# Preparation and Characterization of $BaTiO_3$ Based Dielectric Ceramics

by

**Mohammed Tarcque Chowdhury**



A Thesis

Submitted as the partial fulfillment for the Degree of

**MASTER OF PHILOSOPHY IN MATERIALS SCIENCE**


**DEPARTMENT OF MATERIALS & METALLURGICAL ENGINEERING**

**BANGLADESH UNIVERSITY OF ENGINEERING AND TECHNOLOGY**

**DHAKA-1000, BANGLADESH**

**March 2008**

The thesis titled "Preparation and characterization of $BaTiO_3$ based dielectric ceramics" submitted by Mohammed Tareque Chowdhury, Roll no 020411103P Session April/2002 has been accepted as satisfactory in partial fulfillment of the requirement for the degree of Master of Philosophy in Materials Science on the 31 March, 2008.

**Board of Examiners**

1. Dr. Md. Fakhrul Islam
Professor
Department of Materials and Metallurgical Engineering
BUET, Dhaka
— Chairman (Supervisor)

2. Dr. A K.M. Abdul Hakim
Chief Engineer & Head
Material Science Division
Atomic Energy Center
BAEC, Dhaka
— Member (Co- Supervisor)

3. Dr Md Fakhrul Islam
Professor and Head
Department of Materials and Metallurgical Engineering
BUET, Dhaka
— Member (Ex-officio)

4. Dr. Md. Nasrul Haque
Professor
Department of Materials and Metallurgical Engineering
BUET, Dhaka
— Member

5. Dr. A.K.M Bazlur Rashid
Professor
Department of Materials and Metallurgical Engineering
BUET, Dhaka
— Member

6 Dr Mominul Huq
Professor
Department of Physics
BUET, Dhaka
— Member (External)

## CANDIDATE'S DECLARATION

**It is hereby declared that this thesis or any part of it has not been submitted elsewhere for the award of any degree or diploma.**

( Mohammed Tareque Chowdhury)

Dedicated

**To**

*My Parents*

and

*My wife*

# CONTENTS

## List of Figures

## Lists of Tables

# Acknowledgements

Firstly, I would like to express sincere gratitude to my supervisor Prof. Dr. Md. Fakhrul Islam for his guidance, valuable comments. encouragement, enthusiasms and all round support. This thesis would not have been realized without his extra ordinary support, I am indeed indebted to him.

Dr A.K.M Abdul Hakim, Chief Engineer and Head, Material Science Division (MSD) Atomic Energy Center, Dhaka was kind enough to be my co-supervisor. He guided me with valuable comments, suggestions and facilitated with equipments of his Division. He constantly encouraged me during my thesis work. I would like to express my sincere gratitude to him.

I am grateful to all the teachers of MME Department for their continuous inspiration, help; particularly to for valuable comments. I would like to thanks Mr. Yusuf Khan for SEM, Mr. Faruk Hossain and Mr Abdullah Maksud for DSC and all the technicians and staffs of MME Department for their technical support whenever I needed. I like to thank them all.

Dr. Dilip Kumar Saha and Dr. Sk Manjura Hoque of Material Science Division (MSD) of Atomic Energy Center, Dhaka, BAEC helped me with XRD. I gratefully acknowledged their cooperation and extend my gratitude. All the technical staffs of MSD did extended their help whenever I needed. I like to thank them all.

I am grateful to Dr. Mafizur Rahman, CSO and Head, RPED, INST, Dr Muslehuddin Sarker, CSO, INST and all of my colleagues in RPED who supported me a lot to finish my thesis work.

I like to thank my teacher Dr Md. Nurul Islam, Professor, Department of Physics, University of Chittagong who inspired me to do research in the field of Material Science.

I would like to express my gratitude to my parents, my family, friends and my wife. My wife Tasneem was behind the scene from the starting, inspiring me continuously to complete this thesis.

Mohammed Tareque Chowdhury

Dhaka
March 2008

## ABSTRACT

The microstructure-property relationship of $BaTiO_3$, $Ba_{1-x}Sr_xTiO_3$(x=0.10, 0.15, 0.20) and $SrTiO_3$ has been studied in this thesis. $BaTiO_3$ and $SrTiO_3$ powders of 100nm were used to prepare pellet shaped samples using 130-150 MPa pressure. The green samples were dried and then sintered in the temperature range of 1100°C to 1275°C, varying the holding time from 2 hours to 6 hours. The density, dielectric constant and loss tangent were measured using available equipments at BUET and the Atomic Energy Center, Dhaka (AECD). Optical Microscope, Scanning Electron Microscope (SEM), Differential Scanning Calorimeter (DSC) and X-ray Diffractometer (XRD) were used to observe the microstructure, identify the Curie temperature and different phases to find the correlation between microstructure and property of the sintered samples.

Ninety five percent of the theoretical density has been found for $BaTiO_3$ samples sintered in the temperature range of 1225°C-1250°C. It has been observed from the microstructure that grain growth occurs at higher temperature but porosity still remains inside the grain and in the grain boundaries. Ferroelectric domain twins have been revealed in the chemically etched samples by SEM.

The frequency dependent dielectric constant and loss tangent were measured at room temperature for $BaTiO_3$, $Ba_{1-x}Sr_xTiO_3$ and $SrTiO_3$ samples. The highest dielectric constant was found for $BaTiO_3$ sintered at 1100°C for 3 hours may be due to the small grain size. Loss tangent at 1 kHz for this sample was reasonable compared to the other $BaTiO_3$ sample but at 100 kHz loss tangent was found maximum among all the $BaTiO_3$ samples. The Sr doping was found to have an observable effect on the dielectric properties. The highest dielectric constant obtained for $Ba_{.8}Sr_{.2}TiO_3$ at room temperature was 3000. In the case of $SrTiO_3$, the dielectric constant was found considerably lower. The loss tangent was also found very low for $SrTiO_3$. The temperature dependent dielectric constant was measured for the $BaTiO_3$ and $Ba_xSr_{1-x}TiO_3$ samples. Curie temperature was found at around 130°C for $BaTiO_3$. Tetragonal to cubic transformation was accompanied with a sharp peak for the sample sintered at 1225°C for 4 hours. Curie temperature was found to decrease with an increase of Sr concentration in $Ba_{1-x}Sr_xTiO_3$ sample sintered at 1250°C for 5 hours as expected.

# 1. INTRODUCTION

## 1.1 Barium Titanate

The discovery of ferroelectric Barium Titanate opens the present era of ceramic dielectric materials. The high dielectric constant was first described in the United States in 1942 [1]. Recognition of $BaTiO_3$ as a new ferroelectric compound followed, possibly independently, in several countries [2-4]. A question of historical interest is posed by the lapse of a decade or more between actively ongoing development of titania-based dielectrics and the discovery of $BaTiO_3$. A case can be made that; there may have been earlier syntheses of the material without recognition of its dielectric character. Barium titanate has become the basic ceramic capacitor dielectric material in use today. As earlier with rutile, the main mode of its use has been in combination with other materials. Primary application requisites are a high capacitance and, to the degree possible, stable capacitance over the temperature range of use of the component. Practical temperature ranges of use have been specified from - 55°C to 125°C, or segments within that range. Since pure, crystalline $BaTiO_3$ has a peak permittivity at about 130°C and another secondary peak at 10°C [5]. corrective modification is required for practical applications.

A huge leap in the research on ferroelectric materials followed immediately in the 1950's, leading to the widespread use of barium titanate ($BaTiO_3$) based ceramics in capacitor applications and piezoelectric transducer devices. Since then, many other ferroelectric ceramics including lead titanate ($PbTiO_3$), lead zirconate titanate (PZT), lead lanthanum zirconate titanate (PLZT), and relaxor ferroelectrics like lead magnesium niobate (PMN) have been developed and utilized for a variety of applications. The largest uses of ferroelectric ceramics have been in the areas of dielectric ceramics for capacitor applications, ferroelectric thin films for non-volatile memories, piezoelectric materials for medical ultrasound imaging and actuators, and electro-optic materials for data storage and displays.

## 1.2 Business scenario of titanate materials

Understanding the dielectric materials business is some times a complex process and appears confusing for any companies in the industry. Titanate demand for the merchant market is dependent upon unit growth, since down sizing to smaller, less expensive case sizes by end user of ceramic capacitor require a lower quantity of ceramic capacitor. Each year ceramic capacitor manufacturer is able to produce increasingly larger number of ceramic capacitor with a single pound of dielectric materials. Thus ceramic dielectric material vendor such as Ferro Corporation (which now owns TAM Ceramics), Kyoritsu corporation, Degussa Corporation and Fuji Titanium are dependent upon significant unit growth in the ceramic capacitor industry to increase their shipment volume or to develop technically advanced formulations of dielectrics that are superior to dielectric materials developed in house by the ceramic capacitor companies. Ceramic dielectric materials used in the production of Y5V ceramic capacitors are usually produced in-house by ceramic capacitor. Y5V ceramic dielectric material is predominantly a barium calcium zirconium titanate material. X7R ceramic dielectrics are much harder to produce and require additional additives to be placed in the composition. Even so, about 50% of ceramic capacitor manufacturer produce their own X7R formulation in-house, but still source the titanate vendors for the additive necessary to produce the formulations. The remaining 50% of ceramic capacitor materials for production of X7R ceramic capacitor are sourced directly from the titanate material vendor. The process of producing X7R dielectric materials involves taking the curie point of barium titanate and suppressing it down to create a core shell type structure [6]. The phenomenon growth of integrated circuit technology has been accompanied by increased consumption of discrete circuit component such as resistor and capacitors. Ceramic capacitors account for a major segment of this volume, approximately 2 billion discrete ceramic capacitor being consumed world wide in 1987 with a value exceeding $2.5 billion, and this consumption rate is projected to grow at an average 6% a year [7].

## 1.3 Limitations of Barium Titanate

Although $BaTiO_3$ has, superior dielectric properties compare to other dielectric materials it has some limitations, which must be eliminated, to obtain optimum uses from its dielectric properties. Dielectric constant of $BaTiO_3$ depends on electric field [8] and frequency [9, 10]. At high electric field strength, the domain is more effectively oriented and higher dielectric constant result. Dielectric constant is strongly temperature dependent. That is why circuit characteristic changes even over a moderate temperature range. The temperature dependence of Curie temperature ($T_C$) and dielectric constant ($k'$) can be modified by forming solid solution over a wide range of compositions. For example Pb2÷, Sr2+, Ca2+, Sn2+ can be a substitute for Ba2÷ in the titanate lattice. The possibility of forming solid solution in all of this crystal offers a wide range of values for $k'$, $P_s$ and $T_c$. For example, substitution of Sr2+ for Ba2+ lowers the Curie point. On the other hand, substitution of Pb2+ for Ba2+ increases the $T_c$ to a maximum of 490°C. The effect is due to the lower M-O bonding for Pb<Ba<Sr which offer less resistance to the motion of the Ti ions in their six fold oxygen coordination field. The strain energy introduced by electrostrictive effects on cooling through and below the $T_c$, when some domains change their orientation in relation to the others causes time dependence for the dielectric constant known as aging. The rate of change increases as the initial value of $k'$ increases. Both composition and heat treatment affect aging and also $k'$. In a polycrystalline ceramic, domain orientation is affected by grain size, impurities, and pores. which prevent domain movement due to stresses, imposed by surrounding grains.

# 2. LITERATURE REVIEW

## 2.1. Introduction

For many years, theoreticians avoided the study of ceramic materials, their properties, and their behavior and, understandably, preferred instead to treat the material phenomena associated with metals, single crystals, and the like. In our present highly technological age, it is not possible to ignore ceramics, however complex they are, since more and more applications are being found for these materials in devices affecting our everyday lives in such areas as electronic components, environmental sensors, gas ignitors, intrusion alarms, loudspeakers, ultrasonic cleaners, and medical diagnostic equipment. In fact, many of these applications have come about because of the special nature and properties of ceramics, which set them apart from other materials such as metals or plastics. The relationship of ceramics to other materials can readily be illustrated as shown in Figure 2.1. [7]

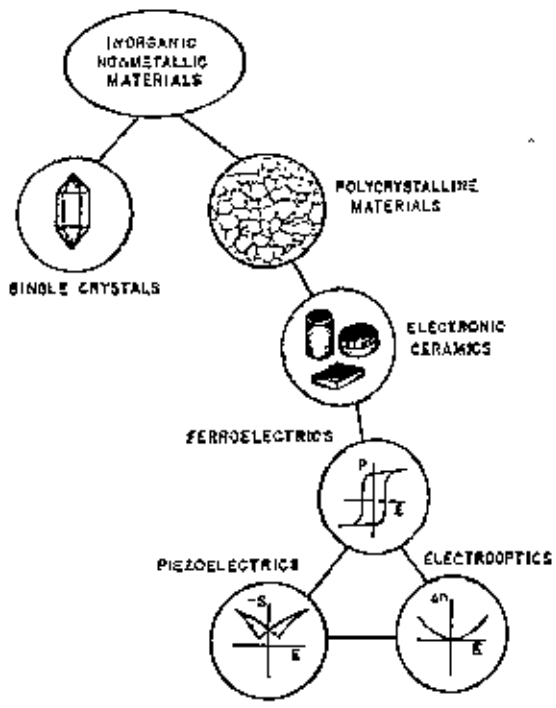


Figure 2.1: Relationship of ceramic and electronic subclasses to all inorganic nonmetallic solids.

In general, all solid materials can be grouped into three major categories: metals, organics (plastics), and inorganics. Similarly, the inorganic solids may be subdivided into the three categories of glasses, single crystals, and ceramics, depending on their microscopic and macroscopic structure. Glasses are distinguished from other inorganic materials by their amorphous nature or lack of long-range internal structure, whereas single crystals are characterized by a well-ordered internal structure on both a long-range ($10^{-4}$-1 cm) and a short-range ($10^{-8}$ - $10^{-5}$ cm) scale. Ceramics are composed of an aggregate of randomly oriented crystallites (small single crystal of less than 100μm or $10^{-2}$ cm average diameter) intimately bonded together to form a solid. Although the crystallites do possess an ordered internal structure just as single crystals do, their random orientation produced during the high-temperature sintering or coalescing operation causes the ceramic to have an overall isotropic (equal in all directions) character in regard to its properties. This isotropic character can be modified, if desired, by special techniques employed during the sintering operation (crystallite orientation by mechanical, electrical, or thermal crystallization means) or after cooling to room temperature. Many of the unique properties of ceramics are thus a direct result of the properties of the small crystallites themselves, their orientation with respect to each other, or the grain (crystallite) boundaries between them.

Ceramics may encompass a wide range of polycrystalline materials; however, our interests here are centered on those types known as electronic ceramics. These materials are highly specialized, being prepared from specifically formulated compositions (usually not found in nature), processed under controlled conditions and fabricated into complex shapes with specific properties, particularly electrical properties. Among these are included insulators, ferrites, capacitors, substrates, varistors, PTCs (positive temperature-coefficient materials), ferroelectrics, pyroelectrics, piezoelectrics, and electrooptic ceramics. We deal here specifically with ferroelectrics, material. The inclusion of piezoelectrics under the category of ferroelectrics as given in Figure 1 is not rigorous, since piezoelectricity is the more general phenomenon; however, today's usage of the term ferroelectric tends to be all-inclusive since most ceramics exhibiting pyroelectric, piezoelectric, and electrooptic behavior are ferroelectric. The actual relationship between these effects

is discussed in succeeding sections.

## 2.2 Piezoelectric Ceramics

### 2.2.1 Symmetric Considerations

Piezoelectricity [11] is a property possessed by a select group of materials. It was discovered in 1880 by Pierre and Jacques Curie during their systematic study of the effect of pressure on the generation of electrical charge by crystals such as quartz, zinc blende, tourmaline, and Rochelle salt; however, the term "piezoelectricity" (pressure electricity) was first suggested by W. Hankel in 1881. Cady [12] defines piezoelectricity as "electric polarization produced by mechanical strain in crystals belonging to certain classes, the polarization being proportional to the strain and changing sign with it." Two effects are manifest in piezoelectricity: the direct effect and the converse or inverse effect. The direct effect is identified with the phenomenon whereby electrical charge (polarization) is generated from a mechanical stress, whereas the converse effect is associated with the mechanical movement generated by the application of an electrical field. Both effects are useful and have found application in present-day devices.

An understanding of the concept of piezoelectricity must necessarily begin deep down inside the structure of the material; and for our purposes here, let's consider a single crystal or single crystallite in the case of a ceramic. This crystal has a definite chemical composition, and hence is made up of ions (atoms with positive or negative charge), which are constrained to occupy positions in a specific repeating relationship to each other, thus building up the structure or lattice of the crystal. The smallest repeating unit of the lattice is called the unit cell, and the specific symmetry possessed by the unit cell determines whether it is possible for piezoelectricity to exist in the crystal. Furthermore, the symmetry of a crystal's internal structure is reflected in symmetry of its external properties.

The elements of symmetry that are utilized by crystallographers to define symmetry about a point in space, for example, the central point of a unit cell, are (1) a point (center) of symmetry, (2) axes of rotation, (3) mirror planes, and (4) combinations of these. Utilizing these symmetry elements, all crystals can be divided into 32

different classes or point groups, as shown in Figure 2. These 32-point groups are subdivisions of seven basic crystal systems, which are, in order of ascending symmetry, triclinic, monoclinic, orthorhombic, tetragonal, rhombohedral (trigonal), hexagonal, and cubic. Of the 32-point groups, 21 classes do not possess a center of symmetry (a necessary condition for piezoelectricity to exist) and 20 of these are piezoelectric. One class, although lacking a center of symmetry, is not piezoelectric because of other combined symmetry elements.

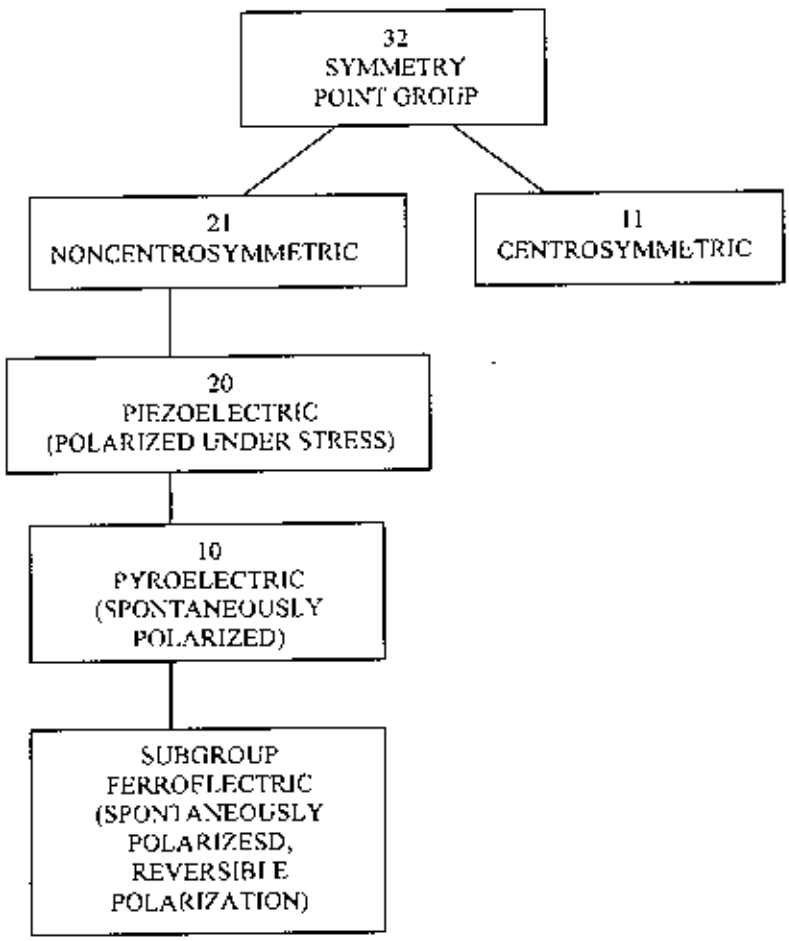


Figure 2.2: Interrelationship of piezoelectrics and subgroups on the basis of internal crystal symmetry.

It can be seen that a lack of a center of symmetry is all-important for the presence of piezoelectricity when one considers that a homogeneous stress is centrosymmetric and cannot produce an unsymmetric result (e.g., a vector quantity such as electric polarization) unless the material lacks a center of symmetry whereby a net movement of the positive and negative ions with respect to each other as a result of the stress produces an electric dipole (polarization).

For piezoelectricity, this effect is linear and reversible; the sign of the charge produced is dependent on the direction of the stress (tensile or compressive). When one now considers a ceramic consisting of a multitude of tiny, piezoelectric crystallites at random orientation, quite a different situation from that of a single crystal is obtained. This random orientation causes the overall ceramic to be inactive, with no piezoelectricity detectable until some means is found to polarize the ceramic as a whole entity. With piezoelectric crystallites, this is possible only through techniques such as extrusion, hot forging, or directional recrystallization, which will orient the crystallites.

## 2.3. Ferroelectric Ceramics

If we again refer to Figure 2.2, we see that there are 10 crystal classes, out of a possible 20, that are designated as pyroelectric. This group of crystals possesses the unusual characteristic of being permanently polarized within a given temperature range. Unlike the more general piezoelectric classes, which produce a polarization under stress, the pyroelectrics develop this polarization spontaneously and form permanent dipoles in the structure. This polarization also changes with temperature-hence the term pyroelectricity. Pyroelectric crystals such as tourmaline and wurtzite are often called polar materials, referring to the unique polar axis existing within the lattice. The length of the polar axis (dipole moment) varies with temperature, changing sign as the temperature is either elevated or lowered. Present-day pyroelectric devices utilize this effect in such applications as intrusion alarms, thermal imaging, and geographical mapping.

A subgroup of the spontaneously polarized pyroelectrics is a special category of

materials known as ferroelectrics. Materials in this group are characterized as crystals that possess a spontaneous dipole, and this dipole is reversible by an electric field of some magnitude less than the dielectric breakdown of the material itself. Because of the empirical nature of determining the reversibility of the dipoles, as detected in a hysteresis loop measurement, one cannot predict the existence of ferroelectricity in a new material with much accuracy. We do see, however, that the basis for the existence of ferroelectricity rests primarily on structural (symmetry) considerations. The number of actual ferroelectrics today is known to be in the thousands when one includes the large number of ceramic solid-solution compositions, and it is no longer the great "accident of nature" that it was once thought to be. Ferroelectricity was first discovered in Rochelle salt by Valesek in 1920. Further significant developments in the history of ferroelectric materials came in the 1940s when ferroelectricity was discovered in single-crystal and ceramic barium titanate and in the 1950s when the ferroelectric lead zirconate titanate ceramic solid-solution compositions were developed [10].

Ferroelectric ceramics have a number of properties, which make them very useful in a variety of applications. These include (1) a high dielectric constant, (2) high piezoelectric constants, (3) relatively low dielectric loss, (4) high electrical resistivity, (5) moisture insensitivity, (6) high electromechanical coupling, (7) medium hardness, (8) fairly high pyroelectric coefficients; and in some special compositions, also (9) high optical transparency and (10) high electro optic coefficients. Although these properties do not always combine to produce an optimum effect in anyone application, one can see that the number of desirable properties provides the possibility for many new and unique applications. This is particularly true when one considers the interactive properties of (1) electromechanical (piezoelectric) behavior relating mechanical and electrical properties, and (2) electrooptic effects relating electrical and optical properties. In addition, these properties in ceramics can be continuously modified over specified ranges because many ceramic compositions form continuous solid solutions (solid solubility) of one or more compounds in each other. Less obvious, but perhaps equally important, is the fact that most ceramics can be fabricated into complex shapes and are more economical to produce.

The most outstanding feature of a ferroelectric ceramic is its hysteresis loop. It describes the nonlinear polarization switching behavior as a function of field. The initial application of an electric field to a virgin ferroelectric electroded disk produces very little effect until the electric field becomes sufficiently high to switch the dipoles in the crystallites. At this field, the polarization (measured as voltage on a large, known, series capacitor) changes sharply and reaches saturation at higher fields. Reducing the field to zero leaves the material with a net permanent polarization known as remanent polarization *($P_R$)*. As the field is reversed, polarization is first reduced to zero and then changes direction (sign) as the field produces saturation polarization in the opposite direction, thus tracing out a hysteresis loop. The field at which the polarization equals zero (changes sign) is known as the coercive field $E_c$. Poling consists of applying one-quarter of a hysteresis loop, leaving the material in a remanently polarized condition at $P_{Ro}$

Although a large number of ferroelectric ceramics are used in piezoelectric applications today, it should be pointed out that devices which are strictly dependent on the ferroelectric (polarization switching) properties of ceramics have not found acceptance in the marketplace. This has been due primarily to (1) undesirable fatigue effects resulting from stress (strain)-induced microcracks developed during switching, and (2) the lack of a definite electrical switching field *(Ec)*, which can cause loss of remnant (memory) polarization states in the material over a period of time when subjected to partial reversing fields. Undoubtedly, these detractors would need to be overcome before ferroelectric-switching devices will be successful.

## 2.4 Ferroelectric phenomena

### 2.4.1 Curie point and Phase Transitions

All ferroelectric materials have a transition temperature called the Curie point ($T_c$). At a temperature $T > T_c$ the crystal does not exhibit ferroelectricity, below $T_c$ it is ferroelectric. On decreasing the temperature through the Curie point, a ferroelectric crystal undergoes a phase transition from a non-ferroelectric phase to a ferroelectric phase. If there is more than one ferroelectric phase, the temperature at which the

crystal transforms from one ferroelectric phase to another is called the transition temperature.

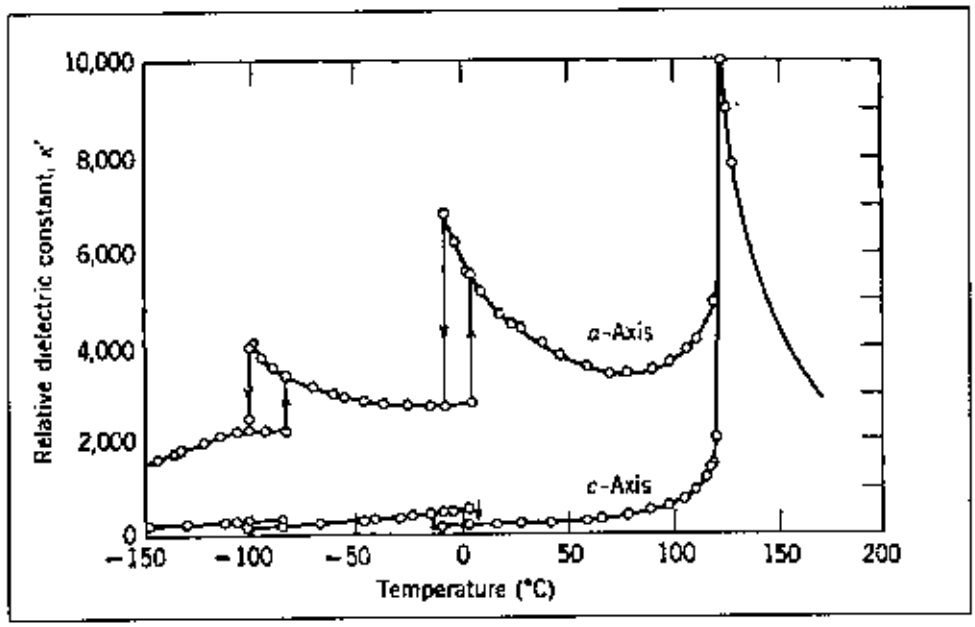


Figure 2.3: Variation of dielectric constants (a and c axis) with temperature for $BaTiO_3$. [13]

The phase transition in $BaTiO_3$ is of first order, and as a result, there is a discontinuity in the polarization, lattice constant, and many other properties, as becomes clear in Figure 2.4. It is also clear in the figure that there is three phase transitions in barium titanate having the following sequence upon cooling: rhombohedral, orthorhombic, tetragonal and cubic. There is a small thermal hysteresis of the transition temperature, which depends on many parameters such as the rate of temperature change, mechanical stresses or crystal imperfections. From a crystal chemical view, the Ba-O framework evokes an interstitial for the central Ti4+ ion, which is larger than the actual size of the Ti4+ ion. As a result, the series of phase transformations takes place to reduce the Ti cavity size. Certainly, the radii of the ions involved impact

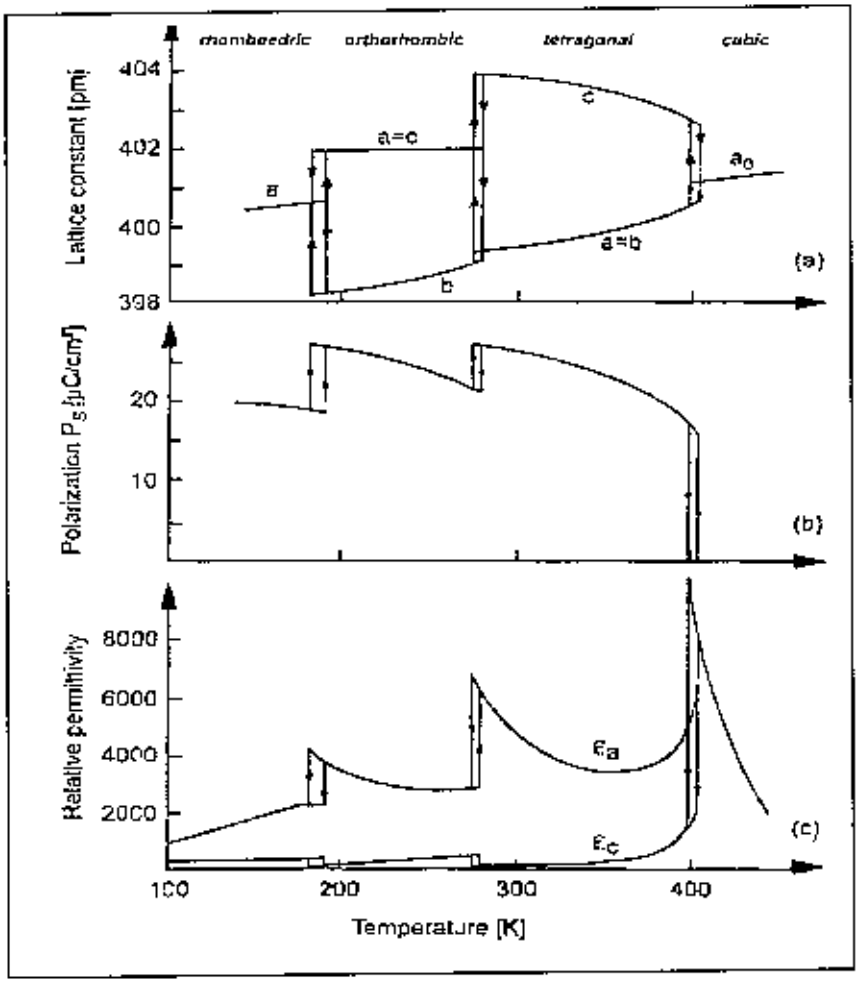


Figure 2.4: Various properties of $BaTiO_3$ as function of phase transformation

the propensity for forming ferroelectric phases; thus both $PbTiO_3$ and $BaTiO_3$ have ferroelectric phases, while $CaTiO_3$ and $SrTiO_3$ do not [14]. Early research work on ferroelectric transitions has been summarized by Nettleton [15, 16]. Figure 2.3 shows the variation of the relative permittivity $\varepsilon_r$ with temperature as a $BaTiO_3$ crystal is cooled from its paraelectric cubic phase to the ferroelectric tetragonal, orthorhombic, and rhombohedral phases. Near the Curie point or transition temperatures, thermodynamic properties including dielectric, elastic, optical, and thermal constants show an anomalous behavior. This is due to a distortion in the crystal as the phase structure changes. The temperature dependence of the dielectric constant above the Curie point ($T > T_c$) in ferroelectric crystals is governed by the Curie-Weiss law.

### 2.4.2 Crystal structure and phase transformation

Large classes of ferroelectric crystals are made up of mixed oxides containing corner-sharing octahedra of $O^{2-}$ ions schematically shown in Figure 2.5. Inside each octahedron is a cation $B^{b+}$ where 'b' varies from 3 to 6. The spaces between the octahedra are occupied by $A^{a+}$ ions where 'a' varies from 1 to 3. In prototype forms, the geometric centers of the $A^{a+}$, $B^{b+}$ and $O^{2-}$ ions coincide, giving rise to a non-polar lattice. When polarized, the A and B ions are displaced from their geometric centers with respect to the $O^{2-}$ ions, to give a net polarity to the lattice. These displacements occur due to the changes in the lattice structure when phase transitions take place as the temperature is changed. The formation of dipoles by the displacement of ions will not lead to spontaneous polarization if a compensation pattern of dipoles are formed which give zero net dipole moment.

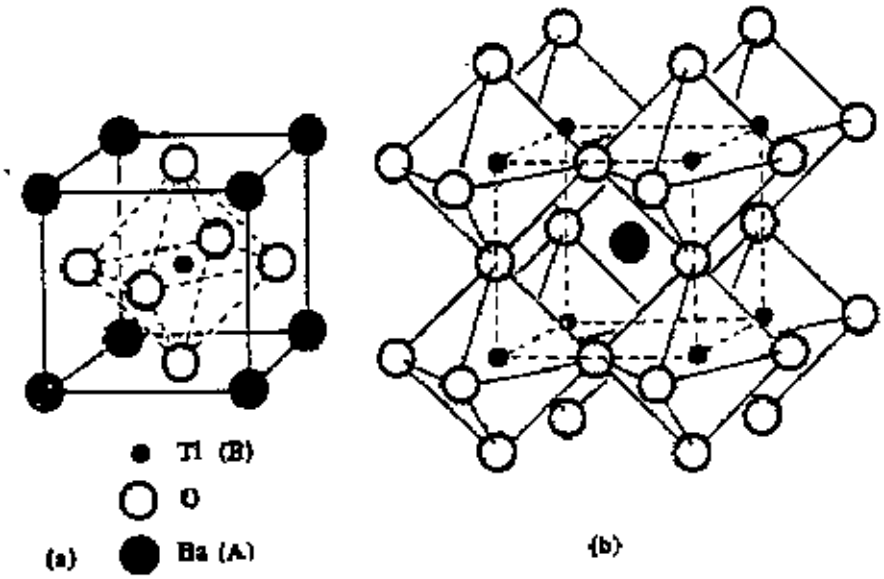


Figure 2.5: (a) A cubic $ABO_3$ ($BaTiO_3$) perovskite-type unit cell and (b) three dimensional network of corner sharing octahedra of $O_2$- ions [ 13].

Perovskite is a family name of a group of materials and the mineral name of calcium titanate ($CaTiO_3$) having a structure of the type $ABO_3$. A wide variety of cations can be incorporated into perovskite structure as long as they obey the relationship:

$$t = (R_A + R_B)/ \sqrt{2}(R_B + R_O)$$

For an ideal perovskite structure t = 1, and $R_A$, $R_B$ and $R_O$ the ionic radius of large cation, small cation and oxygen [17]. The structure takes cubit from with the t value between 0.95 to 1.0; lower this slightly distorted cubic but not ferroelectric but slightly over 1.0 tends to be ferroelectric [18].

Different phase transformations and cell dimensions of $BaTiO_3$ are illustrated in Figure 2.6. $BaTiO_3$ has a paraelectric cubic phase above its Curie point of about 130°C. In the temperature range of 130°C to 0°C the ferroelectric tetragonal phase with a c/a ratio of ~1.01 is stable. The spontaneous polarization is along one of the [001] directions in the original cubic structure. Between 0°C and -90°C, the ferroelectric orthorhombic phase is stable with the polarization along one of the [110] directions in the original cubic structure. On decreasing the temperature below -90°C the phase transition from the orthorhombic to ferroelectric rhombohedral phase leads to polarization along one of the [111] cubic directions.

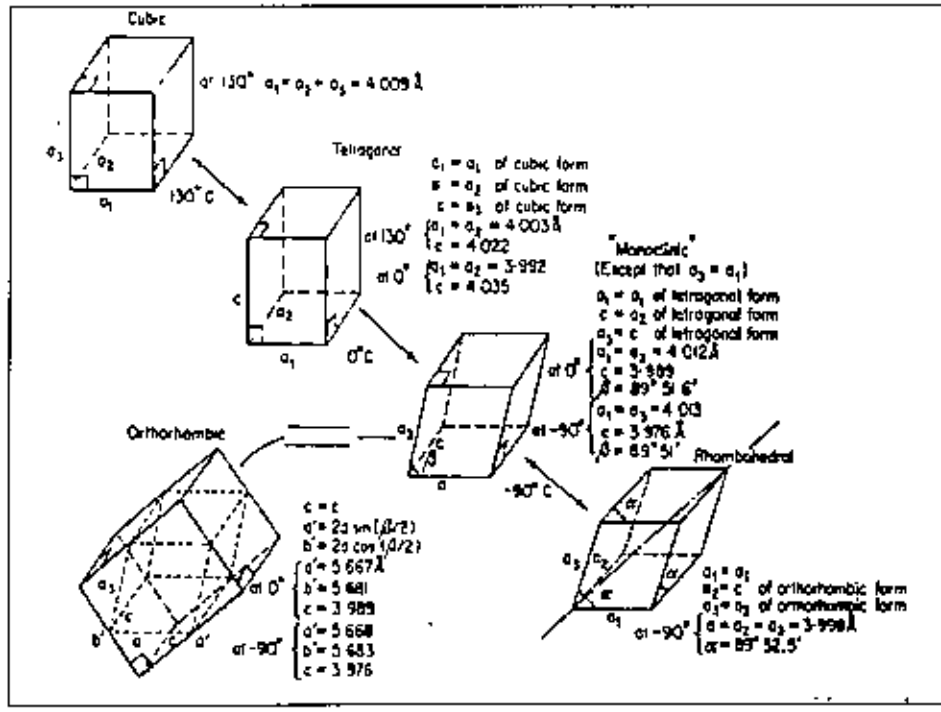


Figure 2.6: Different Phases, transformation and cell dimension of $BaTiO_3$

On cooling from high temperatures, the permittivity increases up to values well above 10,000 at the phase transition temperature $T_c$. The inverse susceptibility as well as the dielectric permittivity follows a Curie-Weiss law. The appearance of the spontaneous polarization is accompanied with a spontaneous (tetragonal) lattice distortion. The phase transition in barium titanate is of first order, and as a result, there is a discontinuity in the polarization, lattice constant, and many other properties, as becomes clear in Figure 2.4.

Many piezoelectric (including ferroelectric) ceramics such as Barium Titanate ($BaTiO_3$), Lead Titanate ($PbTiO_3$), Lead Zirconate Titanate (PZT), Lead Lanthanum Zirconate Titanate (PLZT), Lead Magnesium Niobate (PMN), Potassium Niobate ($KNbO_3$), Potassium Sodium Niobate ($K_xNa_{1-x}NbO_3$), and Potassium Tantalate Niobate ($K(Ta_xNb_{1-x})O_3$) have a perovskite type structure.

### 2.4.3 Ferroelectric Hysteresis Loop

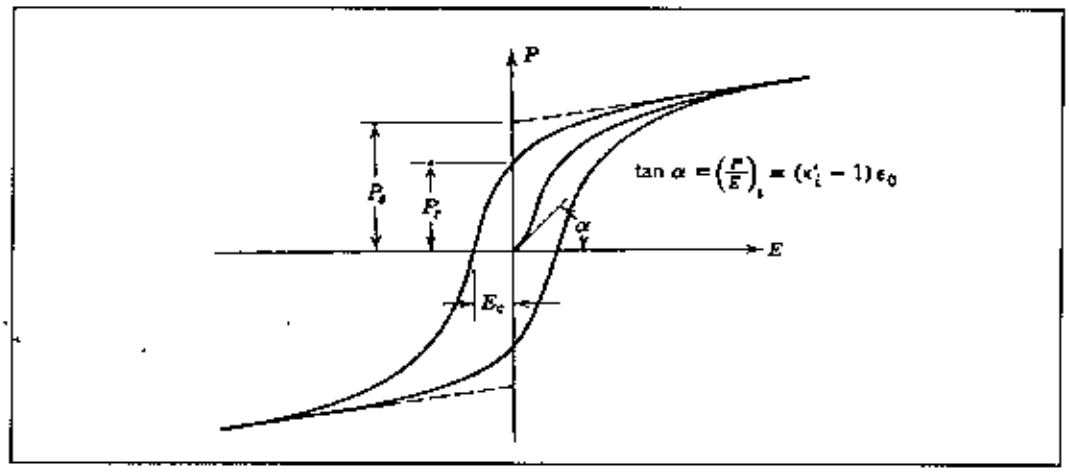


Figure 2.7: A Polarization vs. Electric Field (P-E) hysteresis loop for a typical ferroelectric crystal. [19]

The result of spontaneous polarization of a ferroelectric at $T_c$ is the appearance of very high $k'$ and a hesterisis loop for polarization (Figure 2.7). The hesterisis loop is due to the presence of crystallographic domains within which there is complete alignment of electric dipole. The ferroelectric hysteresis originates from the

existence of irreversible polarization processes by polarization reversals of a single ferroelectric lattice cell. However, the exact interplay between this fundamental process, domain walls, defects and the overall appearance of the ferroelectric hysteresis is still not precisely known. The separation of the total polarization into reversible and irreversible contributions might facilitate the understanding of ferroelectric polarization mechanisms. Especially, the irreversible processes would be important for ferroelectric memory devices, since the reversible processes cannot be used to store information. For ferroelectrics, mainly two possible mechanisms for irreversible processes exist. First, lattice defects, which interact with a domain wall and hinder it from returning into its initial position, after removing the electric field, which initiated the domain wall motion ("pinning"). Second, the nucleation and growth of new domains that do not disappear after the field is removed. In ferroelectric materials, the matter is further complicated by defect dipoles and free charges that contribute to the measured polarization and can interact with domain walls [20].

Reversible ferroelectrics are the basic requisite of dielectric materials for application such as capacitors. Reversible contributions in ferroelectrics are due to ionic and electronic displacements and to domain wall motions with small amplitude. These mechanisms are very fast. The reorientation of dipoles and/or defect or free charges also contributes to the total polarization. These mechanisms are usually much slower, but they also might be reversible (relaxation).

Remnant polarization and coercive voltage are of critical importance to the design of external circuits of FeRAMs.

### 2.4.4 Ferroelectric domain

Ferroelectric crystals possess regions with uniform polarization called ferroelectric domains. Within a domain, all the electric dipoles or the polar axis transformation occur and spontaneous polarization takes place. The electrical stray field energy caused by the non-compensated polarization charges is reduced by the formation of ferroelectric domains as shown in Figure 2.8. The configuration of the domains follows a head-to-tail condition in order to avoid discontinuities in the polarization

at the domain boundary. The polarization may be orientated in any of the six pseudo cubic <001> directions. Therefore, the polar axis may be aligned orthogonally (90° domains) and anti-parallel (180° domains) with respect to each other (Figure 2.9).

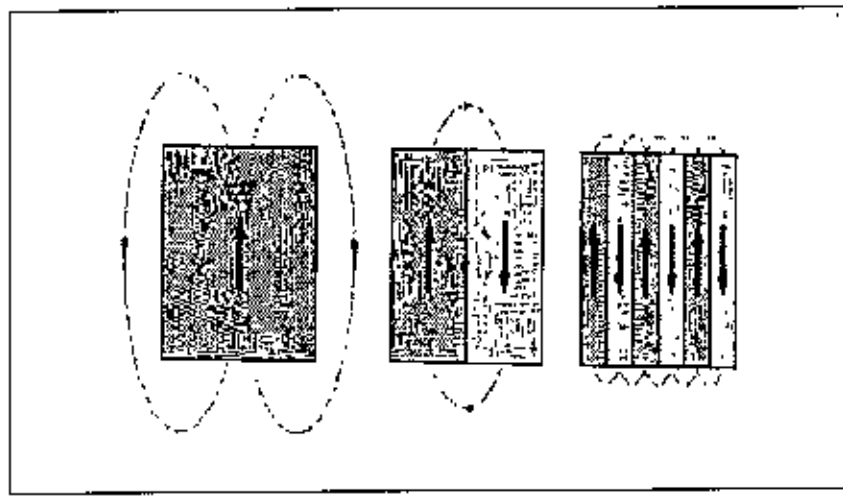

Figure 2.8: Reduction of electrical energy by domain formation.

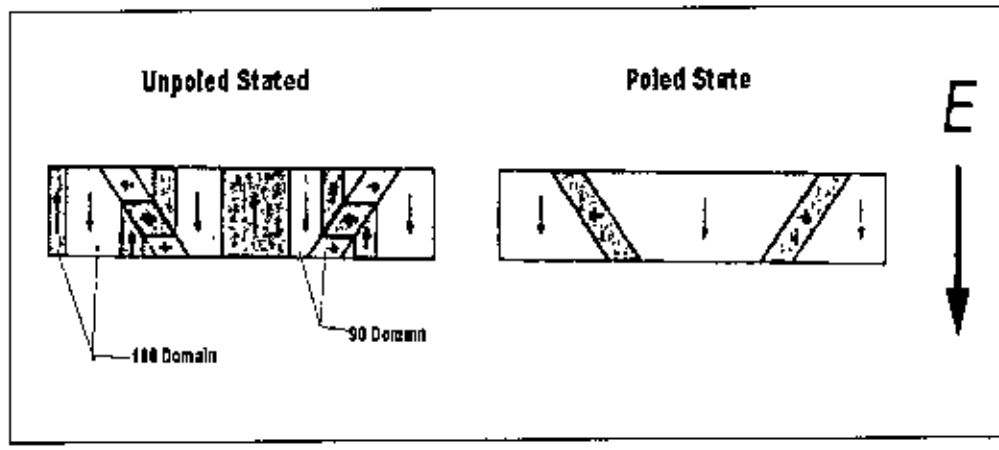


Figure 2.9: Domain polarization direction changed by poling

Atomic force microscopy [21] and TEM [22] was used to characterize domain. A very strong field could lead to the reversal of the polarization in the domain, known as domain switching [23]. The relationships between etch pattern and the domain orientation in $BaTiO_3$ crystal in tetragonal state had been described by Hooton [24].

Domains can be observed under the optical microscope and in SEM after the polished sample being etched with concentrated HCl [25]. During etching processing the positive ends of the electric dipoles etch rapidly, forming a rough surface, the negative ends etch slowly, forming smooth surface and the sides (dipoles parallel to the surface) etch at an intermediate rate, forming a semi smooth surface.

The built-up of domain wall. elastic stress fields as well as free charge carriers counteracts the process of domain formation. In addition, an influence of vacancies, dislocations and dopants exits [26].

## 2.5 Science of $BaTiO_3$ Materials

### 2.5.1 Formation of phases and Phase Diagram

$BaTiO_3$ formed during reaction above through formation number of intermediate phases. Templeton [27] detected the intermediate second phases $Ba_2TiO_4$, $BaTi_4O_9$ and $BaTi_3O_7$.The final conversion to monophase $BaTiO_3$ determined by decomposition of the intermediate phases, ie, the diffusional exchange between Ba and Ti rich region in the powder. The calcinations temperature and the amount of intermediate phases critically depend on the morphology and degree of mixing of the raw material. During ball milling this is an important point aimed to accomplish. According to Bauger et al [28], during this solid-solid reaction BaO act as the mobile agent. At the contact interface BaO is formed which diffuses into the $TiO_2$ forming as intermediate layer of $Ba_2TiO_4$, which slowly reacts with the residual $TiO_2$ to form $BaTiO_3$. Hence, particle size is an important factor especially the size of $TiO_2$ as it determines the particle size of $BaTiO_3$.

The phase diagram of $BaO$-$TiO_2$ is shown in Figure 2.10. As per phase diagram stoichometric $BaTiO_3$ can accommodate little more $TiO_2$ with the compound. Formation of $Ba_2TiO_4$ is inhibited below 1100°C by the presence of a $CO_2$ atmosphere. This phase is particularly harmful, since it is hygroscopic and decomposed with swelling in slightly moist air. Incomplete mixing and reaction will yield small amounts of $Ba_2TiO_4$ and $BaTi_3O_7$ and other intermediate phases. The same kind of harmful phases may also occur when alkaline earth oxides, such as Ca, Sr used in substituted $BaTiO_3$ [29]. Effect of calcination temperature was studied by

Maison *et.al* [30] suggests at 700°C tetragonal $BaTiO_3$ do not form whereas at 1100°C it does at the expenses of particle agglomeration.

Dopent and other additives are added at this stage of processing. A great advantage of this method is that dopes and additives can be homogeneously incorporated into the perovskite lattice during calcinations. The calcining temperature is important as it influences the density and hence the electromechanical properties of the final product. The higher the calcinations temperature, the higher the homogeneity and density of the final ceramic product. Many calcinations temperature and time scheme has been suggested. Higher temperature and longer time usually yield completely reacted powder but coarser particle size posing difficulties during subsequent milling So, proper calcination at the right temperature is necessary to obtain the best electrical, mechanical properties and minimizing the presence of harmful phases

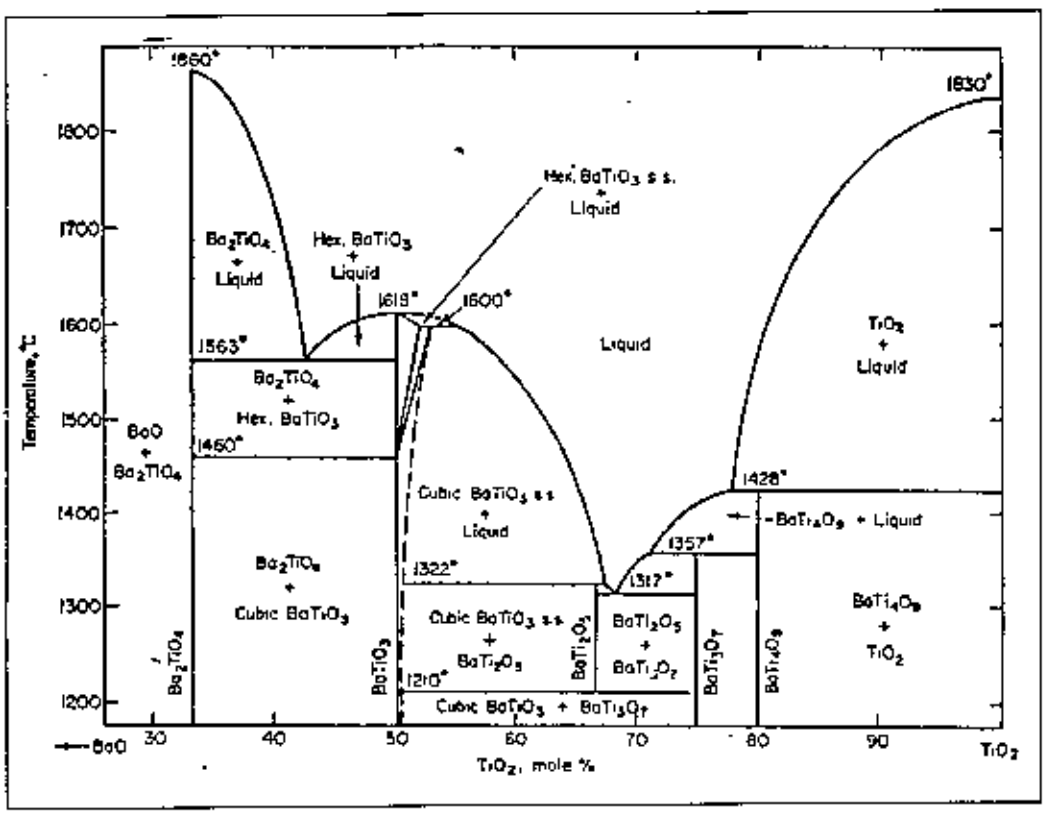


Figure 2.10: Phase Diagram of BaO - $TiO_2$ system

### 2.5.2 Effect of grain size

Reducing the grain size of the barium titanate ceramic below about 1 μm diameter has a flattening effect on capacitance versus temperature. The origin of this effect is in the nature of the symmetry transition associated with the 130°C permittivity peak of $BaTiO_3$. The microstructure of a large-grained ceramic contains "90°" twins formed to relieve the strains generated when the C axis elongates on passing from the cubic to the tetragonal symmetry; in the strained the highest permittivity is displays. The domain boundary plane has have surface energy proportional to the square of the grain diameter; the strain energy responsible for domain formation, a volume effect, is related to the cube of the grain diameter. With decreasing grain size a critical size, Dc I reached where it is energetically less costly to support an elastic strain than to relieve by twin formation. The ceramic in which situation exists will have average grain size of the order of 1 μm or less and be untwined; that is each grain will comprise a single domain and have one orientation of spontaneous polarization, be stressed and tend to be cubic symmetry. The permittivity of ceramic in this condition will be grater than when unstrained, having a room temperature value of average 2000, compared with 1400 for large grained, freely twinned $BaTiO_3$.To take advantage of this effect, $BaTiO_3$ starting material of very fine grain size and processing that minimizes grain growth are required. Fig 2.11 shows the ferroelectric transition of $BaTiO_3$ at $120^0$C for ultra fine particles.

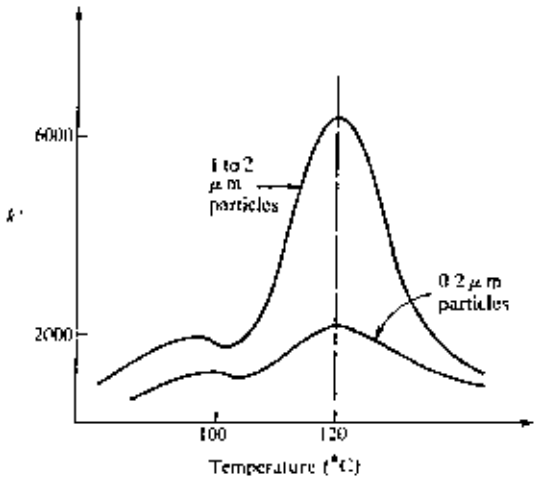


Figure 2.11: Ferroelectric behavior of ultra fine particle size $BaTiO_3$

When this is compared with the single crystalline $BaTiO_3$ we can see a markedly different behavior. For single crystalline material, the transition is extremely sharp. In fact, the derivative goes to infinity. In the case of fine particle, (1 to 2 μm) the transition is gradual. This indicates that there is relationship between the size of the crystalline structure and the equilibrium position of the titanium ions in the polarize state. In ultra fine powder (0.2 μm), there exists little or no orientational relationship. Like wise, the increase in dielectric constant is much less for ultra fine particles. This again shows the interrelationship of the microstructure and the ferroelectric domains. The domain orientation of the ultra fine powder is random. This randomization tends to broaden the ferroelectric transition.

Figure 2.12 shows the variation of dielectric constant with temperature for $BaTiO_3$ ceramics with a fine (<1μm) and coarse (>50μm) grain size. Large grained $BaTiO_3$ (>1μm) shows an extremely high dielectric constant at the Curie point. This is because of the formation of multiple domains in a single grain, the motion of whose walls increases the dielectric constant at the Curie point. For a $BaTiO_3$ ceramic with fine grains (<1μm), a single domain forms inside each grain. The movement of domain walls are restricted by the grain boundaries, thus leading to a low dielectric constant at the Curie point as compared to coarse grained $BaTiO_3$ [31]. The room temperature dielectric constant k′ of coarse grained (>50μm) $BaTiO_3$ ceramics is found to be in the range of 1500-2000. On the other hand, fine grained (~1μm) $BaTiO_3$ ceramics exhibit a room temperature dielectric constant between 3500-6000. The grain size effect on the dielectric constant at room temperature has been explained by the work of Arlt et. al. [22] and Buessem et. al. [32] coworkers proposed that the internal stresses in fine grained $BaTiO_3$ must be much greater than the coarse grained ceramic, thus leading to a higher permittivity at room temperature. Arlt studied the domain structures in BT ceramics and showed that the room temperature k′ reached a peak value at a critical grain size of ~0.7μm. He concluded that the enhanced dielectric constant was due to the increased 90° domain wall density.

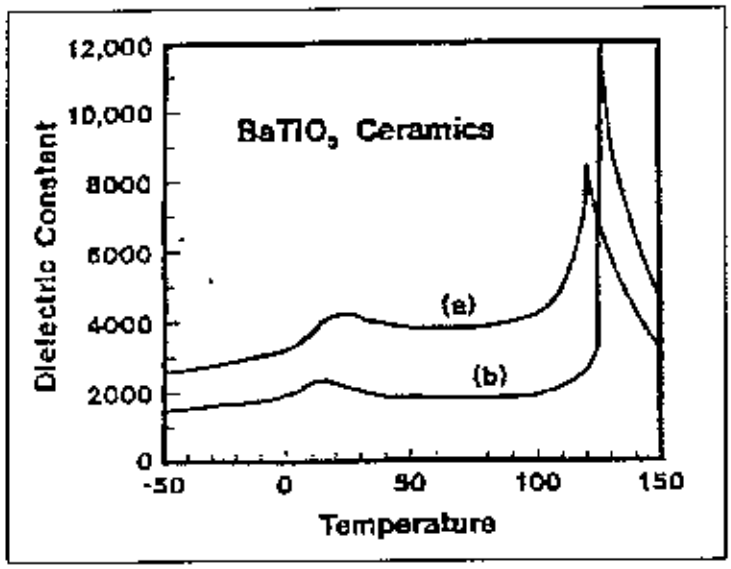


Figure 2.12: Grain size effect of bulk ceramic (a) fine grain (b) course grain

The mobility of the 90° domain walls in very fine-grained BT is hindered and only less than 25 % of the k′ was achieved. As the BT ceramics have a very large room temperature dielectric constant, they are mainly used multilayer capacitor applications. The grain size control is very important for these applications.

Frey et.al [33] reported the results of an investigation into the grain-size dependence of lattice structure for barium titanate ($BaTiO_3$) ceramics prepared by a sol-gel method. Raman and infrared spectroscopy, x-ray diffraction, and differential scanning calorimetry were used in combination with electron microscopy (Figure 2.13) to study the evolution of lattice structure and phase transformation behavior with heat treatment and grain growth from the nano scale to the micron scale for $BaTiO_3$ polycrystals. Raman spectroscopy and optical second-harmonic generation measurements indicated the onset of local room-temperature acentric crystal symmetry with heat treatment and crystallite growth, well before the observation of any tetragonal structure by x-ray diffraction. Analysis of the room temperature Raman spectra for ultrafine grain (grain size < 0.1 μm) polycrystals suggested that a locally orthorhombic structure preceded the globally tetragonal form with grain growth. In support of this observation, differential scanning calorimetry suggested the orthorhombic-tetragonal phase transformation shifts up through room temperature with decreasing grain size. Hot-stage transmission electron

microscopy studies (Figure 2.14) revealed that fine grain (grain size = 0.1μm) ceramics, which showed a thermal anomaly associated with the cubic-tetragonal phase transformation, were un twinned at room temperature, as well as on cycling through the normal Curie temperature, suggesting a single-domain state for individual grains.

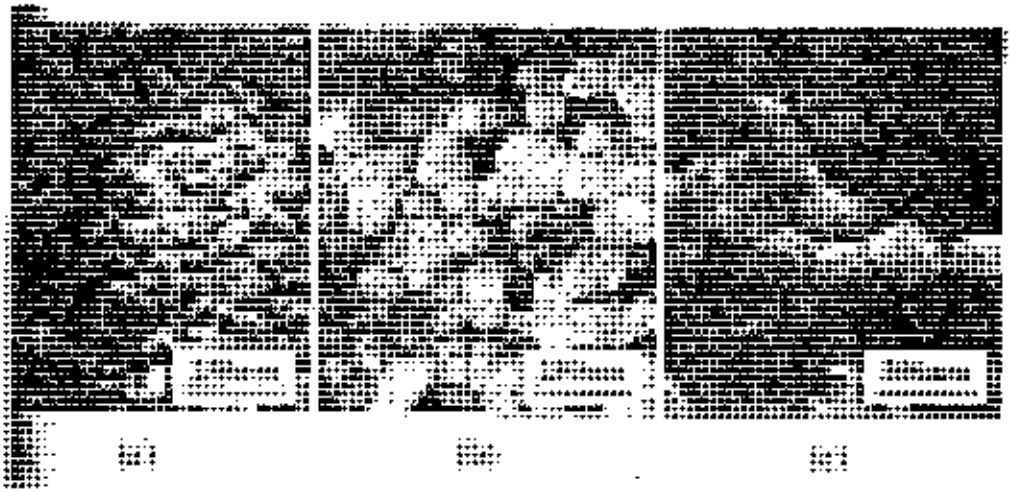

Figure 2.13: SEM photograph illustration the grain growth with increasing heat treatment temperature for sintered for xerogel pieces (a) 800°C (b) 1000°C (C) $1200^0$C

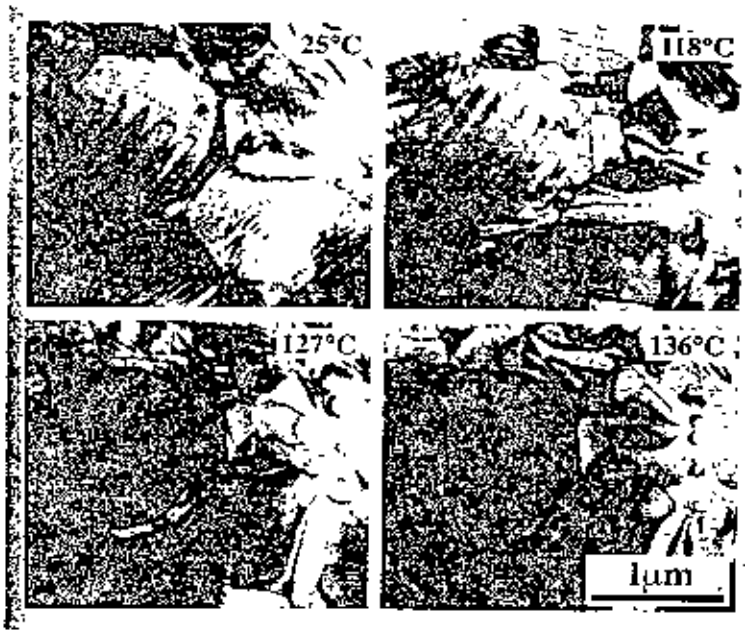


Figure 2.14: TEM photograph illustrating the development of a poly domain subgrain structure for $BaTiO_3$ of grain size 1μm.

Arlt et. el [22] reported that at grain size <10μm the width of the ferroelectric 90° domains decreases proportionally to the square root of the grain diameter. The decreasing width of the domain can be theoretically explained by the equilibrium of elastic field energy and domain wall energy. The smaller the grain, the more the dielectric and elastic constants are determined by the contribution of 90° domain walls. The permittivity below the Curie point shows a pronounced maximum $\varepsilon_r$ ≈5000 at grain sizes 0.8-1μm. At grain sizes less than<0.7μm the permittivity strongly decreases and the lattice gradually changes from tetragonal to pseudocubic. Figure 2.15 shows the microstructure of fine grain $BaTiO_3$.

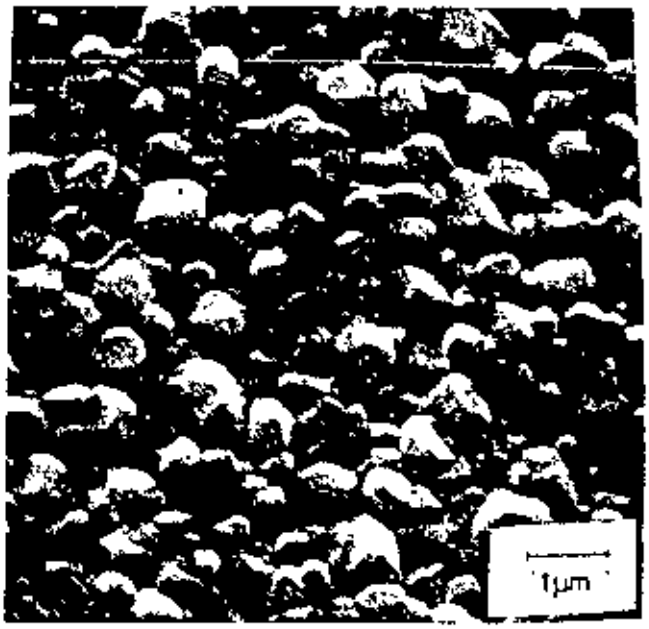


Figure 2.15: Thermal etching of fine grain $BaTiO_3$, 1 h in air at 1100°C; $BaTiO_3$ hot pressed at1130°C.

### 2.5.3 Effect of electric field

The magnitude of the applied filed E has a large effect on the switching of domains and also on the temperature of the onset of electricity. $T_C$ as shown in Figure 2.16, step A-B designate the switching transition, that is reversing domain orientation, due to changing at a constant temperature. Step C-D is a transition to the non-ferroelectric state, which is due to thermal disordering of the dipole in the domains.

Step A-H is a transition from ferroelectric to non-ferroelectric state under a field bias. As indicated, the transition temperature is higher. Step F-G is double loop switching. This field effect in polarization switching is shown in Figure 2.17. When the bias does not exceed 6kV/cm [34], the bias cause finite polarization even at temperature above $T_C$; a linear dielectric response of the material result. When the bias is sufficiently large the spontaneous polarization $P_s$ and the dielectric polarization merge and $T_c$ loses meaning (Figure 2.18).

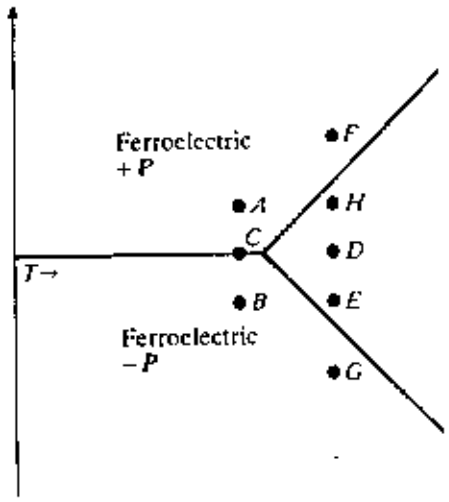


Figure 2.16: Ferroelectric transitions

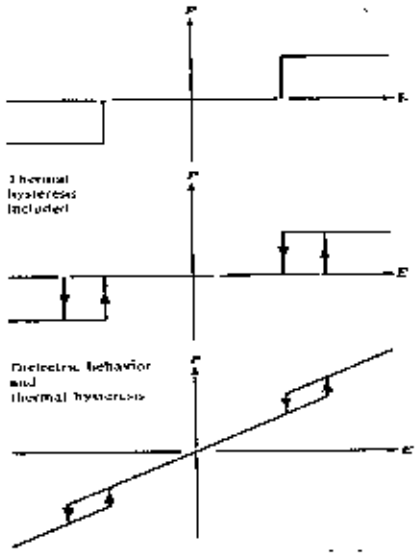

Figure 2.17: field effects on polarization of a ferroelectric

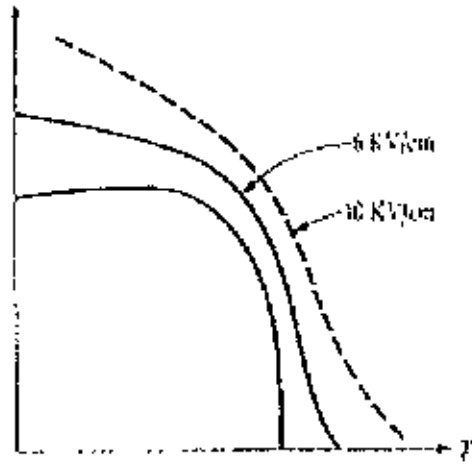

Figure 2.18: Effect of bias on $T_C$

### 2.5.4 Domain structure effect

Many of the properties of ferroelectric ceramics such as dielectric constant, aging, dielectric loss, etc., are related to the motion of domain boundaries. It is therefore of great importance to be able to examine and accurately interpret ferroelectric domain structures. The domain structure of $BaTiO_3$ is of particular interest because of its extensive application in electronic application. Between 1460°C and 130°C $BaTiO_3$ adopts a cubic perovskite structure and is paraelectric. On cooling below 130°C, it undergoes phase transition accompanied by an elongation along one cubic axis (c axis), and a contraction along the other two (a) axes. The result is a tetragonal unit cell with c/a ratio of ≈1.101. The tetragonal phase is ferroelectric, and the direction spontaneous polarization being parallel to the elongated c axis. The phase is stable down to 5°C, where transformations to an orthorhombic structure take place. The knowledge of ferroelectric domains in tetragonal $BaTiO_3$ [35] can be summarized as follows:

(i) In an individual domain, the direction polarization occurs along c axis and parallel to any one of the three original [100] cube axes.

(ii) There are two types of domain boundary, 90° and 180°. The angles refer to the angle between the domain polarization vectors on either side of the boundary.

(iii) 90° boundary walls lie on (110) planes and tend to be straight. The energy of 180° boundary walls, however is less sensitive to crystallographic orientation; thus 180° boundaries are usually 'wavy.'

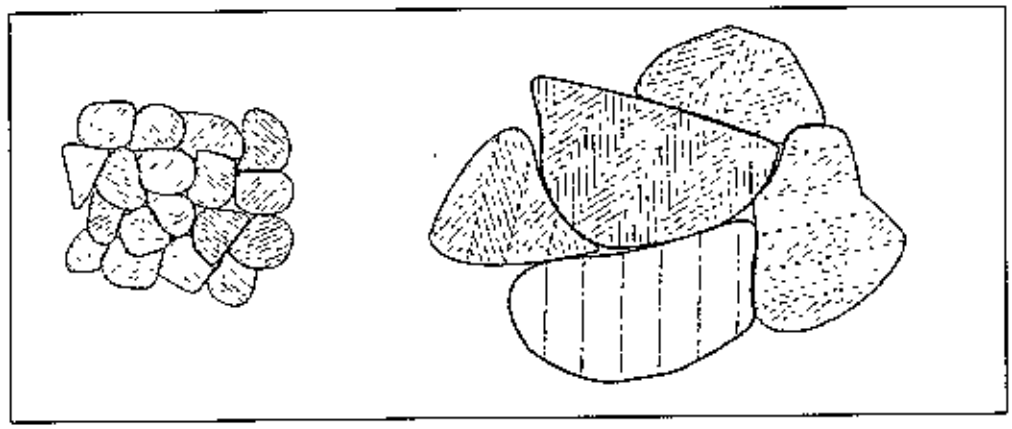

Figure 2.19: Domain pattern of fine grained (left) and coarse grained (right) $BaTiO_3$ ceramic.

(iv) The polarization vectors adopt a head to tail arrangement across a 90° boundary in order to minimize the charge at the domain wall.

In polycrystalline bulk ceramics the pattern of domains is quite different because the domain structure of each grain is formed under elastic clamped conditions by its surrounding neighbors, whereas a single crystal is free [9]. It should be noted that only non-180° domains, i.e. 90° domains (for tetragonal structures) or 71 and 109 domains (for rhombohedral structures), have the potential to reduce elastic energy.

There exist two types of domain in coarse-grained $BaTiO_3$, called herringbone and square net pattern. The first one is by far the most common in unpoled ceramics. As shown in Figure 2.19, by decreasing the grain size the domain pattern changes from a banded to a laminar structure [36].

### 2.5.5 Doping and compositional effect

The temperature dependence of $T_c$ and $k'$ can be modified by forming solid solutions over a wide range of compositions. For example, Pb2+, Sr+, Ca2+, Cd2+ can be substituted for Ba2+ in the titanate lattice. Also, Sr4+, Hf+, Zr4+, Ce4+, Th4+ can

be substituted for Ti4+.The zirconates ($XZrO_3$), niobates ($XNbO_3$), tantalates ($XTaO_3$), tungstates ($XWO_3$) and molybdates ($XMO_3$) also form ferroelectrics [7]. It is reported that substitution of Sr+ for Ba2+ lowers the Curie point. Substitution Pb2+ for Ba2÷ increases $T_c$ to a maximum of 490°C. The effect is due to the lower M-O bonding for Pb < Ba < Sr which offers less resistance to the motion of the Ti ions in their six fold oxygen coordination field. Effect of doping on the transition temperature is shown in the Figure 2.20.

The strain energy introduced by electro-strictive effects on cooling through and below the $T_C$ when some domains change their orientation in relation to others causes time dependence for the dielectric constant known as aging [7] The rate of change increases as the initial value of $k'$ increases. Both composition and heat treatment affect aging and $k'$. In a polycrystalline ceramic, domain reorientation is affected by grain size, impurities, and pores, which prevent domain movement due to stresses, imposed by surrounding grains.

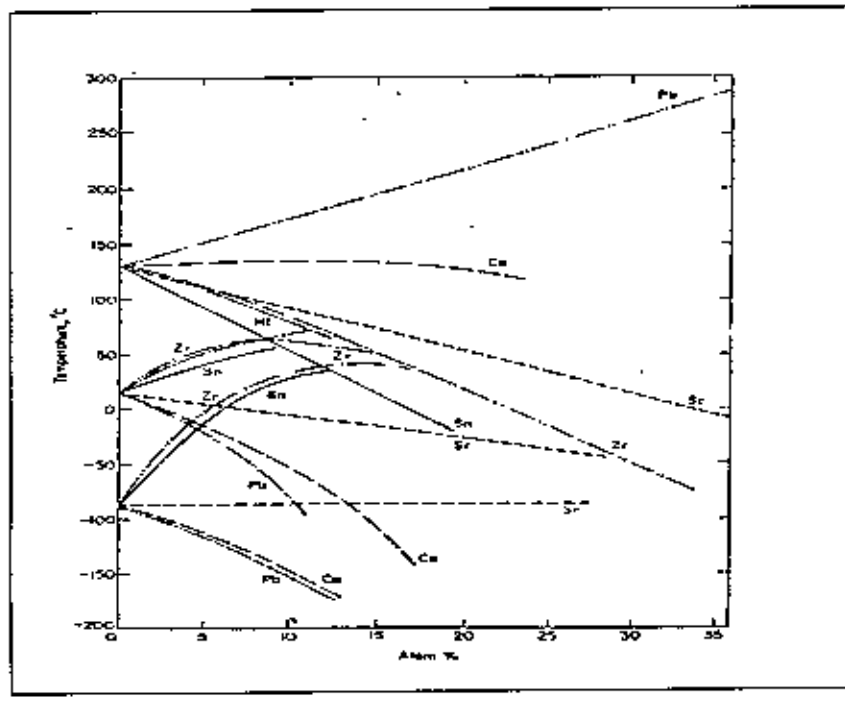


Figure 2.20: The effect of doping on the transition temperatures of $BaTiO_3$ ceramic

### 2.5.6 Observation of Microstructural features

Several investigators have described the ferroelectric or twin domains that can be seen in the single crystal of Barium titanate. For most practical application polycrystalline Barium Titanate ceramics are the most important than single crystal. R.C. DeVRIES et.al [38] described elaborately the micro structural features of polycrystalline barium titanate. Polising and etching are very important part of Microstructural observation. It is interesting however that the different methods of polishing and etching do not reveal all the microstructural features of the structure. It should be noted that the thermally etched sample reveal grain boundaries but no domains, where the chemical etched samples exhibit domain pattern and few or no grain boundaries. The reason is that at elevated temperatures where thermal etching (partial melting) takes place there are no domains since the material is in the non polar, cubic phase, whereas at room temperature where the chemical etching occurs, domain have spontaneously formed when the material is bought below its Curie point [7]. The investigators [37] fabricated the sample in such a condition that resulted in a ceramic of about 15% porosity containing large domain (70 to 100μ) in which ferroelectric domain structure could be readily distinguish. In the commercial based ceramics is usually considerably smaller than this..

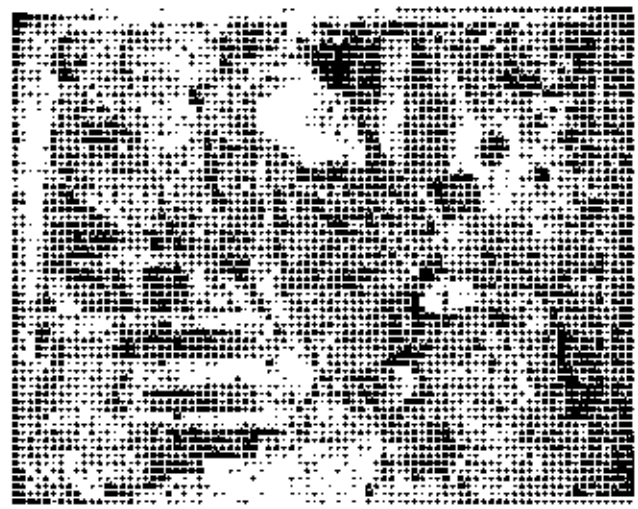

Figure 2.21: Polycrystalline $BaTiO_3$ after polishing and etching. Fine black and white strips are 90° domains; irregular line crossing 90° domains are 180° boundaries (×500).

The microstructure of the polycrystalline aggregates has two obvious features not shown in a single crystal microstructure (1) pores which arise from the ceramic having been made from powder and (2) grain boundaries. The finest black and white stripes (about 0.5 to 2μ wide) are 90° domain as shown in Figure 2.21. Another observation of domain in $BaTiO_3$ reported by Arlt et.al [35] shown in Figure 2.22.

(a) (b)

Figure 2.22: Ferroelectric domain pattern (a) $BaTiO_3$ sintered 2 hour at 1330°C, chemically etched. (b) $BaTiO_3$ hot pressed at 1080°C; sintered 60hour at 1250°C; ion beam etched.

They are revealed in this way because the differently oriented twin domains etch to give different surface roughness, which reflects light differently. In considering the thickness of the domain boundaries, it is helpful to recall that these domains are also crystallographic twins. A frequent characteristic structure is a straight line, which always extends completely through a grain with the structures on the either side of this trace changing direction in to it. Such a structure is very similar in appearance to the (111) annealing twins frequently observed in face centered cubic metals. An analysis of the trace directions in the grain shown. with the aid of a stereographic projection and making the assumption that all 90° domain boundaries are traces of {101} types planes, leads to the solution that the line referred to is indeed a trace of (111) plane, and thus supports the conclusion that these markings are interfaces

between (111) twins. One micro structural feature, which is very evident in the ceramic and absent in most single crystals is the arrangement of families of {101} twins in broad bands as shown in Figure 2.21. These bands (about 10μ wide) are define by the change in direction of the included fine twins (never more than two different directions within a band) and the interfaces are reasonably close to straight lines with the exception of a few orientations which have wedge like shape.

## 2.6 Dielectric Properties

Ceramics are mostly covalently bonded material hence electrically non-conductive or insulator. Importance of particular property depends on the application demand. For instance, dielectric strength is an important parameter for application of ceramic as insulators used in power transmission line, load bearing general insulators, in house hold appliances, etc. In this kind of applications where frequency do not exceed 1 kHz, the breakdown strength, measured in kV/cm, together with mechanical strength are prime important factors. The dielectric constant (k′) or loss factor (k′′) does not matter much. On the other hand, for capacitor and electronics applications just the opposite required. The values of k′ and k′′ are of prime importance. not only their room temperature values but also as function of temperature and frequency. These are intrinsic properties of material, especially of polycrystalline ceramic, can be modified by doping, micro structural variation, etc. $BaTiO_3$ is used extensively as a principal ingredient for multi layer ceramic capacitor (MLCC) manufactured commercially in billions. In the following sections basic concept and factors governing dielectric constant. dielectric loss is discussed. Materials are treated as polycrystalline and linear dielectric.

### 2.6.1 Dielectric constant

The overall Dielectric constant (k′) of an insulator material is given by the relation:

$$D = \varepsilon_0 E = \varepsilon_0 \kappa' E \qquad \text{--- --- } \{1\}$$

D represents the electric displacement, E the electric field in the dielectric, k′ the dielectric constant and $\varepsilon_o$ permittivity of vacuum. The electric displacement describes the extent to which the electric field has been altered by the presence of the dielectric material. The dielectric constant k′ is an intrinsic property of a material and a measure of the ability of the material to store electric charge relative to vacuum. It is measured indirectly from the capacitance of a capacitor in which the material is used as electrode separator or dielectric. From eq.{2} and the capacitive cell illustrated in Figure 2.23, the dielectric constant k′, total charge Q (coulombs) and capacitance C (farads) can be developed as follows:

$$\kappa' = \frac{D}{\varepsilon_o E} = \frac{Q/A}{\varepsilon_o V/d} \qquad \text{--- ---} \qquad \{2\}$$

Therefore, $$Q = \varepsilon_o \kappa' \frac{A}{d} V = CV \qquad \text{--- ---} \qquad \{3\}$$

Where, $$C = \varepsilon_o \kappa' \frac{A}{d} \qquad \text{--- ---} \qquad \{4\}$$

$$C_o = \varepsilon_o \frac{A}{d} \qquad \text{--- ---} \qquad \{5\}$$

and $$\kappa' = \frac{C}{C_o} = \frac{\varepsilon}{\varepsilon_o} \qquad \text{--- ---} \qquad \{6\}$$

Here, A represents the area of the capacitive cell, d its thickness (or gap between the electrodes), Co and C the respective capacitance of the capacitor with air and material, V the voltage across the cell and ε the material permittivity (F/m). Thus, k′ represents the ratio of the permittivity or charge storage capacity relative to air or vacuum as dielectric. It is clear from eq. {5} that for a given size capacitor and applied voltage the higher the k′ the higher the capacitance of the capacitor. This is the only variable left with the material scientist to increase the capacitance per unit volume value of capacitor for modern electronics applications.

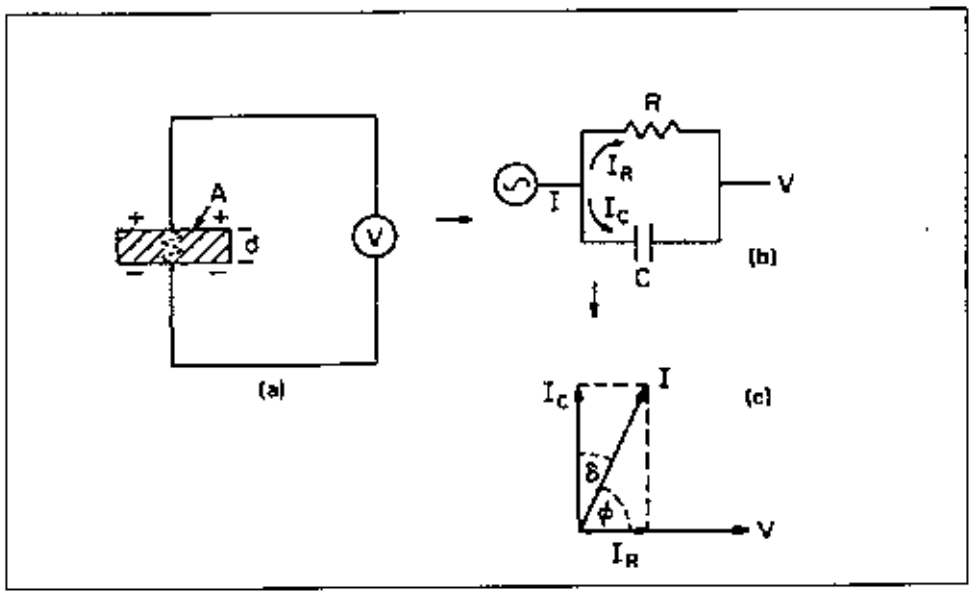


Figure 2.23: Equivalent circuit diagrams a) Capacitive cell, b) Charging and loss current c) loss tangent

### 2.6.2 Dielectric Loss

An ideal dielectric would allow no flow of electronic charge, only a displacement of charge via polarization. If a plate of such ideal material were placed between the capacitive cell shown in Figure 2.23(a) and a dc voltage was applied, the current through the circuit would decay exponentially to zero with time. But this would not be case if an alternating (sine wave) electric field were applied. In this case the eq. {4} may be written as:

$$Q = CV_o e^{i\omega t} \qquad \text{--- ---} \qquad \{8\}$$

Therefore,

$$I = \frac{dQ}{dt} = i\omega CV = i\omega C_o \varepsilon_o \kappa' V \qquad \text{---} \qquad \{9\}$$

here, $I$ represent the current flow on discharge of the capacitor in time t. For real dielectric material, the current $I$ has two vector components, real $I_R$ and imaginary $I_C$. The condition of a lossy (not so good) dielectric illustrated in Figure 2.23(c) as an equivalent circuit analogous of a resistance in parallel with the capacitor. The current $I_C$ represents a (watt less) capacitive current proportional to the charge stored in the

capacitor. It is frequency dependent and leads the voltage by 90°. On the other hand, the current $I_R$ is ac conduction current in phase with the voltage V, which represents the energy loss or power dissipated in the dielectric. The resultant angle between the current and the voltage is φ somewhat less than 90°. Ideal dielectric under this circumstance would not absorb any power and the capacitor would have zero loss. The current would lead the voltage exactly 90°. The current in real capacitor lags slightly behind what it would be in an ideal capacitor. The angle of lag is defined as δ and the amount of lag becomes tan δ or loss tangent.

Eq. {9} can be written for real and imaginary part,

$$I = I_C + I_R \qquad \text{--- ---} \qquad \{10\}$$

$$= i\omega C_o \varepsilon_o \kappa' V + \omega C_o \varepsilon_o \kappa'' V \qquad \text{---} \qquad \{11\}$$

By definition, $$\tan\delta = \left|\frac{I_R}{I_C}\right| = \frac{\kappa''}{\kappa'} \qquad \text{--- ---} \qquad \{12\}$$

Dielectric loss often attributed to ion migration, ion vibration & deformation and electronic polarization. Ion migration is particularly important and strongly affected by temperature and frequency. The losses due to ion migration increase at low frequency and the temperature increases.

### 2.6.3 Mechanism of Polarization

In general, there are five different mechanisms of polarization which can contribute to the dielectric response.

• Electronic polarization exists in all dielectrics or all solids up to optical frequencies ~ $10^{16}$Hz [Buchanan].It is based on the displacement of the negatively charged electron shell against the positively charged core. The electronic polarizability $\alpha_e$ is approximately proportional to the volume of the electron shell. Thus, in general $\alpha_e$ is temperature-independent, and large atoms have a large electronic polarizability.

• Ionic polarization is observed in ionic crystals and occurs up to the infrared region $10^{10}$-$10^{13}$Hz. It describes displacement of the positive and negative sublattices under an applied electric field.

• Orientation polarization is both frequency dependent and temperature dependent, since it represents dipole orientation and ion jump polarization.

• Space charge polarization could exist in dielectric materials which show spatial inhomogeneities of charge carrier densities. Space charge polarization effects are not only of importance in semiconductor field-effect devices, they also occur in ceramics with electrically conducting grains and insulating grain boundaries (so-called Maxwell-Wagner polarization).

• Domain wall polarization plays a decisive role in ferroelectric materials and contributes to the overall dielectric response. The motion of a domain wall that separates regions of different oriented polarization takes place by the fact that favored oriented domains with respect to the applied field tends to grow.

### 2.6.4 Materials Aspect

Intrinsic properties such as k′and k′′ can be explained in terms of chemical composition and structure. Material behavior in a dielectric field is a direct result of three vector quantities a) dielectric displacement D. b) electric field E, and c) polarization P:

$$D = \varepsilon_o \kappa' E = \varepsilon_o E + P \qquad \text{--- ---} \qquad \{13\}$$

Affect of dielectric in capacitor illustrated in Figure 2.24. The contribution of vacuum is the term $\varepsilon_o E$ and is the electrical polarization contribution of the dielectric.

Therefore, $$P = \varepsilon_o(\kappa'-1)E = \varepsilon_o \chi E \qquad \text{--- ---} \qquad \{14\}$$

It is clear from eq. {1} and {14} polarization is the key factor attributing to the dielectric property of material. For ceramic material, polarization can be further

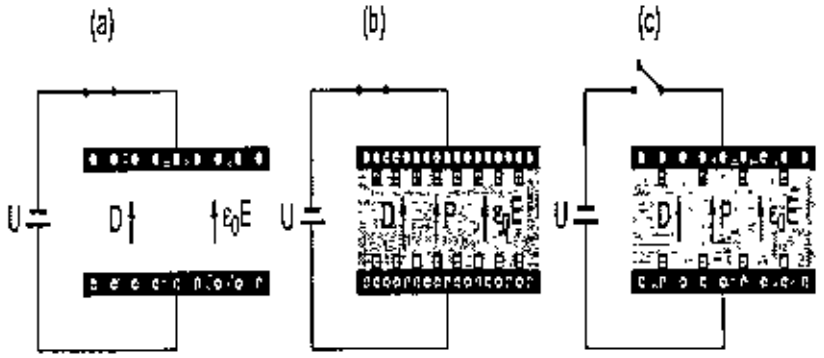


Figure 2.24: Parallel plate capacitor: a) without dielectric b) with dielectric E constant c) with dielectric with D constant.

described in terms of a volume charge density related to the concentration of dipole per unit volume N and the local field E' in the dielectric:

$$P = \alpha N E' \qquad \text{--- --- } \{15\}$$

and $$E' = \frac{\kappa' + 2}{3} E \qquad \text{--- --- } \{16\}$$

Where, α represents the polarizability, arising from different polarization mechanism of the material: $$\alpha = \alpha_e + \alpha_i + \alpha_o + \alpha_s \qquad \text{--- --- } \{17\}$$

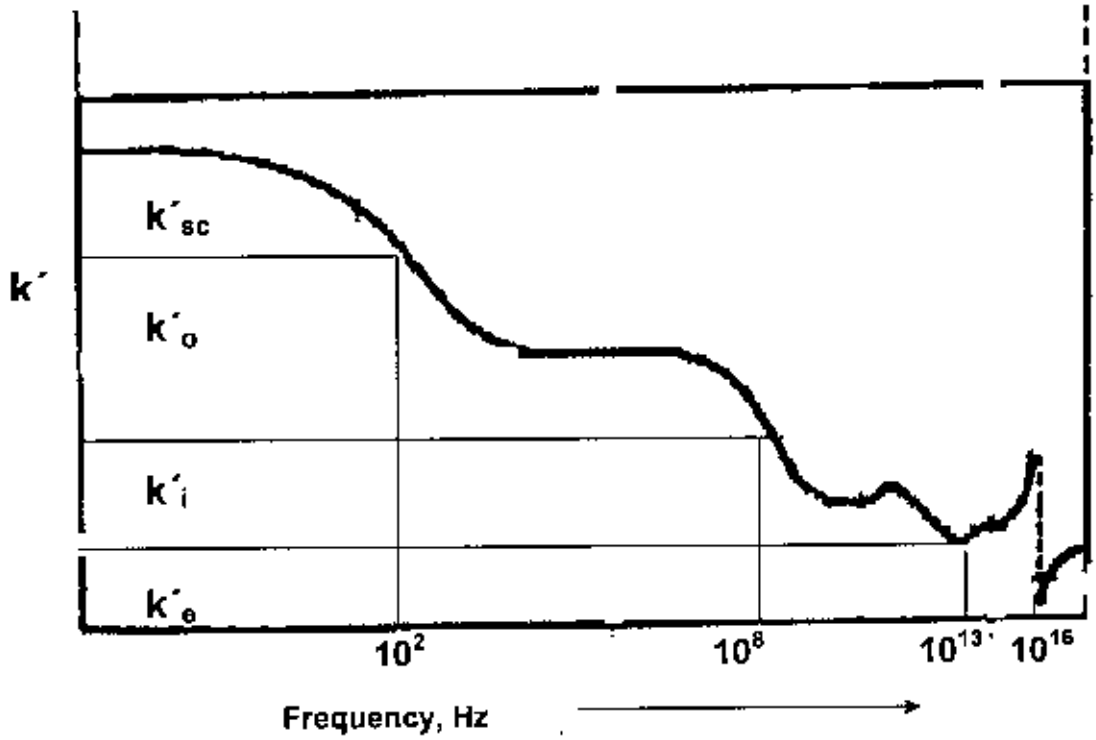


Figure 2.25: Frequency dispersion behavior of dielectric material as function of frequency.

representing the susceptibility associated with electronic, ionic, orientational and space charge polarization, respectively. For cubic structures and for induced dipoles (ionic and electronic polarization), the calculation reveals a relation between the atomic polarizability $\alpha$, and the macroscopic permittivity $\varepsilon = \varepsilon_0\varepsilon_r$ which is referred to the Clausius-Mossotti equation [14].

$$\varepsilon = \frac{\varepsilon_o + 2N\alpha}{\varepsilon_o - N\alpha} \qquad \text{--- ---} \qquad \{18\}$$

In Figure 2.25, the frequency dependence of k´ and associated polarization mechanism are illustrated. Affect of different polarization mechanism to the overall dielectric constant is related to the composition, frequency and temperature of the dielectric material. In general, $\alpha_e$ increases with ion concentration, ion size and ion polarizability, hence ions like $Ba^{2+}$, $Pb^{2+}$, $La^{3+}$ are used in order to achieve a higher dielectric constant and refractive index. In ionic solids, (such as MgO, $Al_2O_3$) $\alpha_i$ is

the predominant polarization mechanism, where ion size and separation have the significant effect. For ceramic materials with mobile ion, the orientational polarization can be a factor. This can be attributed to ion jump polarization $\alpha_j$, where

$$\alpha_o = \frac{p^2}{3kT} \quad \text{and} \quad \alpha_j = \frac{(ezd)^2}{3kT} \qquad \text{---} \qquad \{19\}$$

$p = ezd$. represents the dipole moment associated with the jump of an ion of charge $ez$ through a distance $d$. The relaxation time $\tau$ and the number of successful ion jumps per second are given in Arhenius form:

$$\tau = \tau_o e^{\mu/kT} \quad \text{and} \quad n = n_o e^{-\mu/kT} \qquad \text{---} \quad \text{---} \qquad \{20\}$$

Here, $\mu$ is the activation energy, $k$ Boltzman constant and T absolute temperature. In other word, for ceramic $\tau$ decreases with temperature, the relaxation move to higher temperature with increasing frequency and $n$ increases with the temperature. Hence it is normally observed k′ to increase with the temperature at a given frequency and at a given temperature k′ decreases as frequency increased

## 2.7 Science of Barium-Strontium Titanate Materials

### 2.7.1 Formation of Solid solution

Solid solution with an iso structural compound broadens the Curie pick. This was first perceived in $BaTiO_3$-$SrTiO_3$ solid solution (Figure 2.26).

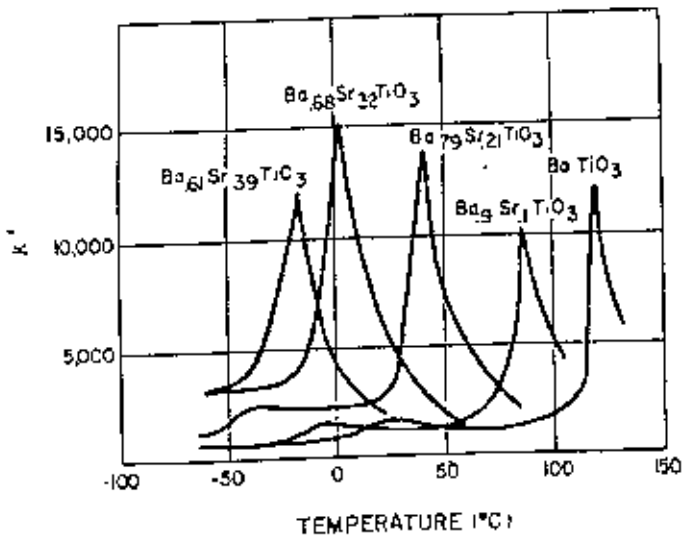


Figure 2.26: Effect of solid solution on dielectric constant versus temperature characteristic [7]

Ceramic based on $BaTiO_3$-$SrTiO_3$ solid solutions are frequently used to manufacture ceramic capacitors and thermistors. Mixed titanates are also considered for other applications such as delay lines, slow wave structures, optical modulators, etc. (Ba,Sr)$TiO_3$ solid solution ceramics are usually made by shaping and firing ceramic bodies from mixtures of $BaTiO_3$ and $SrTiO_3$ powders. D Kolar et.al [38] investigated in detail the Mechanism of (Ba,Sr)$TiO_3$ solid solution formation. During sintering, a solid solution is formed which results in a shift of the Curie temperature and changes in other properties. $BaTiO_3$ and $SrTiO_3$ crystallize in the same perovskite structure. Both compounds form a complete series of solid solutions [39]. The lattice parameter of the perovskite cell decreases monotonically from pure $BaTiO_3$ to pure $SrTiO_3$. The system shows a minimum in melting temperature at 1585°C and 2.5 mol% $SrTiO_3$. In view of the similarity of crystal structures and ionic sizes, (Ba,Sr)$TiO_3$ solid solutions were expected to form by the simple interdiffusion of Ba2+ and Sr+ ions in a relatively rigid Ti-O lattice. It was confirmed by the present authors using X-ray microprobe analysis that Ba2+ ions diffuse faster into the $SrTiO_3$ lattice than Sr2+ ions into the BaTiO3 lattice. This conclusion was based on the shift of $SrTiO_3$ X-ray diffraction lines.

On the Ba-rich side of the system $BaO$-$BaTiO_3$, only one compound, $Ba_2TiO_4$ (barium orthotitanate), with a high melting point (higher than 1860°C) is known. This compound forms an an extensive solid solution with $Sr_2TiO_4$ which end at a composition with a Ba2+ :Sr2+ ratio of about 1:3. On the SrO rich side of the system $SrO$-$SrTiO_3$, There exist several polytitanates such as $Sr_3Ti_2O_7$ and $Sr_4Ti_3O_{10}$ All of them may take some Ba in to solid solution.

(1) Mechanism of solid solution formation in the system $BaTiO_3$-$SrTiO_3$

X-analysis of sintered $BaTiO_3$ 1:1 powder mixture confirmed Namura's observation, i.e. a shift of $SrTiO_3$ reflections towards the higher d values at the same time, $BaTiO_3$ reflections intensity. However, some additional very faint diffraction lines also appeared after firing at T= 1300°C to 1400°C. After a 30-h anneal at 1400°C, $BaTiO_3$ was reduced to only a trace quantity and the position of (Ba.Sr)$TiO_3$ diffraction lines revealed the composition $Ba_{0.5}Sr_{0.5}TiO_3$, indicating .that homogenization was practically complete. The faint additional lines disappeared. The faint diffraction lines were found to correspond to $Ba_6Ti_{17}O_{40}$ and $(Ba,Sr)_2$ $TiO_4$ solid solutions, which are thus formed as intermediate compounds in (Ba,Sr)$TiO_3$ formation from mixtures of $BaTiO_3$ and $SrTiO_3$ powders. X-ray microprobe analysis of the neck formed during sintering of a polycrystalline $BaTiO_3$ sphere to a polished $SrTiO_3$ plate at 1300°C shows that Ba ion diffused along the surface of $SrTiO_3$) and into its bulk. To maintain the electrical neutrality, it is assumed that O2- ions accompany the diffusion of Ba2+ ions or that oxygen is transported via the vapor phase. Penetration of Sr ions into the $BaTiO_3$) sphere was much slower (Figure 2.27). It may be further observed that the neck area became rich in titanium. Quantitative analysis of this area revealed a BaO: $TiO_2$ ratio of approximately 1:2.5. The analysis of a hot-pressed (1200°C,5h) $BaTiO_3$-$SrTiO_3$ region. Next to the Ba poly titanate layer, which is formed on the $BaTiO_3$ side, there is a layer rich in Sr and containing some Ba. The Ti concentration level is slightly lower than in $SrTiO_3$ (Figure 2.28). Careful examination of this layer under an optical microscope showed a small amount of apparently solidified liquid phase.

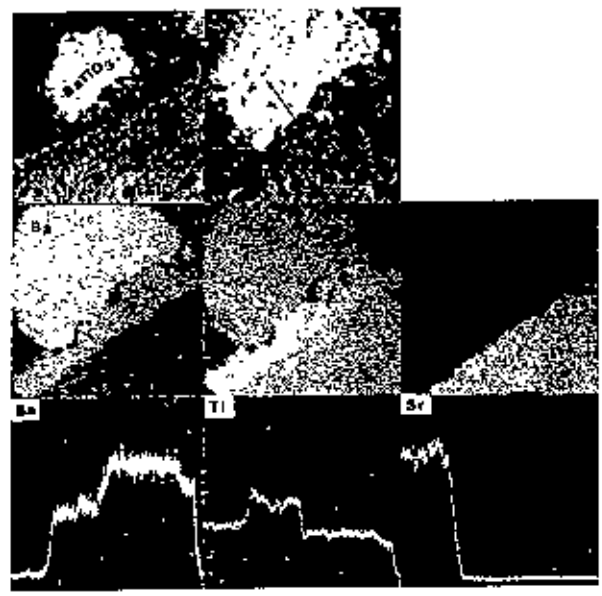


Figure 2.27: Electron beam microanalysis of $BaTiO_3$ sphere –$SrTiO_3$ plate neck area (1300, 12h)

The composition of the Ti-rich compound (poly titanate) formed on the $BaTiO_3$ side of the contact area and the alkaline earth-rich compound (orthotitanate) formed on the surface of $SrTiO_3$ grains and in the contact area depends on temperature and the phase relations in the ternary system BaO-SrO-$TiO_2$. On the basis of the experimental evidence and the phase equilibrium data discussed in the introduction, the first step of $(Ba,Sr)TiO_3$ formation is:

$$BaTiO_3 + SrTiO_3 \qquad BaTi_xO_{2x+1} + (Ba,Sr)_2\,TiO_3(ss) \qquad (1)$$

where ss=solid solution and $x=2.5$ in barium poly titanate depends on the temperature and the diffusion rate of $Ba^{2+}$ ions into $SrTiO_3$. On the basis of the composition indicated by X -ray microanalysis, the probable compounds are $Ba_6Ti_{17}O_{40}$ and $BaTi_2O_5$. However, on the basis of the faint diffraction lines which appeared in the powdered specimen after firing, it is concluded that the compound is $Ba_6Ti_{17}O_{40}$. Poly titanate forms a low-temperature (1320°C) eutectic liquid with $BaTiO_3$ The consequent $BaTiO_3$-$SrTiO_3$ solid solution formation above 1300°C is assisted by solution and precipitation. Accordingly, the mechanism of consequent $BaTiO_3$-$SrTiO_3$ solid solution formation may be described as:

$(BaTiO_3\text{-}BaTiO2x+1\ )(liq) + (Ba,Sr)_2\ TiO_4(ss\ )$-+$(Ba,Sr)Ti0_3(ss)$ .....

(2)

Dissolution of (Ba,Sr) $TiO_2$(ss) in a reactive ($BaTi0_3$-BaTix02x+1) eutectic creates a ternary system with a still lower eutectic temperature.

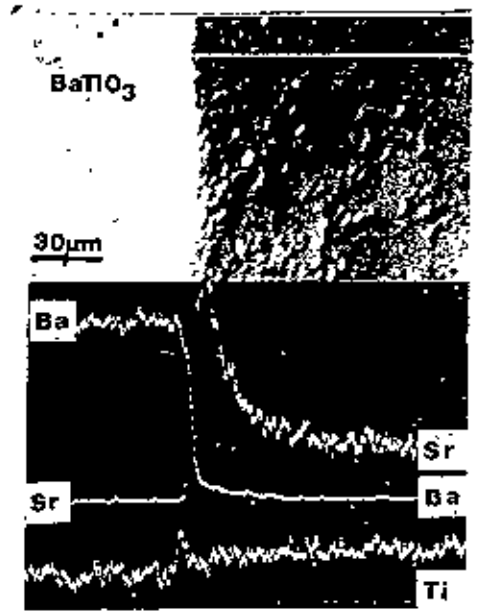


Figure 2.28: Electron beam microanalysis of hot pressed (1200.5h) $BaTiO_3$–$SrTiO_3$ diffusion couple.


Figure 2.29: Scanning electron micrograph of neck formed during sintering ($1300^0$C, 24 H) between polycrystalline $BaTiO_3$ and $SrTiO_3$ spheres)

Differential thermal analysis of mixtures of $Ba_6Ti_{17}O_{40}$ and $BaSrTiO_4$ (ss) showed

an endothermic effect, indicating melting at 1280°C. A further indication that (Ba, Sr)$TiO_3$(ss) crystallizes from the melt is given by Figure 2.29, which shows the neck grown between polycrystalline $BaTiO_3$ and $SrTiO_3$ spheres during sintering at 1300°C for 24 h. The polygonal large grains of the neck seem typical for melt-grown crystals. Similar large grains formed in the contacts between $BaTiO_3$ spheres and $SrTiO_3$ plates, as shown on Figure 2.30(A). On the contrary, such large grains never formed in contacts between the spheres and plates of the same chemical composition, as shown on Figure 2.30(B).

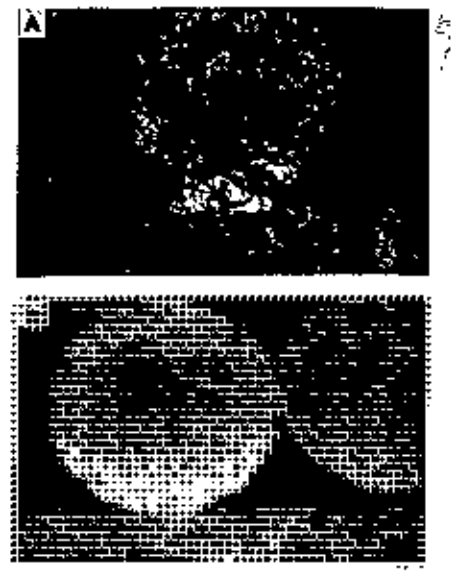


Figure 2.30: Micrograph of polished neck area between (A) $BaTiO_3$ ppheres/$SrTiO_3$plate and (B) $BaTiO_3$ sphere/$SrTiO_3$plate ($1300^0$C, 12h)

Formation of (Ba,Sr)$TiO_3$(ss) from non equilibrium compounds according to Eqs. (I) and (2) was analyzed in more detail by examining the microstructure of the diffusion couple prepared by pressing and sintering layers of $BaSrTiO_4$. and $BaTi_{17}O_{40}$ at 1300°:± 20°C for 4 h.

In Figure 2.31, the presence of a liquid phase is clearly visible between the grains of the reaction product. The presence of liquid is easily explained as a consequence of the formation of (Ba,Sr)$TiO_3$(ss), which in turn gives the eutectic liquid with $BaTi_{17}O_{40}$. The reactive eutectic dissolves both starting phase $Ba_6Ti_{17}O_{40}$ and $BaSrTiO_4$.

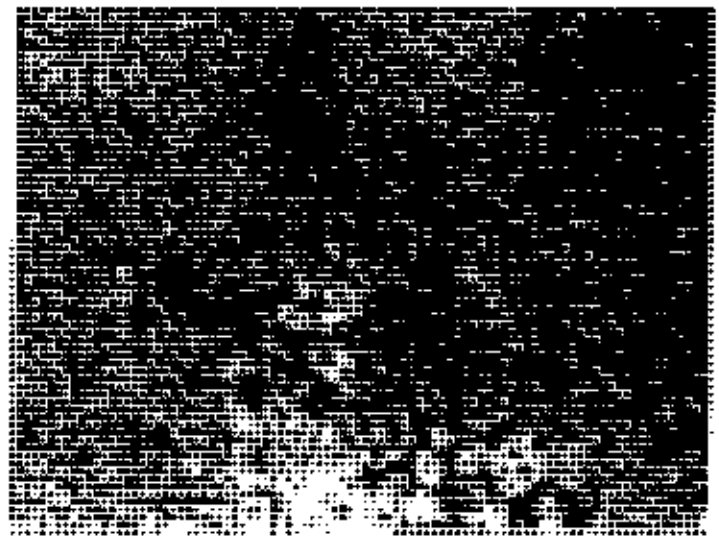

Figure 2.31: Microstructure of sintered $BaSrTiO_4$-$Ba_6Ti_{17}O_{40}$ sandwich (1300°C, 4 h) with liquid layer among grains of reaction product.

Equilibrium (Ba.Sr)$TiO_3$(ss) precipitates from the supersaturated solutions. X-ray analysis of the fired samples confirmed the presence of a perovskite (Ba,Sr)$TiO_3$ phase besides the phases initially present. The Ba/Sr ratio in (Ba,Sr)$TiO_3$(ss).depends on the local composition of the melt. Electron microprobe analysis revealed the composition of reaction product as $Ba_{0.75}Sr_{0.25}TiO_3$. The solidified liquid phase among (Ba,Sr)$TiO_3$ grains in Figure 2.31 was difficult to analyze accurately due to the limited size. The approximate composition was determined as BaO: SrO:$TiO_2$. = 1 :0. 1: 2.5, which is in accordance with the proposed explanation. Line analysis across the diffusion couple revealed, besides the facts already discussed, a thin layer rich in Sr between the (Ba,Sr)TiO. and (Ba,Sr)$TiO_3$(ss) layer. Analysis of the Sr-rich layer gave the composition BaO: SrO: $TiO_2$ 0.35: 1: 1, indicating the existence of $(Sr,Ba)_3Ti_2O_7$. solid solution. Transient formation of this phase during equilibrium in the system (Ba,Sr)$Ti0_4$-$Ba_6Ti_{17}O_{40}$ is possible on the basis of BaO-SrO-$TiO_2$ equilibrium dataS and compatible with composition analysis of other phases in the (Ba,Sr)$TiO_4$-$Ba6Ti_{17}O_{40}$ diffusion couple.

. The analysis described above may also explain the existence of the Sr-rich layer in the $BaTiO_3$-$SrTiO_3$ diffusion couple, as indicated in Figure 2.28.

(2) Consequences of the Mechanism of (Ba,Sr)$TiO_3$ Solid Solution Formation of Densification and Microstructure Development During Sintering of $BaTiO_3$-$SrTiO_3$ Mixtures.

It is shown in Figure 2.32 that 50: 50 mixtures sinter to much lower density (73% of theoretical) than mixtures with 5% $BaTiO_3$ or $SrTiO_3$, respectively. Comparison of Figs. 2.30(A) and 2.30(B) demonstrates the disturbance in neck geometry caused by differences in chemical composition.

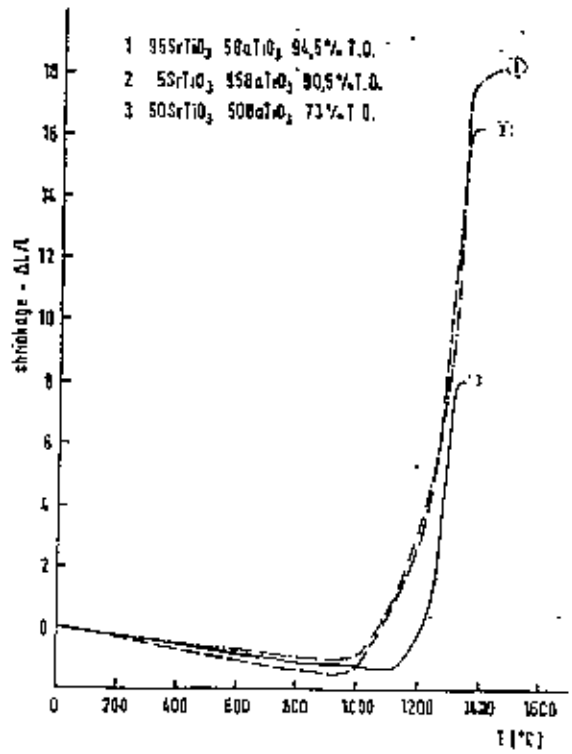


Figure 2.32: Shrinkage curves of $BaTiO_3$-$SrTiO_3$ powder mixtures during sintering at a rate of $5^0$C/min.

The neck formed between the $BaTiO_3$ sphere and the $SrTiO_3$ plate is uneven and resembles "mushroom" shapes. On the contrary, the neck between the $BaTiO_3$ sphere and the $BaTiO_3$ plate (Figure 2.30(B) is "normal," such as postulated in model sintering experiments. It is to be expected that disturbance in neck geometry in the early sintering stage and Kirkendall-type porosity brought about by preferential diffusion in $BaTiO_3$-$SrTiO_3$ powder mixtures opposes densification during firing of

green compacts. Hence, high density is not easily achieved in sintering heterogeneous $BaTiO_3$-$SrTiO_3$ mixtures, as confirmed by experiment. The microstructure of sintered $BaTiO_3$-$SrTiO_3$ powder mixtures is uneven. Figure 2.33 shows exaggerated grain growth in sintered $SrTiO_3$-5 wt% $BaTiO_3$ after 3 h and 1350°C.

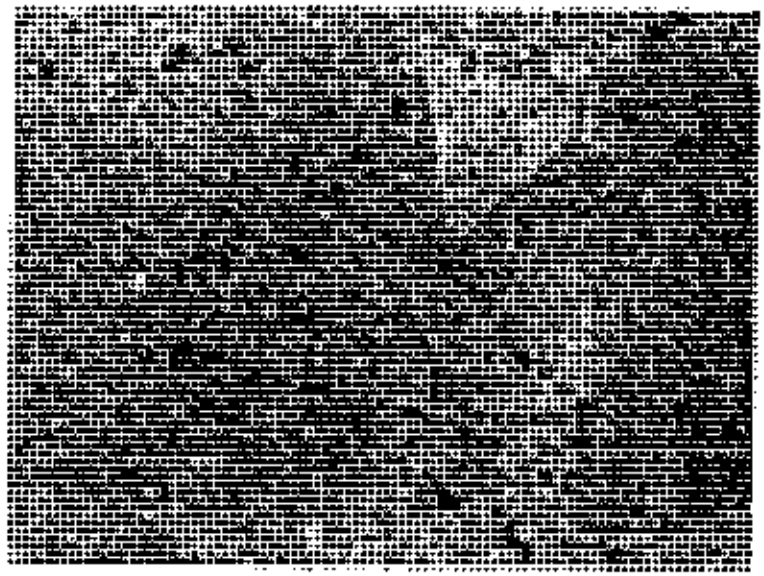

Figure 2.33: Microstructure of $SrTiO_3$-5 wt% $BaTiO_3$, mixture sintered for 3 h at 1350°C.

Microstructure of this is believed to result from the presence of minute amounts of liquid phase during sintering. The $SrTiO_3$-$BaTiO_3$ mixture was sintered well below the liquid phase formation temperature in this system. However, the present analysis of $BaTiO_3$-$SrTiO_3$ solid solution formation explained the necessary presence of a eutectic liquid below 1300°C. Therefore, the structure shown in Figure 2-30 represents further evidence for the proposed mechanism of $(Ba,Sr)TiO_3$ solid solution formation during sintering.

Electron beam microanalysis of the large triangular grain in Figure 2-33 confirmed that the grain represents $(Sr,Ba)TiO_3$ solid solution (Figure 2.34). The grain is richer in *Ba(ss)* than the surrounding $SrTiO_3$, which is in accordance with the mechanism of liquid phase-assisted solid solution formation.

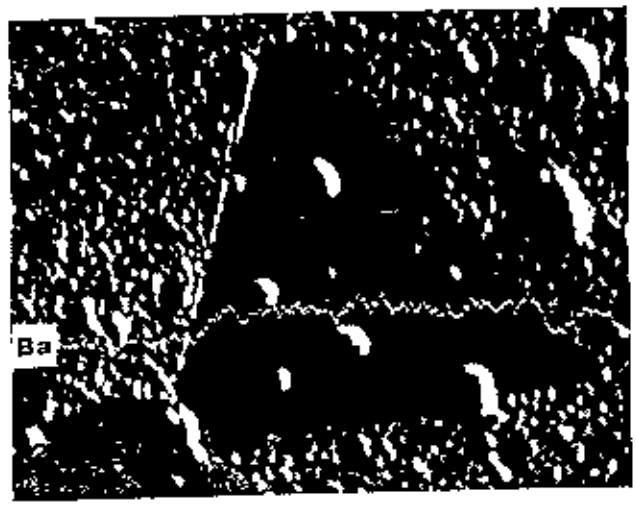


Figure 2.34: Electron beam microanalysis of large grain in $SrTiO_3$-5wt% $BaTiO_3$ sample sintered for 3 h at $1350^0$C. Ba tracing is shown.

Lemanov et.al [40] studied a dielectric (Figure 2.35) and ultrasonic study of phase transitions in $Sr_{1-x}$ $Ba_xTiO3$ with $x$ ranging from 0.0 to 1.0.

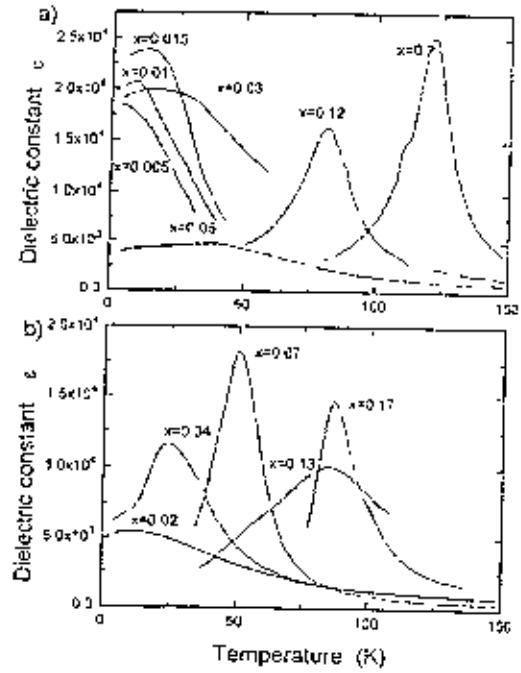


Figure 2.35: Temperature dependence of dielectric constant at frequency of 1 kHz in ceramics (a) and single crystal (b) (the number near the curve refer to $BaTiO_3$ concentration)

The full phase diagram is derived from dielectric measurements for ferroelectric phase transitions and from ultrasonic measurements for structural phase transition. The cubic-tetragonal ferroelectric phase transition, which is of the first order in pure, $BaTiO_3$ (x= 1.0) transforms to the second order phase transition at $x$ dose to 0.2. The transition temperature $T_c$ is a linear function of $x$ at x values from 0.2 10 1.0. For $x<0.2$ the transition temperature is proportional to $(x-x_c)^{1/2}$ ,where $x_c$=0.035. For $x<x_c$ a glasslike behavior is observed. The structural phase transition temperature $T_a$ goes down as compared to pure $SrTiO_3$ when x increases and levels off near x =0.05.

### 2.7.2 Dielectric properties

The microelectronic industry has been emphasizing on reduction in size of the device element such as transistor resist or and capacitor. However there are practical difficulties to these achievements including the lack of ultra fine precursors to manufacture these components, poor dissipation of the tremendous heat generated due to faster speeds, poor reliability etc. Thus, there is a need to pure materials of nanometer size, which have high energy density and better thermal conductivity. Hence, it has become extremely important to synthesize dielectric materials with higher density and higher surface area, more uniform size distribution and less brittleness at elevated temperatures. This necessitates investigation of nano-sized particles of well-known dielectric materials. Ganguli et.al. [41] carried out detail studies of the gel, precursor and they fine powder using powder X-ray diffraction (Figure 2.36) (PXRD), transmission electron microscopy (TEM) (Figure 2.37) and dielectric measurement (Figure 2.38). They discussed their result on the synthesis and the characterization of barium strontium titanate $Ba_{1-x}Sr_xTiO_3(0\leq x\leq 1)$ (BST), barium lead titanate $Ba_{1-x}Pb_xTiO_3(0\leq x\leq 1)$(BPT) and $PbZr_{1-x}Ti_xO_3$ by the polymeric citrate precursor method. Ganguli et.al [41] found that with the increase in strontium substitution the dielectric constant decrease. The value of dielectric constant varies from 510 for $BaTiO_3$ to 190 for $SrTiO_3$.The composition of x=0.5, namely $Ba_{0.5}Sr_{0.5}TiO_3$, the dielectric constant decreases in a regular fashion with increase in temperature from room temperature to $300^0$C.

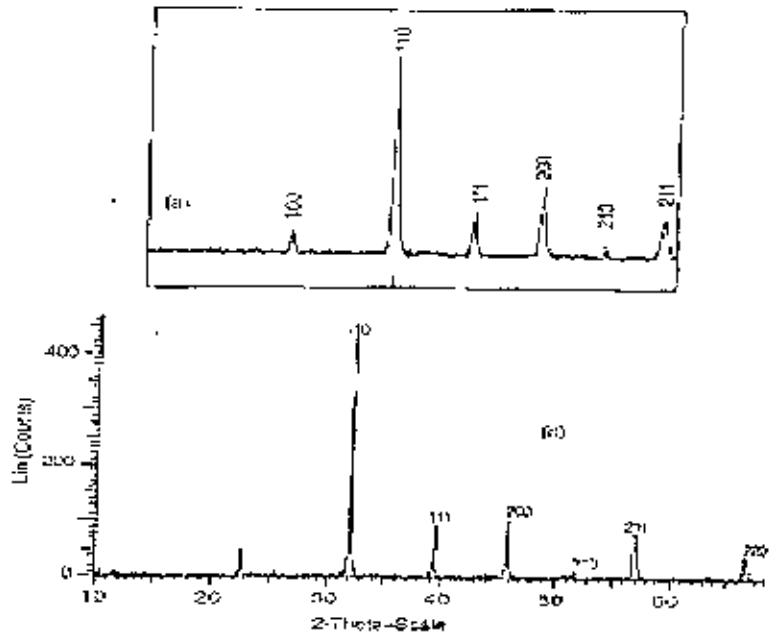


Figure 2.36: Powder X-ray diffraction pattern for the composition $Ba_{0.5}Sr_{0.5}TiO_3$ after being heated at (a) 500°C (b) 1100°C.

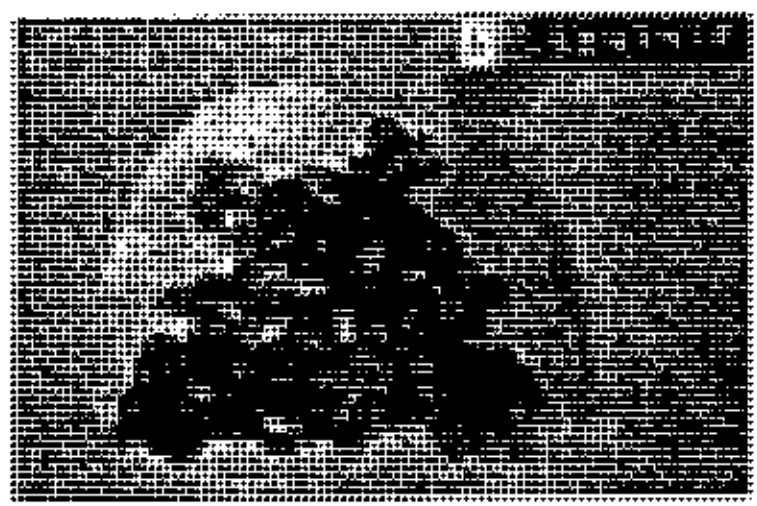

Figure 2.37: Transmission electron micrograph of $SrTiO_3$.

For $BaTiO_3$ the dielectric constant shows a minor change with a temperature 150°C beyond which it shows a decrease. The dielectric constant shows a very slight variation with a frequency till 300kHz.The dielectric loss also remains almost

constant till 200 kHz beyond which it follows a considerable rise with increasing frequency. For $Ba_{0.5}Sr_{0.5}TiO_3$, the dielectric constant shows negligible variation in the frequency range 100 to 500 kHz in the entire range of temperature studied.

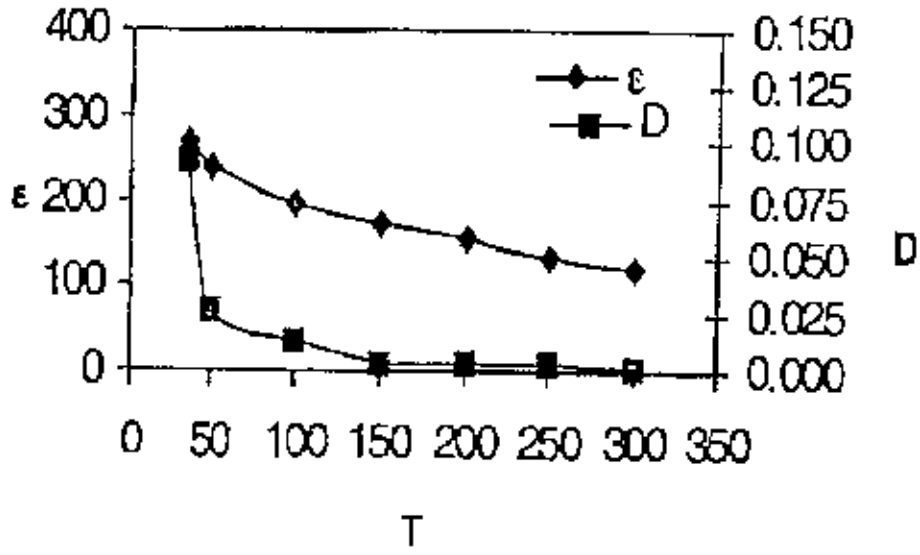


Figure 2.38: Variation of dielectric constant and dielectric loss with temperature for composition $Ba_{0.5}Sr_{0.5}TiO_3$ (sintered at 1100°C) at 100 kHz

Similar behaviors are seen for $BaTiO_3$ and $SrTiO_3$. Also no peak has been observed in the dielectric constant versus temperature curve in the temperature range of $50^0$C to$150^0$C for $BaTiO_3$ [41].

It has been pointed earlier that the cubic structure and absence of ferroelectricity for $BaTiO_3$ occurs for small grain size. As grain size decreases polarization decreases and thus ferroelectricity is lost.

Manfred [42] reported about the high dielectric constant materials which are relatively homogeneous barium titanate formulations that have grain more than 3 μm. Their high dielectric constant stems from the addition of substituents with the same valences. These shift the Curie point to the room temperature region. Sr2+ or Zr4+ is often used, making peak dielectric constant as high as 18000 available. Such materials can loose up to 50% of their dielectric constant at $50^0$C, but find general

application in computers and other low power electronic equipment requiring a limited temperature range.

In an article of Igor Lubomirsky et.al [43] showed that due to the graded composition the ceramic doesn't show a sharp change in dielectric constant near the relaxation frequency. Instead they observed gradual decrease in dielectric constant with frequency with the loss tangent remain practically unchanged (below 0.02 everywhere within the frequency range 0.0003-3 GHz). The investigators synthesized high purity $(Ba,Sr)TiO_3$ and $SrTiO_3$ powder with a average grain size 0.2μm by solgel method. $BaTiO_3$ and $SrTiO_3$ were thoroughly mixed in a molar ratio of 4:1. They were than pressed in to disks of 6.3mm diameter. Pure $BaTiO_3$ powder was also pressed in to disks by the same method. The length of time and temperature of sintering were adjusted in the range of 0.5-4h at 1300-1400°C so that different degree of $BaTiO_3/SrTiO_3$ interdiffusion could be obtained. The experimental finding by the above researcher were as follows

(i) The partial interdiffusion of $BaTiO_3$ and $SrTiO_3$ powder forms a ceramic material with intragrain concentration gradient.

(ii) Graded composition ceramic exhibit a very broad dielectric relaxation region with almost flat Cole-Cole diagram.

(iii) An unusually flat Cole-Cole diagram appears when an intra grain composition gradient is present. The diagram approaches arc-like shape when the intra grain composition gradient declines. The $\varepsilon''$-$\varepsilon'$ dependence follows the debye semicircle when the intragrain composition vanishes completely

Ferro electric thin film is currently being considered for variety of electronic application. Some of this application takes advantage of the voltage dependence of dielectric constant. This feature can be used to produce voltage tunable microwave devices such as resonator, filters and phase shifter. For this application it is desirable to produce thin films which have maximum tenability (change in capacitance under applied dc bias.) with minimum loss factor. Since the tenability of a ferroelectric is maximum near the Curie point. H.N Al Shareef et.al [44] found that high temperature post deposition annealing of both sputtered $SrTiO_3$ and Sol-

gel derived $BaTiO_3$ films markedly improve their tuning and loss factor characteristics.

## 2.8 Processing of Barium Titanate based ceramics

Property of the final product depends on the processing from raw material to the final sintering. Every step in the process chain has its own influence on the successive step and the final product. Many methods are used to syntheses $BaTiO_3$

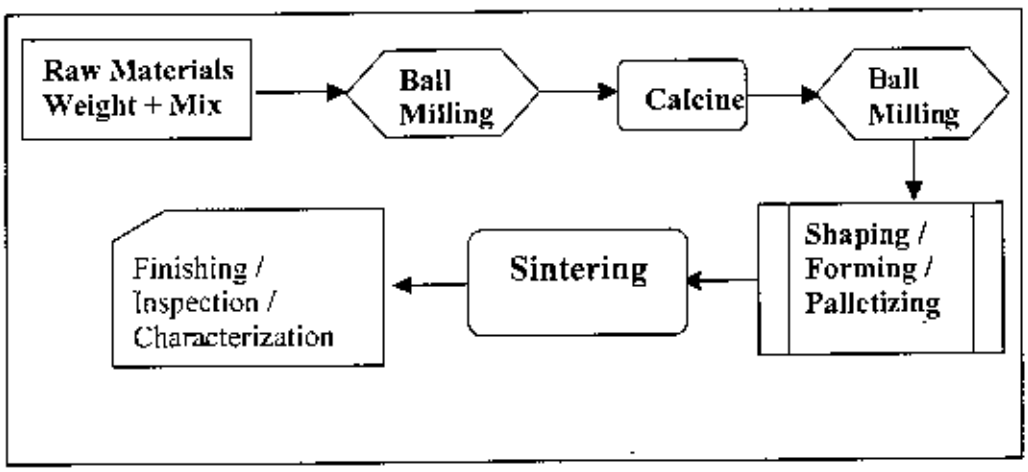


Figure 2.39: Flow chart of Mixed Oxide route

a) Conventional mixed oxide, b) sol-gel, c) chemical precipitation. d) hydrothermal and e) combustion reaction. Choice of route depends on the application. Nano-powders are prepared using the electrophorectic (EPD) method for making films. Even thin film was prepared from bulk single crystal using ion slicing method [45]. Ultra fine $BaTiO_3$ powder obtained by combustion reaction are used to make bulk material was described as relatively efficient method [46]. By far the first method is widely in the industrial application as well as at laboratories. However, powder obtained in other routes is superior in terms of homogeneity and fineness. This method also known as solid-state method was used to prepare sample in this study.

Processing route of this method illustrated in Figure 2.37. In the following sections important steps are discussed briefly with their influence on dielectric property of $BaTiO_3$ ceramics. The raw materials are $BaCO_3$, TiO2 and $SrCO_3$. Almost same

procedures are followed in the solid solution of $BaTiO_3$ and $SrTiO_3$. In the solid solution reaction process mixing is completed by ball milling. Solid state reaction is completed during the sintering process.

### 2.8.1 Ball Milling

The weighted powders are mixed mechanically by either ball milling or attrition milling. Milling is carried out to reduce the particle size of the powders to the sub-micron range for the solid phase reactions to occur by atomic diffusion. The schematic of a ball mill was illustrated in Figure 2.40.

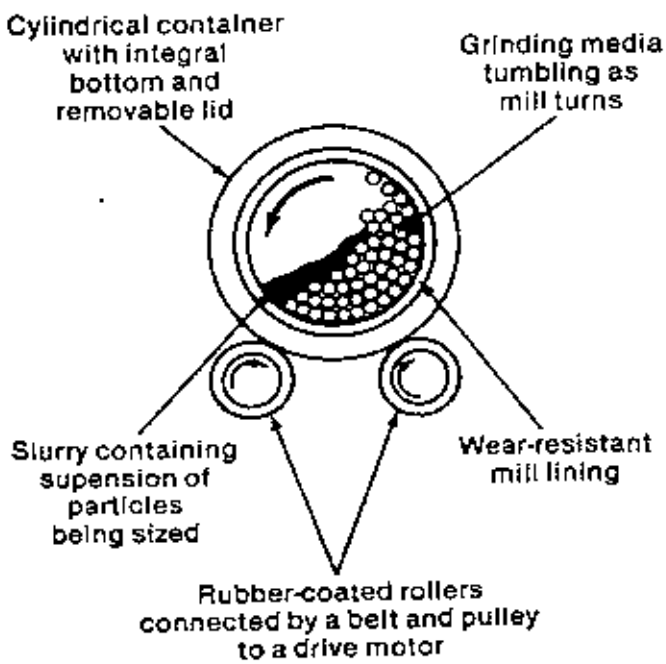


Figure 2.40: Schematic of a Ball Mill

Size and distribution of the ball is an import factor determining the product quality. Thumb rule is, smaller the size of balls finer the particle but it take longer time to break down big particles, hence use mix of different size balls. Motion of ball is controlled by the rotation speed of the mill. At higher speed balls cling at the inner side of the mill due to centrifugal force, too low speed would set the balls almost

stationary at the bottom. In both case insufficient friction between balls and particle would not break down the particle. Optimum speed is achieved when balls are in circular motion and roll back to bottom from about three quarter way to the top as shown in Figure 2.40. Media is another important consideration for two reasons. It must not react with the ball, the container, or the powder. Secondly, must avoid decrease of colloidal stability. For instance, milling of $BaTiO_3$ in water media set of tribochemical reaction. The reaction forms strongly alkaline $Ba(OH)_2$ which upset the pH balance, decreasing the colloidal stability of the suspension [47]. Either non-polar liquid such as acetone, alcohol, is used or polyelectrolyte stabilizers are used with water. Usually the same set up is used for milling the calcined powder. Finer particle can lower the sintering temperature and firing time significantly. Extent of ball milling is usually assessed by particle size analysis. If very fine initial raw materials is used in the case of solid solution then ball milling is used for mixing fine powder homogeneously.

### 2.8.2 Shaping and drying

After calcining, the lumps are ground by milling as described previously. The milled powder ready for further processing is commonly referred at 'green' body. The green bodies should have a certain minimum density before they can be sintered. Common practice is to achieve 60% of the theoretical density during shaping and pre-sintered state. The desired shape and a minimum green density can be provided by various techniques including powder compaction, slip casting, extrusion, doctor blading, dipping, etc. Hot pressing (both axial and isostatic), although expensive method is becoming popular for better quality ceramic material used in high-end application. The choice of the method depends on the type of powder used, particle size distribution, and state of agglomeration, desired shape, and thickness of the part. Hydraulic or mechanical presses are used to press powder in to desired shape at the pressure of ~100 to 300MPa. Owing to the nature of this process, only simple and symmetric shape can be prepared. No sintering aid or liquid is added to the powder for solid phase sintering route. Hence, strength of the green powder compact is achieved through addition of a suitable binder such as PVA, glycol phthalate, etc.

After shaping, the green bodies are heated very slowly to between 400-600°C in order to remove any binder present. Initial heating rate to burnout the binder is about ~1-2°C/min in order to allow the gases to come out slowly without forming cracks and blisters in the ceramic part. After the binder burnout is over, the samples are taken to a higher temperature for sintering to take place.

### 2.8.3 Sintering

In this step, powder so prepared finally transforms to usable ceramic body. In ceramic industries this step is also known as firing. $BaTiO_3$ matures in the 1350°C to 1450°C range [22]. This is the most important processing step in making of ceramic material. All properties of ceramic depends on the sintered body which is the direct result of the sintering parameter such sintering temperature, hold time, atmosphere, thermal profile, etc. There are many sintering methods used but this discussion would be limited to solid phase method.

Heat causes the powder particles to develop inter granular bonds by surface diffusion and other physical driving force. Mechanism of sintering and allied topics detailed elsewhere [48]. The typical green density of ceramic body at the start is about 60% of TD. Strength starts to develop gradually as more and more particles bond. At about ~80% to 90% density the pores are still open and the ceramic has a typical "chalky" appearance. The dielectric constant is usually low and the $T_c$ is not pronounced strongly. The pores of a ceramic are generally closed at ~95% of TD. Additional heat work causes grater densification as trapped gasses diffuse out along grain boundaries. At densities below 95% of TD the presence of open pores would cause the dielectric loss and undoubtedly inferior dielectric properties.

Setting of sintering temperature is not that straight forward. Low temperature sintering results in ceramic of poor density and formation of $Ba_2TiO_4$. On the other hand, too high temperature and long hold time may cause open structure with low density [22]. Also, at high temperature grain growth is accelerated resulting in low dielectric properties. Another harmful hexagonal phase of $BaTiO_3$ may form at the temperature higher than 1460°C. The sintering temperature and time should be optimum for proper densification to occur without abnormal grain growth. This is

best done by trail and error for particular material, volume and other process parameters.

Sintering temperature of nanopowder is much lower than that of the micron size particles. Ganguli et al [42] sintered the $BaTiO_3$. $Ba_xSr_{1-x}TiO_3$ and $Ba_xPb_{1-x}TiO_3$ $Pb_xZr_{1-x}TiO_3$ compacted sample in the temperature range of 900°C to 1100°C.

In MLC manufacturing industries, sintering high temperature such as 1300°C is not practicable, due to use of low melting point electrode material. Commercial formulation is aimed to lower temperature (~1100°C) sintering with the addition of many sintering and docents, for instance X7R, Z5U, etc.

## 2.9 Commercial formulations

As discussed in detail so far, the permittivity of ferroelectric perovskites shows marked changes with temperature, particularly close to the phase transition. From the device point of view a high dielectric permittivity with stable properties over a wide temperature range is required. There are various commercial specifications which have to be fulfilled {e.g. X7R: $C/C_{T=25°C} < \pm 0.15$ in a range between -55°C and 125°C}. By
substitution or doping it becomes possible to tailor the ferroelectric materials to different properties. In Figure 2.39 dielectric constant vs. temperature behavior of commercial formulation as illustrated.

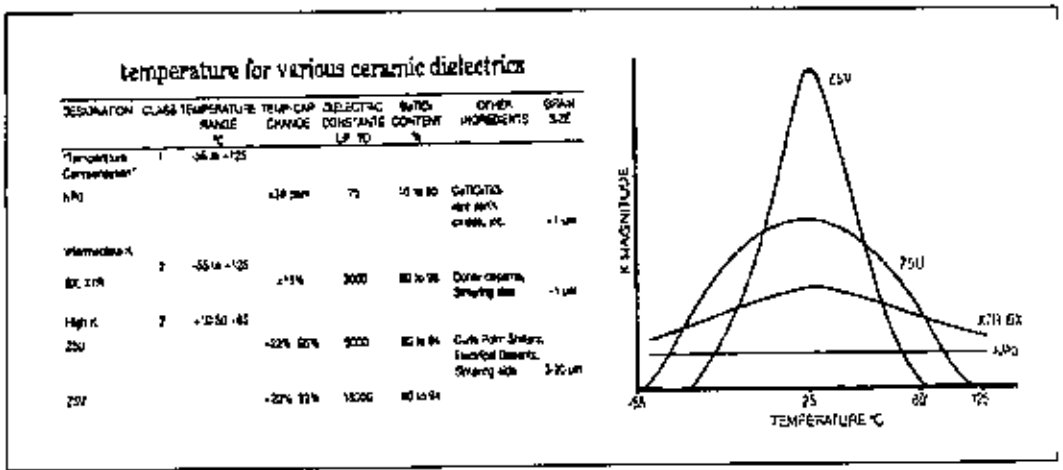


Figure 2.41: Commercial formulations and their k' vs T characteristics [42]

## 2.10 Relaxor Ferroelectric

These are special type of ferroelectric ceramic in their own right. Strictly, they are neither a derivative of $BaTiO_3$ nor a result of doping effect. The reason of their relevance in this study was to high light few aspects, which was observed in the $BaTiO_3$ samples of this study. Relaxor ferroelectrics are a class of lead based perovskite type compounds with the general formula $Pb(B_1,B_2)O_3$ where $B_1$ is a lower valency cation (like $Mg^{2+}$, $Zn^{2+}$, $Ni^{2+}$, $Fe^{3+}$) and $B_2$ is a higher valency cation (like

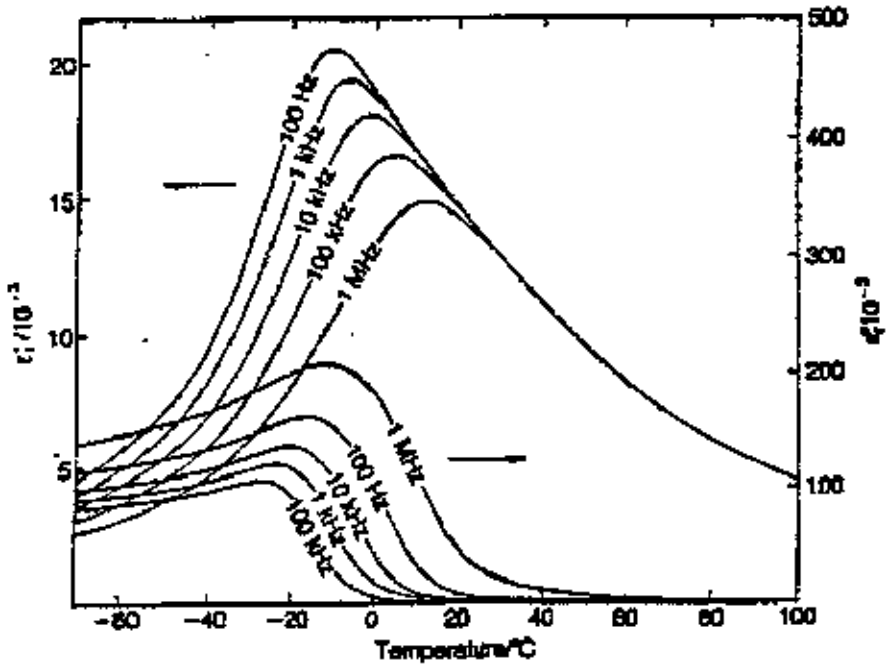


Figure 2.42: Variation with dielectric constant PMN with temperature[49]

$Nb^{5+}$, $Ta^{5+}$, $W^{5+}$). Pure lead magnesium niobate (PMN or $Pb(Mg_{1/3}Nb_{2/3})O_3$) is a representative of this class of materials with a Curie point at $-10^{o}C$. Relaxor ferroelectrics like PMN can be distinguished from normal ferroelectrics such as $BaTiO_3$ and PZT, by the presence of a broad diffused and dispersive phase transition on cooling below the Curie point. Figure 2.39 shows the variation in the dielectric properties with temperature for PMN ceramic. It shows a very high room

temperature dielectric constant and a low temperature dependence of dielectric constant. The diffused phase transitions in relaxor ferroelectrics are due to the compositional heterogeneity seen on a microscopic scale.

The relaxors also show a very strong frequency dependence of the dielectric constant. The Curie point shifts to higher temperatures with increasing frequency. The dielectric losses are highest just below the Curie point, $T_c$. Relaxors which have a second order phase transition, the remnant polarization, $P_r$, is not lost at the Curie point but gradually decreases to zero on increasing the temperature beyond $T_c$ [50].

## 2.11 Applications

Barium titanate can be regarded as 'role model' of electronic ceramic from application point of view. Its piezoelectric, pyroelectric and ferroelectric properties were successfully applied in many commercial applications. Vast majority of commercially important application are in polycrystalline bulk or film form. In the following sections, property wise applications are briefly discussed. Since dielectric properties of $BaTiO_3$ based ceramics were studied in this thesis, capacitor application especially MLCC emphasized.

### 2.11.1 Multilayer ceramic capacitors (MLCs)

Multilayer capacitors structure, as shown in Figure 2.41, enables the maximum capacitance available from a thin dielectric to be packed into the minimum space in a mechanically robust form [51].

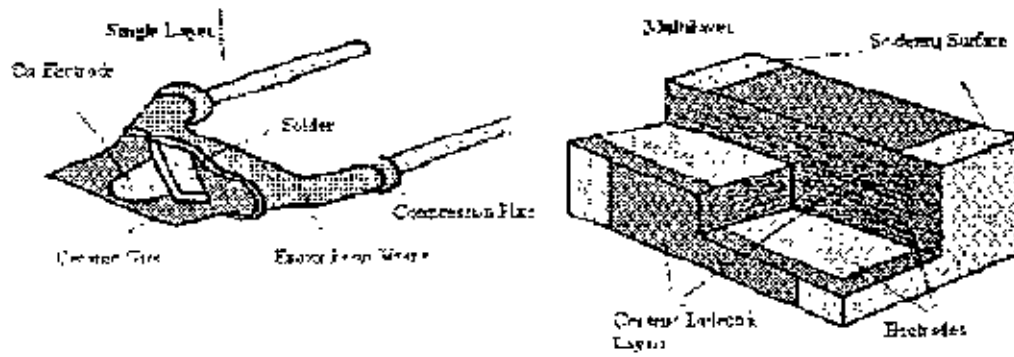


Figure 2.43: Schematic diagram of a multilayer ceramic capacitor construction [52]

Recently, multilayer ceramic capacitors (MLCs) with Ni electrodes have been increasingly produced to meet growing requirements for miniaturization, large capacitors and cost reduction [52]. Firing the dielectric materials in a low-oxygen partial pressure to prevent Ni from oxidizing is one method to miniaturize MLCs. Then addition of MgO and Li2O-SiO2-CaO glass components are effective not only in preventing the dielectric material from reducing and but also in controlling the temperature dependency of the dielectric constant. Because of appealing of heterogeneous microstructure, so-called core-shell structure that showed a typical ferroelectric domain pattern, microstructure controlling becomes extremely important to improve the reliability of MLCs within very thin dielectric layer thickness. It was suggested that the microstructures and the electrical properties were influenced by the change of substitution modes of Mg and rare-earth oxide in perovskite [53]. For larger ion (La, Sm)-doped samples larger amount of MgO is necessary to suppress the grain growth and form the core-shell structure than smaller one (Dy, Ho, Er)-doped samples. Also, the solubility of rare-earth ions in BaTiO3 has a linear relationship with the ionic radius. It is confirmed that the larger ion acting as donors mainly dissolves Ba site, while the smaller ion acting as both donors and acceptors dissolves both Ba- and Ti-sites. In recent years, MLCs with Ni internal electrodes composed of about 400 dielectric layers of below 2μm thickness have been developed [54].

### 2.11.2 Positive temperature coefficient (PTC) thermistors

Positive temperature coefficient (PTC) materials prepared from doped semiconducting barium titanate ceramics can be used in various kind of electronic circuitry as a switching device or as a constant temperature heater [55]. In addition, PTC thermistors applications such as the measurement/detection/control of temperature or parameters related to temperature are also important. These PTC materials are known to have a high temperature coefficient of resistance around Curie point and the ability of self-limiting, so they are as well come out to be a very useful device for sensor applications.

The positive temperature coefficient of resistance (PTCR) can be classified as critical temperature resistors because of the positive coefficient being associated with the ferroelectric Curie point. In fact, PTCR materials can be divided into four groups: polymer composites, ceramic composites, $V_2O_3$ compounds and $BaTiO_3$-based compounds ($BaSrTiO_3$, $BaPbTiO_3$...) [56]. For $BaTiO_3$-based compounds, $BaTiO_3$ is an insulator at room temperature. After doping with trivalent donors (e.g. La, Sb, Y) that substitute for the Ba+2 or with pentavalent donors (e.g. Sb, Nb, Ta) that substitute for Ti+4, $BaTiO_3$ becomes semiconductive that shows a PTCR effect as shown in Figure 2.42.

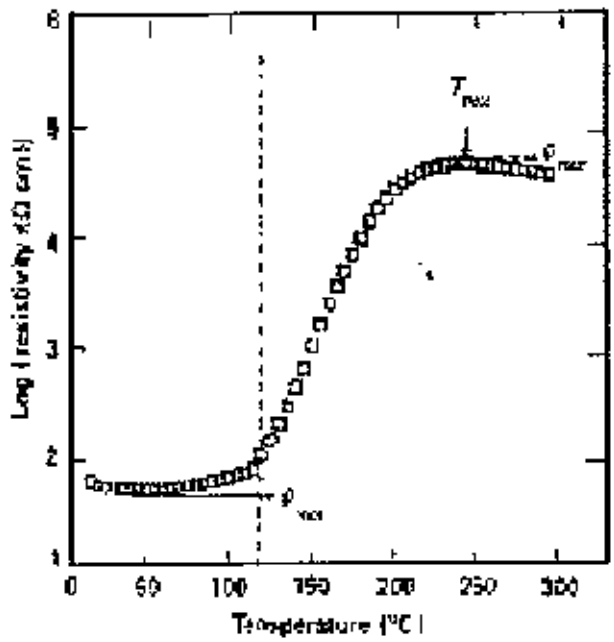


Figure 2.44: Typical resistivity behavior of a $BaTiO_3$ –type PTCR material [55].

### 2.11.3 Microwave device

Ferroelectric thin films are currently being considered for a variety of electronic application. Some of these applications take advantage of the voltage dependent of the dielectric constant. This feature can be used to produce voltage tunable microwave devices such as resonators, filters, and phase shifters. For these

applications, it is desirable to produce thin films, which have maximum tunability (change in capacitance under applied dc bias) with a minimum loss factor. Since the tunability of a ferroelectric material is maximized near its Curie point, different materials are preferred for different application temperatures. Thus material such as $SrTiO_3$ useful for tuning application at cryogenic temperature, whereas material such as $BaTiO_3$ and $Pb(Zr,Ti)O_3$ are more suitable for room temperature application.

## 2.12. Summery of literature Review

$BaTiO_3$ is a ferroelectric material offers a very high dielectric constant. It undergoes a series of phase transition as the temperature increases. The cubic to tetragonal transition temperature is known as Curie temperature. The grain size of the polycrystalline sample has much effect on the dielectric properties of $BaTiO_3$ –based on ceramics. In the small grain size materials, room temperature dielectric constant was observed to be high. On the other hand, at room temperature dielectric constant was found to be low for course grained materials. Internal stress models suggested that in the fine-grained material, it is energetically favorable to accommodate an elastic stress (this stress developed during the tetragonal-cubic phase transformation) than to relieve it by twin formation. So, a material having fine-grained microstructure is stressed untwined and offers high dielectric constant. To be stressed and untwined, the grain size should be as low as 1μm or less. But crystallite size should not be too small. In the ultra fine powder there exist little or no orientational relationship. Ferroelectric crystals possess regions with uniform polarization called ferroelectric domains. Within a domain, all the electric dipoles or the polar axis transformation occur and spontaneous polarization takes place. The electrical stray field energy caused by the non-compensated polarization charges is reduced by the formation of ferroelectric domains. Many of the properties of ferroelectric ceramics such as dielectric constant, aging, dielectric loss, etc., are related to the motion of domain boundaries. It is therefore of great importance to be able to examine and accurately interpret ferroelectric domain structures. The banded structure, butterfly twins are some of the interesting microstructural features observed in $BaTiO_3$. Solid solution with an iso structural compound broadens the Curie pick. Ceramic based on $BaTiO_3$-$SrTiO_3$ solid solutions are frequently used to

manufacture ceramic capacitors and thermistors. Mixed titanates are also considered for other applications such as delay lines, slow wave structures, optical modulators, etc. (Ba,Sr)$TiO_3$ solid solution ceramics are usually made by shaping and firing ceramic bodies from mixtures of $BaTiO_3$ and $SrTiO_3$ powders. D Kolar et.al [38] investigated in detail the Mechanism of (Ba,Sr)$TiO_3$ solid solution formation. Lemanov et.al [40] studied a dielectric and ultrasonic study of phase transitions in $Sr_{1-x}$ $Ba_xTiO3$ with $x$ ranging from 0.0 to 1.0. Ganguli et.al. [41] carried out detail studies of the gel, precursor and they fine powder using powder X-ray diffraction (PXRD), transmission electron microscopy (TEM) and dielectric measurement. They discussed their result on the synthesis and the characterization of barium strontium titanate $Ba_{1-x}Sr_xTiO_3(0\leq x\leq 1)$ (BST), barium lead titanate $Ba_{1-x}Pb_xTiO_3(0\leq x\leq 1)$(BPT) and $PbZr_{1-x}Ti_xO_3$ by the polymeric citrate precursor method. Many methods are used to syntheses $BaTiO_3$. a) Conventional mixed oxide, b) sol-gel. c) chemical precipitation, d) hydrothermal and e) combustion reaction. Choice of route depends on the application.

## 2.13 Scope of this study

The ferroelectric and dielectric properties of metal oxides with the perovskite structure are of utmost important in the electronic industry. Among these materials Barium titanate based dielectric materials are very important for their extensive as high dielectric constant capacitor, PTC resistor, ferroelectric memories and MLCC multilayer ceramic capacitor). Structure property relation of $BaTiO_3$ was studied extensively. A handsome number of microstructures have been analyzed so that structure property relation can be understood. Ferroelectric domain pattern is also revealed in the present study and some other interesting micro structural feature was studied.

Substitution of Strontium in place of Ba in $BaTiO_3$ through solid solutions $BaTiO_3$ and $SrTiO_3$ lowers the Cuire temperature. Effect of different level of substitution on sintered body density; dielectric constant and dielectric loss were measured. Results were explained in the light of finding of crystal structure through XRD investigation, DSC and microstructural study by SEM.

# 3. EXPERIMENTAL

## 3.1 Introduction and sample identification

Five different composition including pure Barium Titanate nano powder and Strontium titanate nano powder were used to prepare the disk shape sample. Table 3.1 shows the set name of the samples. Table 3.2 shows the process variables of the samples. Specifications of raw powders used are given in Appendix.

Table 3.1: Sample identification according to the substitutional doping level

| $BaTiO_3$ | $Ba_{0.90}Sr_{0.10}TiO_3$ | $Ba_{0.85}Sr_{0.15}TiO_3$ | $Ba_{0.80}Sr_{0.20}TiO_3$ | $SrTiO_3$ |
|---|---|---|---|---|
| **A** | **B** | **C** | **D** | **E** |

Table 3.2: Process variables in sample preparation

| SET | Composition | Sintering temp | Holding time (Hour) | Pressure (MPa) |
|---|---|---|---|---|
| A | $BaTiO_3$ | 1250°C | 2 | 150 |
| | $BaTiO_3$ | 1250°C | 3 | 130 |
| | $BaTiO_3$ | 1250°C | 3 | 150 |
| | $BaTiO_3$ | 1250°C | 5 | 150 |
| | $BaTiO_3$ | 1225°C | 4 | 130 |
| | $BaTiO_3$ | 1225°C | 4 | 150 |
| | $BaTiO_3$ | 1225°C | 6 | 150 |
| | $BaTiO_3$ | 1275°C | 3 | 150 |
| | $BaTiO_3$ | 1100°C | 3 | 150 |
| B | $Ba_{0.90}Sr_{0.10}TiO_3$ | 1250°C | 5 | 150 |
| | $Ba_{0.90}Sr_{0.10}TiO_3$ | 1100°C | 3 | 150 |
| C | $Ba_{0.85}Sr_{0.15}TiO_3$ | 1250°C | 5 | 150 |
| | $Ba_{0.85}Sr_{0.15}TiO_3$ | 1275°C | 3 | 150 |

| | | | | |
|---|---|---|---|---|
| | $Ba_{0.85}Sr_{0.15}TiO_3$ | 1100°C | 3 | 150 |
| D | $Ba_{0.8}Sr_{0.2}TiO_3$ | 1250°C | 5 | 150 |
| | $Ba_{0.8}Sr_{0.2}TiO_3$ | 1100°C | 3 | 150 |
| E | $SrTiO_3$ | 1200°C | 3 | 130 |
| | $SrTiO_3$ | 1250°C | 3 | 150 |
| | $SrTiO_3$ | 1250°C | 5 | 150 |

## 3.2 Sample Preparation

Pure $BaTiO_3$ and pure $SrTiO_3$ pellet were prepared from the nano powder of $BaTiO_3$ and $SrTiO_3$. PVA (poly vinyle alcohol) were used as a binder. Other compositions are made by mixing with the stoichiometric rario of $BaTiO_3$ and $SrTiO_3$. Samples were prepared by pressing the powder with 150 MPa pressure. Also there are few samples which are prepared by using 130 MPa pressure to see the effect of compaction pressure on dielectric properties.

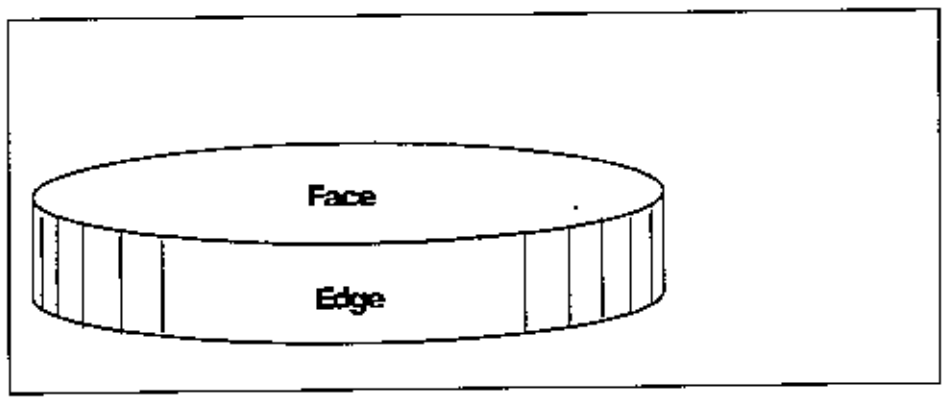


Figure 3.1: Disk shape sample.

### 3.2.1 Ball Milling

Milling pot was made of High Density Polyetheline (HDPE) and $Y_2O_3$-stabilised zirconia balls manufactured by Inframat (USA) were used for milling. Two different size of balls (dia=5mm and 3mm) and acetone (purity>99%Merk. Germany) were used as milling media as shown in Figure 3.2.

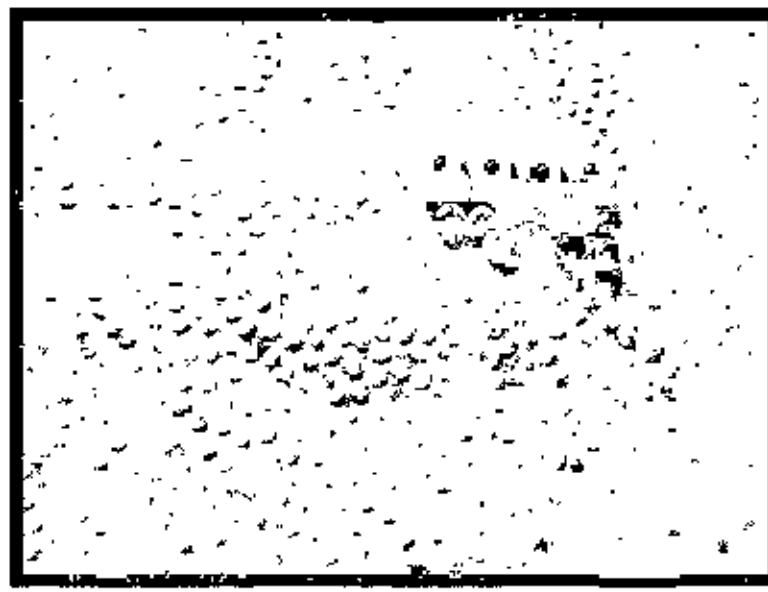

Figure 3.2: Two different size of Yitria Stabilized $ZrO_2$ ball.

Locally made motor driven ball mill was used for this purpose is shown in Figure 3.3. The speeds of the rotation of the pots were 140rpm. In this milling process, though mixing of the powders was the sole objective. Size reduction was not intended. Milling time was 15 hours for each cycle.

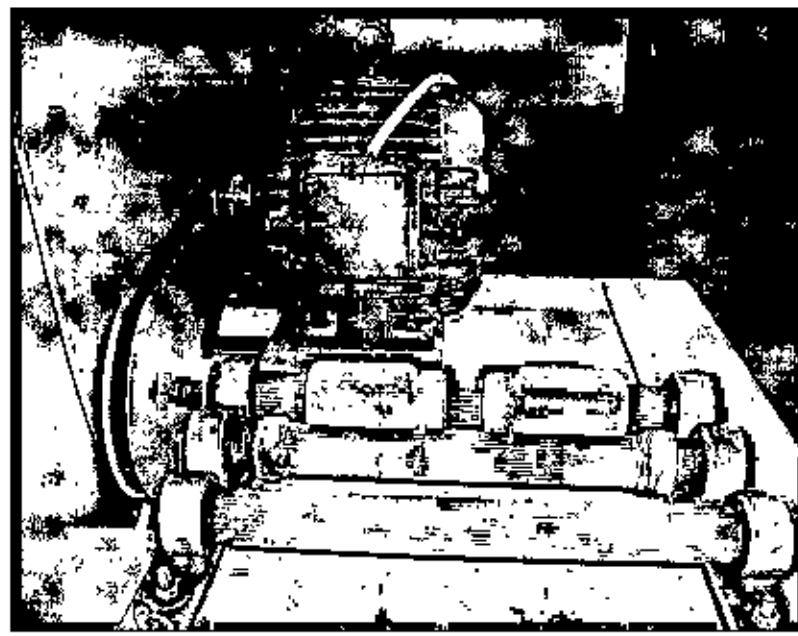

Figure 3.3: Locally made ball mill.

### 3.2.2 Compaction

Milled calcined powder was mixed with 2% Poly Vinyl Alcohol (PVA) and then dried in oven at 100°C before pressed into pallets. Samples were pressed into pallets using pressure of ~150 MPa for all the samples using hydraulic press. At highest-pressure level, holding time was five minutes. Green sample was not made too much thick to avoid pressure gradient in the sample. The Green pallets were dried in oven, and then lightly ground with grit #500 and #800 SiC paper to a flat and smooth surface, removing surface irregularities.

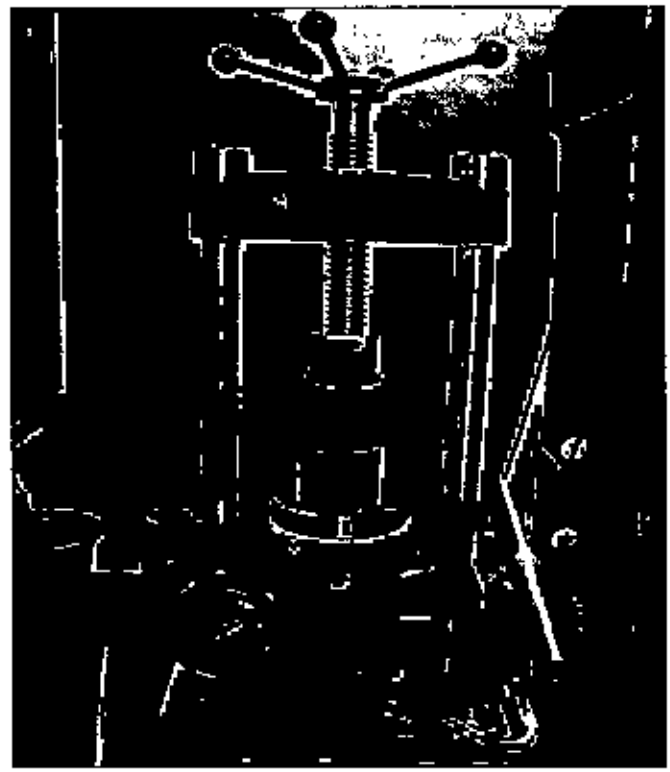

Figure 3.4: Hydraulic press used to make pellet shaped samples.

### 3.2.3 Sintering

Muffle furnace( Thermolyne High Temperature Furnace , Model 46200) was used to sinter the pallets in air atmosphere shown in Figure 3.4.

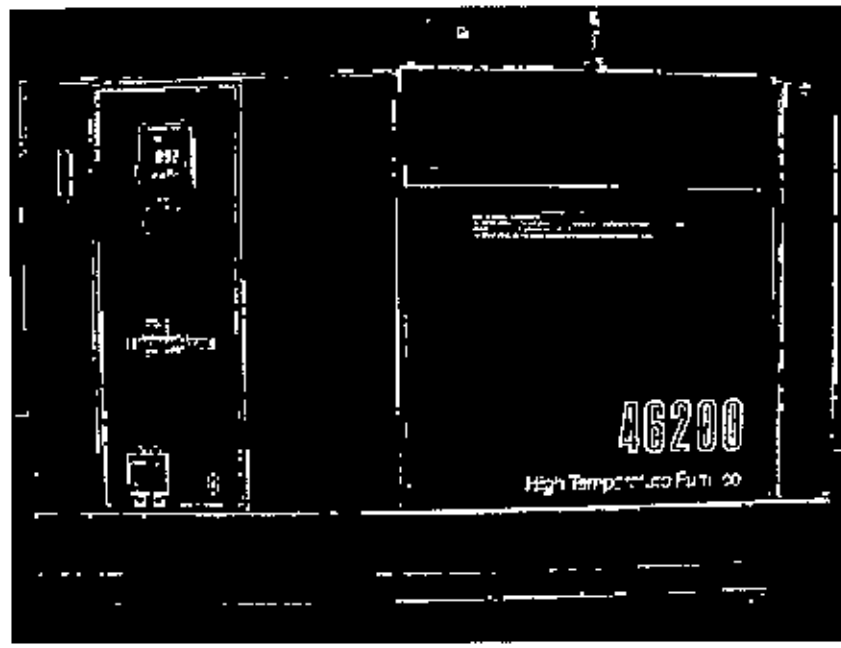


Figure 3.5: High temperature furnace used for firing the ceramics samples.

General thermal profile of sintering is given in Figure 3.5. Pallets were placed in the furnace on alumina plate. Binder burnout temperature was 600°C, while the hold time was 1 hours. Heating and cooling rate used in the sintering process is 2°C/min. Sintering temperature and hold time was varied to observe their effect on the density and dielectric properties .The final shape of the pellet is shown in Figure 3.1

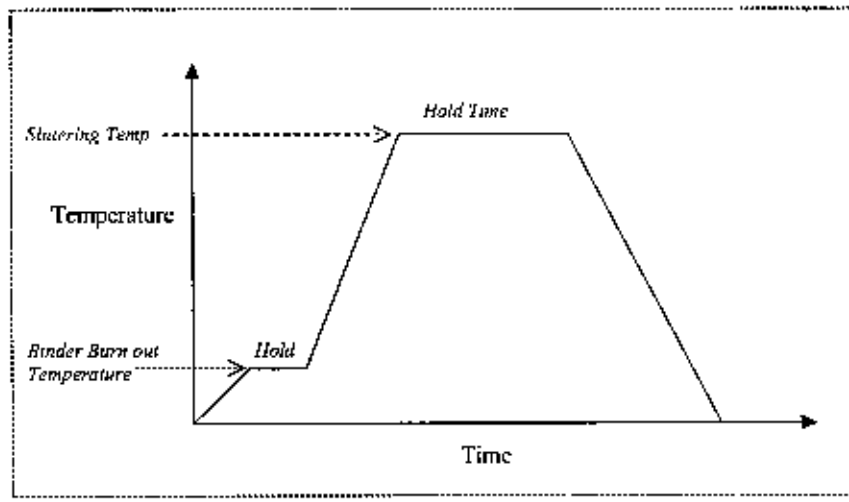


Figure 3.6: Sintering thermal profile in general

### 3.2.4 Post Sintering

After sintering, the samples were ground successively with SiC paper of grit #500, #800 and #1200 to obtain a flat and polished surface. Dimension of the pallets were taken for dielectric constant and density calculation. Prior to electrical measurements samples were cleaned and dried then, painted with high purity conductive silver paint on the both faces of the sample. Edges were ground and cleaned with acetone.

## 3.3 Property Measurement

### 3.3.1 Density

Dimension of the sample were taken using micrometer with digital read out and weighed using analytical weighing scale. Density of the sample was calculated from these data. Density results were presented as percentage of theoretical density (TD). TD of doped samples was calculated based on volume fraction of respective phase as shown in Table 3.3.

Table3.3: Theoretical Density of $BaTiO_3$ and doped sample in $g/cm^3$ [7, 50]

| $BaTiO_3$ | $Ba_{0.90}Sr_{0.10}TiO_3$ | $Ba_{0.85}Sr_{0.15}TiO_3$ | $Ba_{0.80}Sr_{0.20}TiO_3$ | $SrTiO_3$ |
|---|---|---|---|---|
| 6.017 gm/cc | 5.934604gm/cc | 5.88395gm/cc | 5.8396gm/cc | 5.13gm/cc |

### 3.3.2 Dielectric constant and loss

Samples were polished carefully so that both the surfaces of the sample were parallel. Silver paste was painted and dried in the oven at 500°C for 1 hour so that all the absorbed moisture is evaporated. Samples were connected with impedance analyzer and the dielectric properties were measured. Temperature dependence of dielectric properties of $BaTiO_3$ based samples were also measured with the help of a very highly insulated tube furnace. Very slow heating rate was maintained during the experiment, especially in the temperature range where the tetragonal-cubic phase transformation was expected to occur.

Electrical properties of the sample were measured using a Hewlett-Packard 4194A impedance and phase gain analyzer at AECD as shown in Figure 3.7. Dielectric

constant k' was calculated from the capacitance value obtained from the analyzer according to the equation below:

$$\kappa' = \frac{C_p d}{\varepsilon_0 A} \qquad \text{--- ---} \qquad \{20\}$$

A tube-furnace type oven was used for heating the sample at AECD.

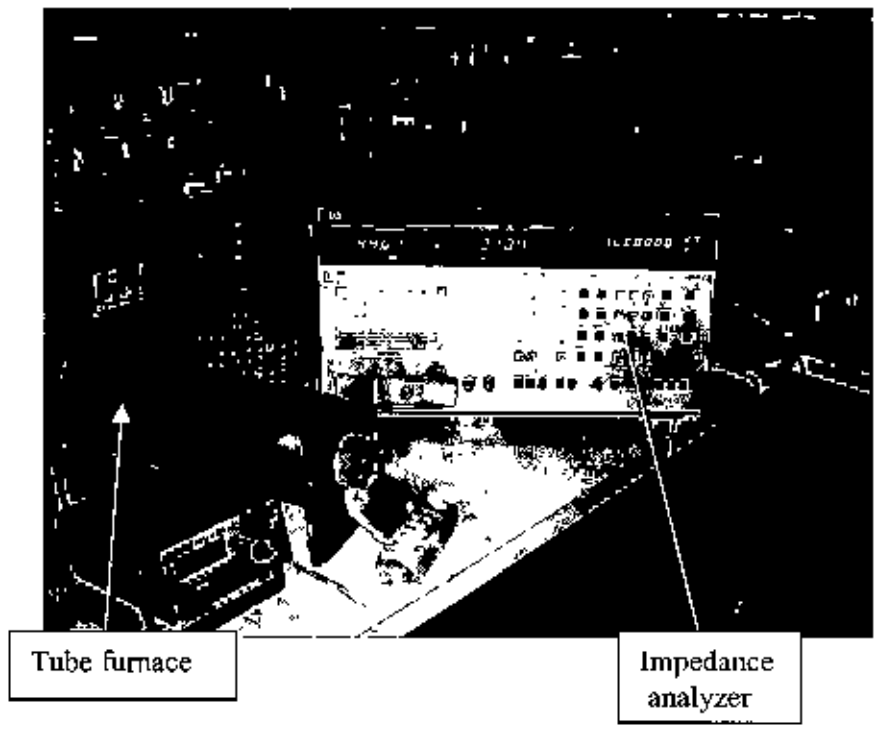


Figure 3.7: Impedance Analyzer ( LCR meter) Model- Hewlett-Packard 4194A

## 3.4 Microstructure study

Many of the properties of ferroelectric ceramics such as dielectric constant, aging, dielectric loss are related to the microstructural features such as grain size, and their shapes, grain boundary, porosity, ferroelectric domains etc. It is therefore of great importance to be able to examine these features and accurately interpret these microstructural effect on the overall properties of materials [32, 34]. Microstructure of the polycrystalline $BaTiO_3$ sample was revealed through a series of polishing and etching (thermal /chemical). After every polishing step the samples were cleaned with acetone and dried.

### 3.4.1 Optical Microscopy

Optical microscopy is a very useful tool for examining whether the surface is sufficiently polished to observe the microstructure. Before going for Scanning electron microscopy the thermal or chemical etched or chemical etched sample was, finally check in the optical microscope.

### 3.4.2 Scanning Electron Microscopy

Sintered samples (disc shaped) were polished using conventional ceramographic technique. At first, sintered samples were polished using 500, 800, and 1200 grit paper & then wheel polishing with Alumina abrasive paste with 1600 grit was carried out. Polished samples were thermally etched at 100°C to 50°C below the sintering temperature with 5 minutes holding time. The microstructure of samples was examined using Scanning Electron Microscope (SEM). Samples were gold sputtered (few nanometer thick) prior to SEM examination. A Phillips XF 30 was used with acceleration voltage of 10kV. If a sample is well, polished then thermal etching reveals the grain size distribution of the sample. As we know that grain boundary, is a high free energy area and we can attack the grain boundary using heat so that the boundary is prominent and grains are isolated from one grain another grain. To observe ferroelectric domain, twin and other microstructural features, chemical etching was used. The composition of the chemical etching reagent was reported elsewhere [57]. A sample having microstructure of small grains with less porosity is the ultimate goal of all commercial polycrystalline ceramics. This microstructure was revealed by thermal etching.

## 3.5 Differential Scanning Calorimetriy (DSC)

DSC was carried out using DSCQ10 of MME department to observe phase transition at Curie temperature. For $BaTiO_3$ the heating rate was 5°C/min because the phase transition is observed at relatively high temperature that is at temperature around 130°C. For the $Ba_{1-x}Sr_xTiO_3$, sample-heating rate was 2°C/min because the tetragonal-cubic phase transition was expected to occur at low temperature depending upon the Sr concentration in $BaTiO_3$.

## 3.6 X-ray Diffraction (XRD)

Crystal structure of $BaTiO_3$ and the doped samples were examined by XRD in powder form. At Material Science Division (MSD) of AECD *Phillips X'Pert Pro* were used following identical scanning parameter given in Table 3.4 in all XRD experiment:

Table 3.4: XRD operational conditions

| | | |
|---|---|---|
| X Ray Source: | **Cu Kα** | for calculation |
| Tube Voltage: | **40 kV** | Cu Kα **λ = 1.54056 Å** |
| Current: | **20 mA** | Used |
| Degree range: | **20° to 80°** | Speed: **0.02° per sec** |

# 4. RESULTS AND DISCUSSION

## 4.1 Sintered density measurement

Green samples (pellets) were prepared by pressing the powder using the hydraulic press. Three parameters are very important for pellet preparation. These are pressure, holding time and thickness of the sample. These three parameters must be optimized to get good green samples, which will, later on experience extensive heat treatment during sintering process. In the thick sample, there is a possibility of density gradient, which is not expected. In the same way proper pressure and holding time is also very important. Pressure must be applied slowly so that pressure can be distributed uniformly throughout the sample. In our case at the highest load holding time is 5 minutes.

Densities were measured taking the mass and volume of the sintered sample and presented as percentage of theoretical density (TD) calculated based on the data given in Table 3.3. First of all, the samples were polished smoothly with the SiC grit paper. Thickness of the sample was measured from different locations of the plane to ensure the accuracy of volume calculation. Table 4.1 shows the density of all the samples sintered at different temperatures, holding time and pressure.

Three different categories of samples were used in the present experiment; Pure Barium Titanate (BT), Barium Strontium Titanate (BST) and Strontium titanate (ST). In the figure, samples were identified in the following way. Three examples were given below;

Example 1: Suppose a sample name is BT-1225/4H

Here BT means $BaTiO_3$ (Barium Titanate).

1225/4H means this sample is sintered at 1225°C for 4 hours.

Example 2: A sample name is BST10-1250/5H.

Here BST10 means $Ba_9Sr_1TiO_3$

1250/5H means this sample was sintered at 1250°C for 5hours.

Example 3: A sample name is ST-1250/5H.

It means that Strontium titanate was sintered at 1250°C for 5hours.

Table 4.1: Densities of the Samples.

| Sample Composition | Sintering Temperature (°C) | Holding time (Hour) | Pressure (MPa) | Thickness (mm) | Bulk density (%) |
|---|---|---|---|---|---|
| $BaTiO_3$ | 1225 | 4 | 130 | 3.32 | 94.24 |
| | 1225 | 4 | 150 | 2.47 | 95.07 |
| | 1225 | 6 | 150 | 2.34 | 95.53 |
| | 1250 | 2 | 150 | - | - |
| | 1250 | 3 | 130 | 3.13 | 95.60 |
| | 1250 | 3 | 150 | 2.30 | 95.34 |
| | 1250 | 5 | 150 | 2.34 | 95.39 |
| | 1275 | 3 | 150 | 4.557 | 91.69 |
| | 1100 | 3 | 150 | 2.87 | 77.45 |
| $Ba_{.9}Sr_{.1}TiO_3$ | 1250 | 5 | 150 | 1.59 | 94.63 |
| $Ba_{.9}Sr_{.1}TiO_3$ | 1100 | 3 | 150 | 2.01 | 71.98 |
| $Ba_{.85}Sr_{.15}TiO_3$ | 1250 | 5 | 150 | 1.67 | 94.96 |
| $Ba_{.85}Sr_{.15}TiO_3$ | 1275 | 3 | 150 | 2.88 | 89.64 |
| $Ba_{.85}Sr_{.15}TiO_3$ | 1100 | 3 | 150 | 1.91 | 78.43 |
| $Ba_{.8}Sr_{.2}TiO_3$ | 1250 | 5 | 150 | 1.67 | 95.63 |
| $Ba_{.8}Sr_{.2}TiO_3$ | 1100 | 3 | 150 | 2.34 | 77.05 |
| $SrTiO_3$ | 1200 | 3 | 150 | 4.02 | 90.49 |
| | 1250 | 3 | 150 | 2.73 | 93.69 |
| | 1250 | 5 | 150 | 2.71 | 93.47 |

Table 4.1 shows that the $BaTiO_3$ sample sintered at 1100°C for 3 hours have the lowest bulk density, which is 77% of the theoretical density. Figure 4.1 shows that, this $BaTiO_3$ is not sintered properly. The bulk densities of two other $BaTiO_3$ samples prepared with 130Mpa pressure but sintered at 1225°C for 4 hours and 1250°C for 3 hours were found to be 94% and 95 % respectively. This analysis confirms that the cause of low density is the low sintering temperature. The bulk

density of the $BaTiO_3$ sintered at 1275°C for 3 hours was found to be 91% of the theoretical density. This is quite interesting because, the bulk densities of other $BaTiO_3$ samples are found to be 95%. The reason of the low density can be attributed to the much higher thickness of the sample, which caused density gradient. It means some part of the sample has higher sintered density and some part of the sample has lower sintered density. Therefore, the average density is lower.

The cause of lower bulk density of the sample $Ba_9Sr_1TiO_3$, $Ba_{85}Sr_{15}TiO_3$ and $Ba_8Sr_2TiO_3$ sintered 1100°C for 3 hours, may be also due to the very low sintering temperature.

$SrTiO_3$ sintered at 1200°C for 3 hours has bulk density 90%, which is little lower compared to the other two samples. The reason can be explained in two fold. The sample thickness is too high and $SrTiO_3$ is a very hard particle. Therefore, pressure may not be adequate for the $SrTiO_3$ to have a good sintered sample for which bulk density might be 95%. Another reason may be, the melting point of $SrTiO_3$ is over 2000°C. So the sample thickness must be lower and applied pressure must be higher than 150 MPa. In such a case, higher sintering temperature is used for obtaining high bulk density.

## 4.2 Microstructural Study

### 4.2.1 Microstructure of Barium Titanate

One thing that is very important to remember before going to the details of the microstrucrural study is the size of the barium titanate particles that were used to fabricate the studied samples. If the starting material were micron size then the sintering temperature would be high. In the present study, nano size particles (≈100nm) were used. Low sintering temperature of the nanoparticles was reported elsewhere [41]. Figure 4.1 shows the microstructure of $BaTiO_3$ sintered at 1100°C for 3 hours. The importance of this poorly sintered sample will be described later on. Figure 4.2 shows the microstructure of the $BaTiO_3$ sintered at 1250°C for 2 hours. This is a good microstructure as far as the grain size is concerned. From the microstructure, it is seen that there are some pores on the surface. Some small grains

have no pores and in large grains, there are few pores inside the grain. So it is expected that if the holding time is increased at the same temperature of 1250°C the porosity may be decreased. The SEM Micrograph of the $BaTiO_3$ sample sintered at 1250°C for 3 hours is shown in the Figure 4.3. The SEM picture showed the mark improvement in the microstructure. When the holding time is increased from 3 hours to 5 hours, no significant change was observed in the sample. Grain growth continues but the pores were not removed in the sample. The microstructures shown in Figure 4.2 and Figure 4.3 were prepared using pressure 150MPa. To see the effect of compaction pressure on the microstructure of the sample another sample was prepared at 130MPa and sintered at 1250°C for 3hours. The microstructure of this sample is shown in Figure 4.4.

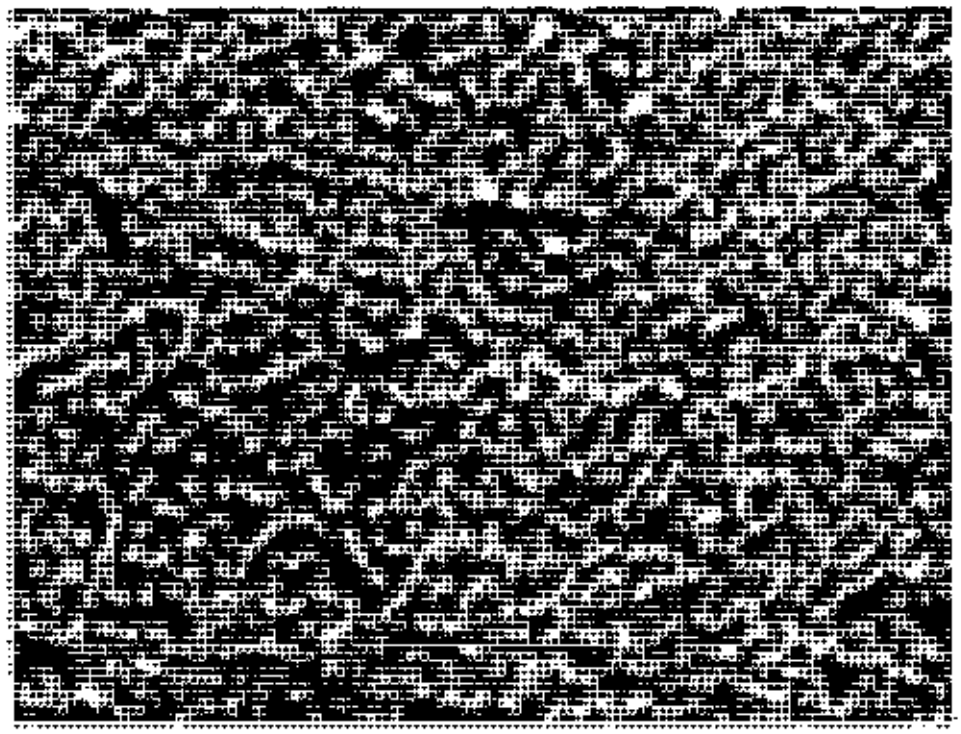

Figure 4.1: SEM micrograph of $BaTiO_3$ sintered at 1100°C for 3 hours (150MPa)

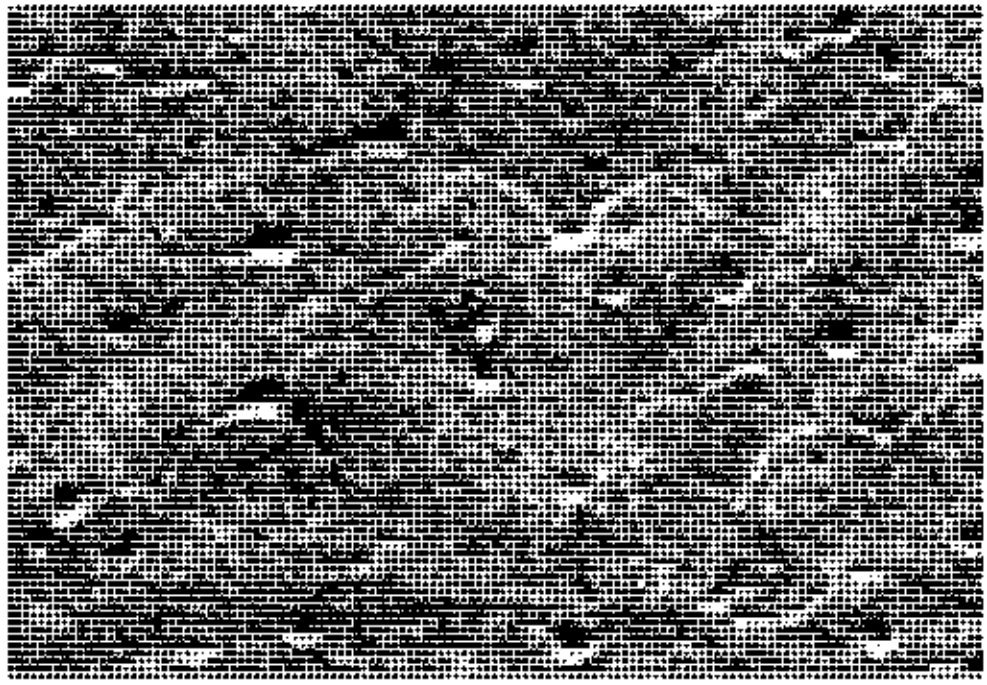

Figure 4.2: SEM Micrograph of $BaTiO_3$ sample at temperature 1250°C for 2 hours (150MPa).

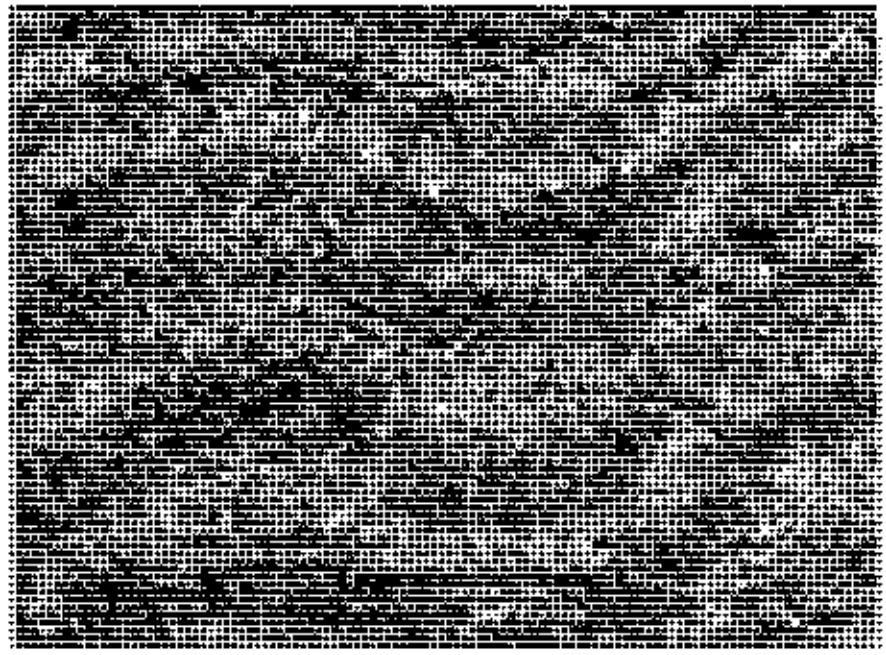

Figure 4.3: SEM Micrograph of $BaTiO_3$ sintered at 1250°C for 3 hours (150MPa)

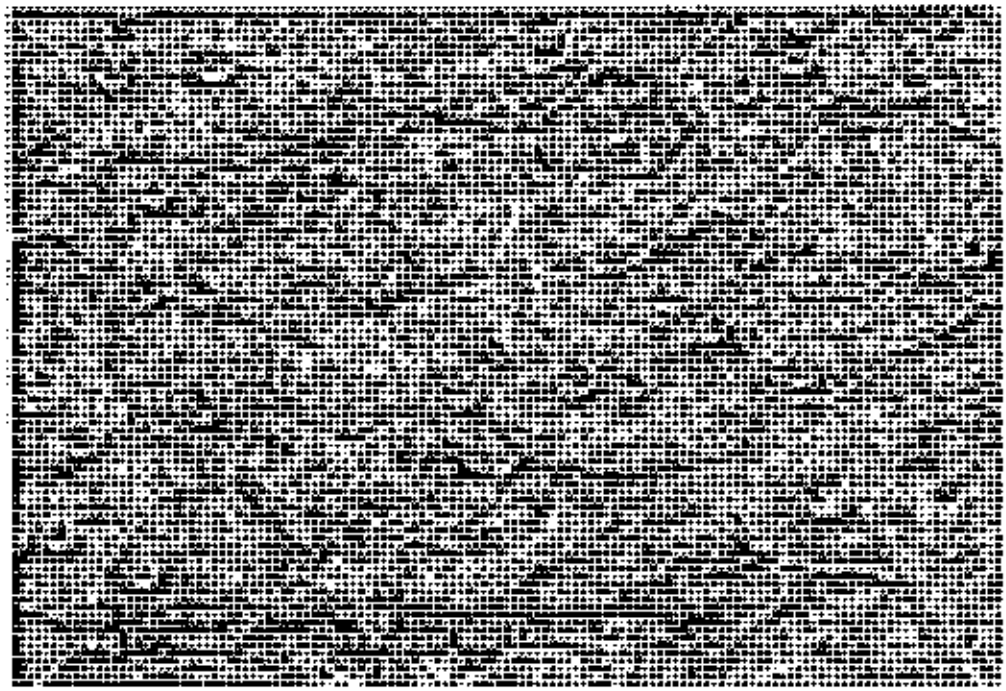

Figure 4.4: SEM Micrograph of $BaTiO_3$ sintered at 1250°C for 3 hours (130MPa)

From the Figure 4.3 and Figure 4.4 it is clearly visible that higher compaction pressure lowers the porosity. In both the case grain growth occurs.

To lower the porosity content, the holding time is further increased to 5 hours. The microstructure (Figure 4.5) shows that porosity is not removed but some of the grains are as big as 20μm. Most of the pores are at the grain boundary or at the triple point. Still some of the pores are inside the grain, which deteriorates the property.
So another option to control the grain growth is to sinter the sample at lower temperature. Figure 4.6 and Figure 4.7 show the microstructure of the a $BaTiO_3$ sample sintered at 1225°C for 4 hours and 6 hours respectively. From Figure 4.6 it is clearly visible that grain size is smaller than the sample sintered at 1250°C for 3 hours. The sample sintered at 1225°C for 4 hours has smaller grains and only less grain have been found to grow.

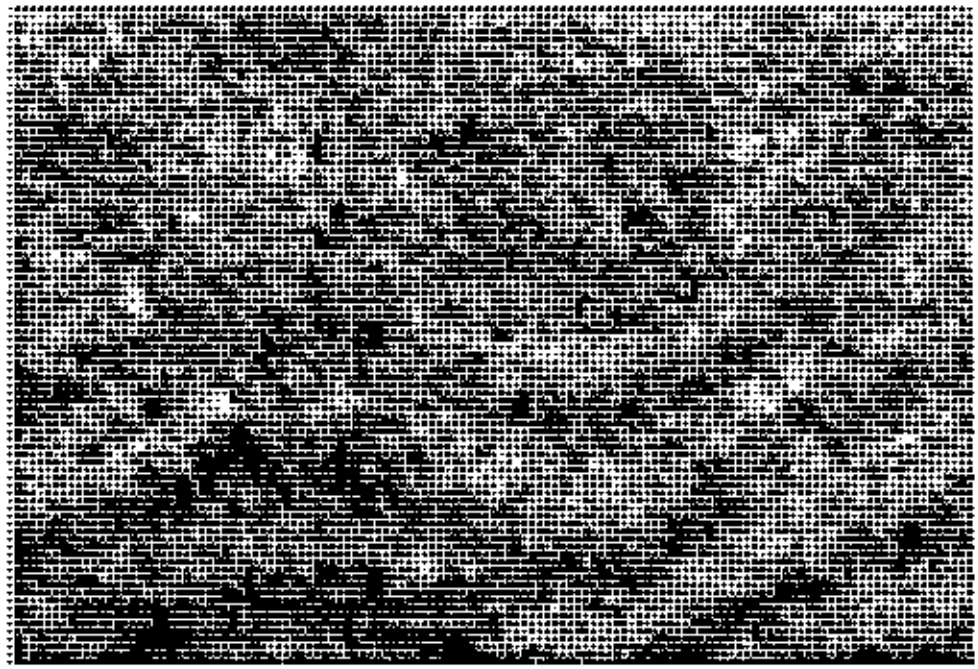

Figure 4.5: SEM Micrograph of $BaTiO_3$ sintered at 1250°C for 5 hours (150MPa)

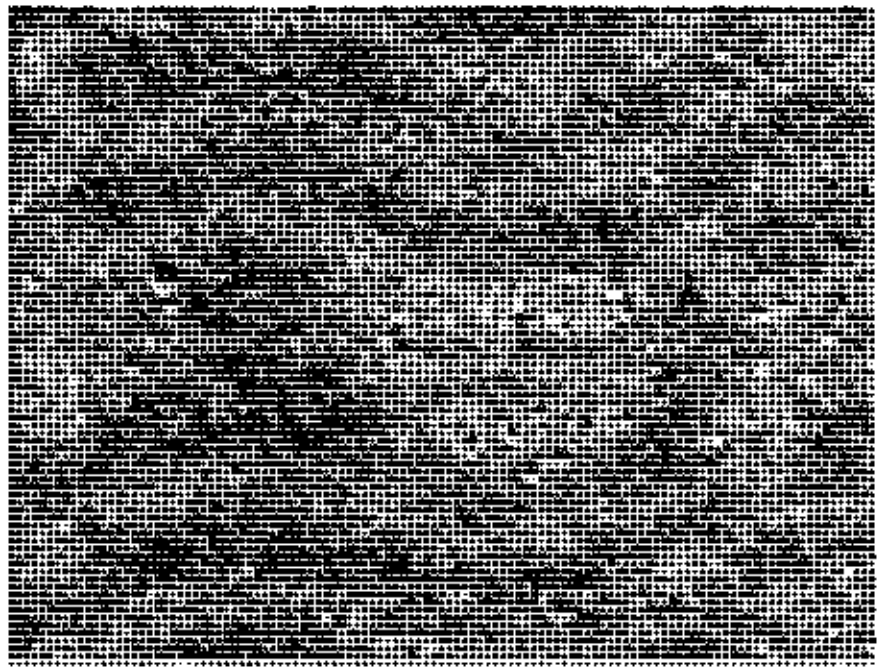

Figure 4.6: SEM Micrograph of $BaTiO_3$ sintered at 1225°C for 4 hours (150MPa)

Figure 4.7: SEM Micrograph of $BaTiO_3$ sintered at 1225°C for 6 hours (150MPa)

On the other hand, for a sample sintered at 1250°C for 3hours grain growth occurs extensively (Figure 4.3). Figure 4.7 shows that when the holding time is increased to 6 hours at 1225°C; grain growth occurs but the rate of grain growth is slower in the sample sintered at 1225°C for 6hours (Figure 4.7) than 1250°C for 5hours (Figure 4.5). Figure 4.8 shows the grain size distribution of $BaTiO_3$ sample sintered at 1225°C for 4 hours and applied pressure for compaction of 130MPa. The average grain size is less than 4μm as it is expected. The porosity remains at the grain boundary and the bulk density of the sample is less than that of the sample prepared by using 150MPa.

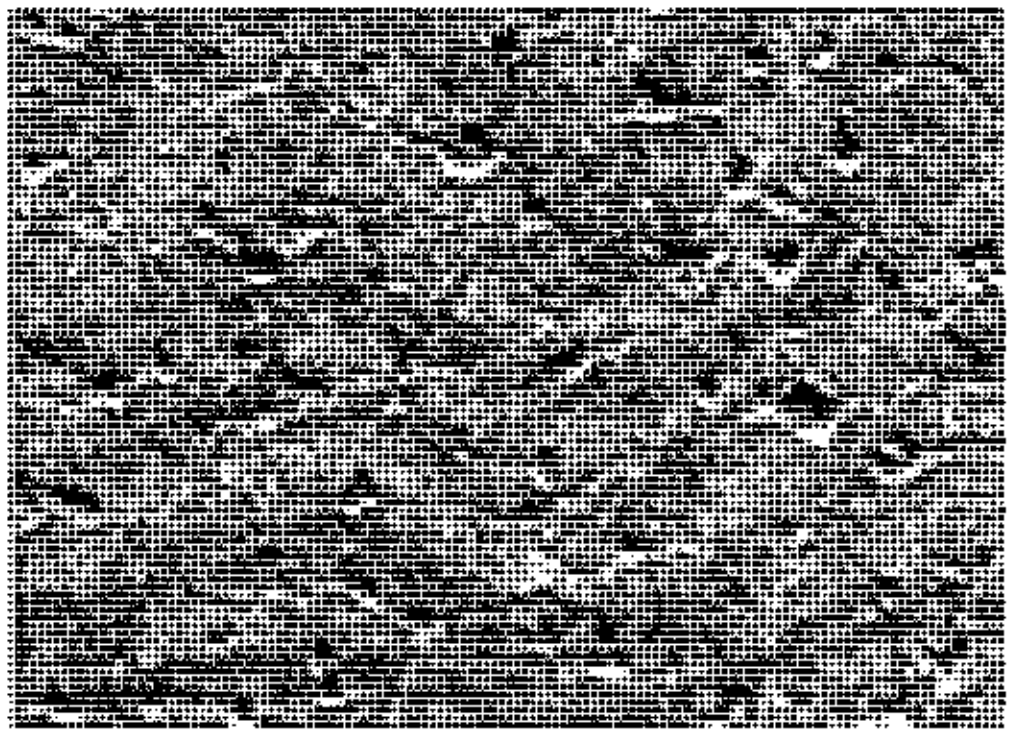

Figure 4.8: SEM Micrograph of $BaTiO_3$ sintered at 1225°C for 4hours (130MPa)

This microstructure is better than the Figure 4.6 as far as the grain size is concerned. The sample prepared by the compaction pressure 150MPa has higher grain size (Figure 4 6). The increased grain size may be due to the higher compaction pressure. So, better microstructure can be obtained if lower sintering temperature and higher compaction pressure are being used.

### 4.2.2 Ferroelectric domain in $BaTiO_3$

The finest black and white stripes shown in Figure 4.9 are the 90° ferroelectric domains. These microstructures are revealed by chemical etching. These 90° domains are so much finer in the polycrystalline aggregate than they are found in the single crystal.

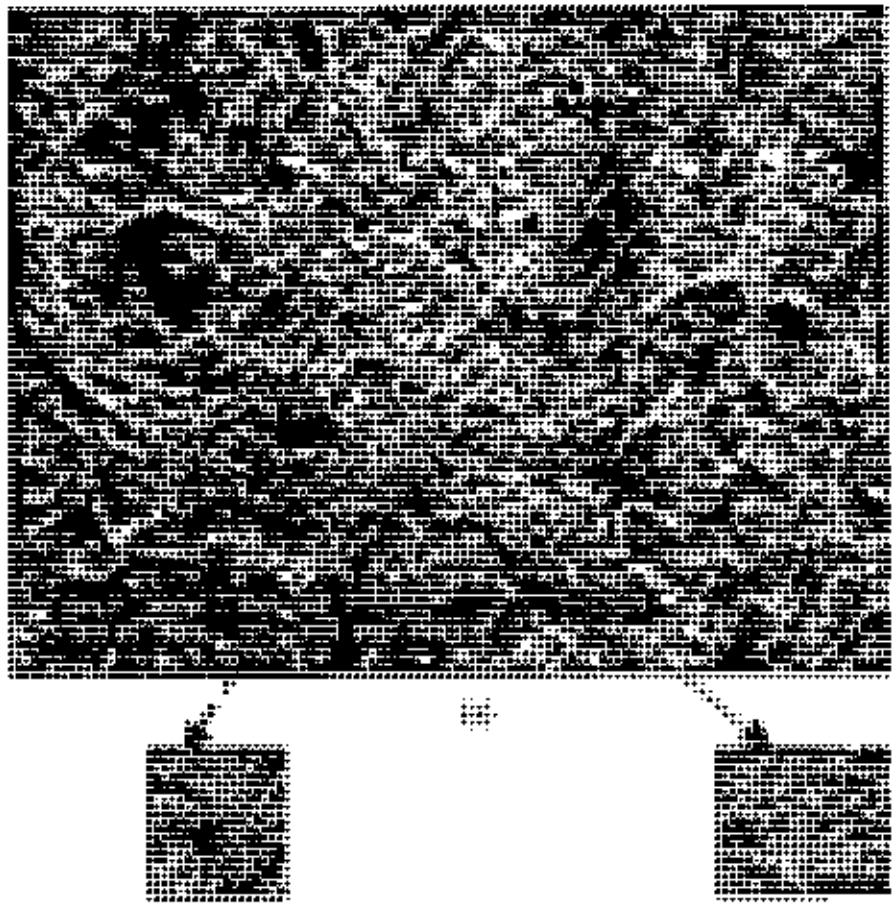

(b) (c)

Figure 4.9: SEM micrograph of $BaTiO_3$ sintered at 1250°C for 5 hours (chemically etched)

In considering the thickness of the domain boundary it is helpful to recall that these domains are also called twins. From Figure 4.9(c) it is evident that twinning interface has zero thickness. Its seems reasonable to assume that as a first approximation that this configuration may be obtained for the interfaces between 90° twins and is even more likely for 180° domains in barium titanates. The banded structure shown in Figure 4.10 is also another microstuctural feature of barium titanate polycrystalline ceramics.

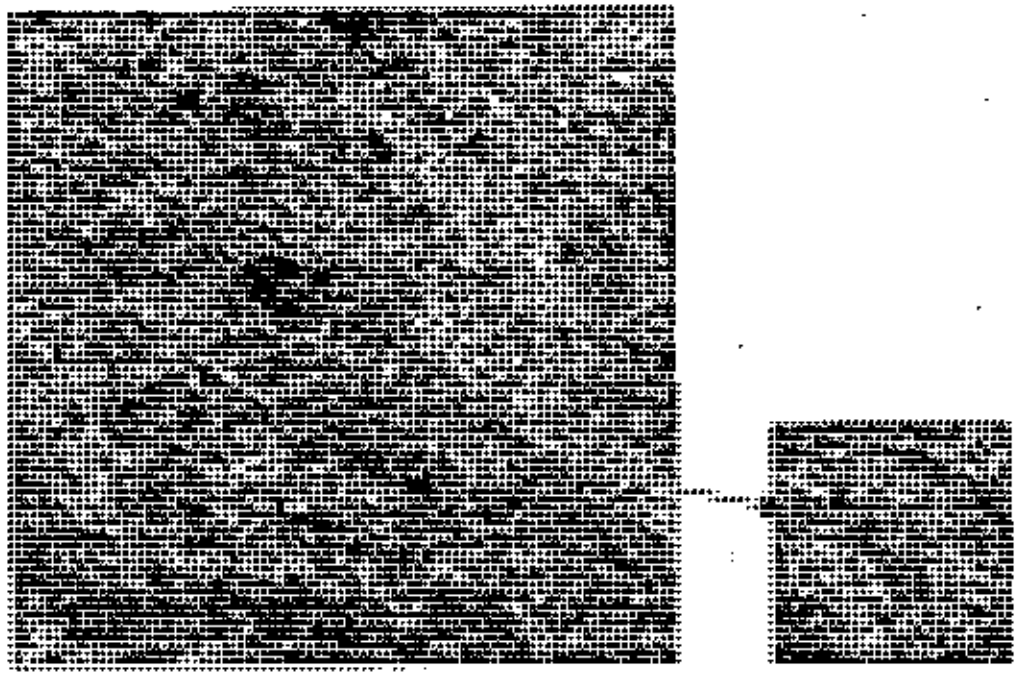

Figure 4.10: SEM micrograph of polycrystalline $BaTiO_3$ sintered at 1250°C for 5hours after polishing and etching.

These bands of about 10μm wide are defined by the change in direction of the included fine twins (never more than two different directions within a band) and the interfaces are reasonably close to straight lines with the exception of a few orientations, which have wedge like shape. DeVries et al [37] also found the similar feature in the $BaTiO_3$. They noticed that the band characteristic of the ceramic structure was associated with the restrain imposed by the surrounding materials during transformation. It was also observed that grains near cracks in the ceramic materials frequently had relatively unbanded structure similar to those in single crystal. From Figure 4.10 it can be seen that the orientation of the straight line is slightly changed at the grain boundary. According to Devries et. al.[37] this can be explained in the following way, when one grain has transformed from cubic to tetragonal and has a banded structure, the stresses at the periphery of the grain will not be uniform. This non-uniform stress will make certain orientation in neighboring grains more favorable. Thus when they transform there will be tendency for band edges to maintain the stress to a minimum. An interesting feature found by us called

butter fly twin [37] in the sample of $BaTiO_3$ sintered at 1225°C for 6 hours shown as shown in Figure 4.11 and Figure 4.12

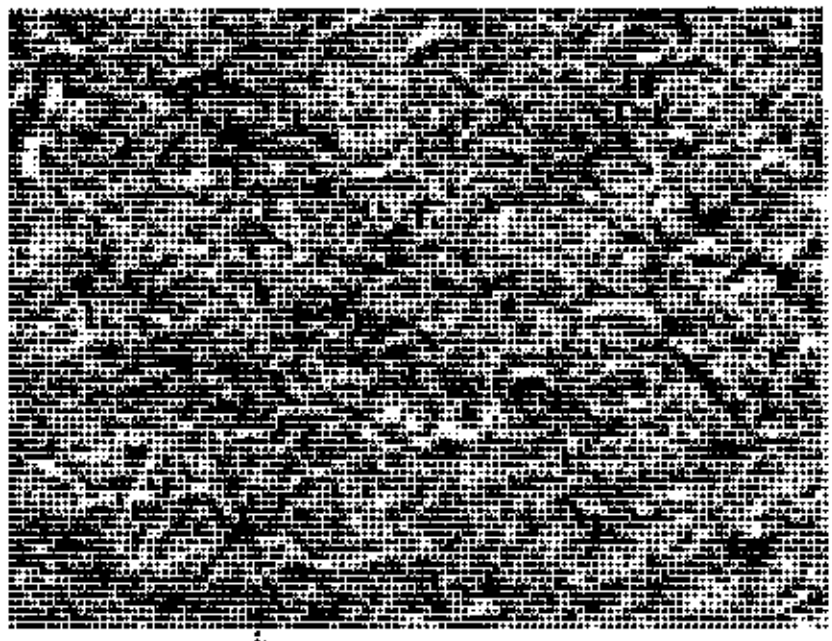


Figure 4.11: SEM micrograph shows twinning in polycrystalline $BaTiO_3$ in the polished and chemically etched section.(×2000)

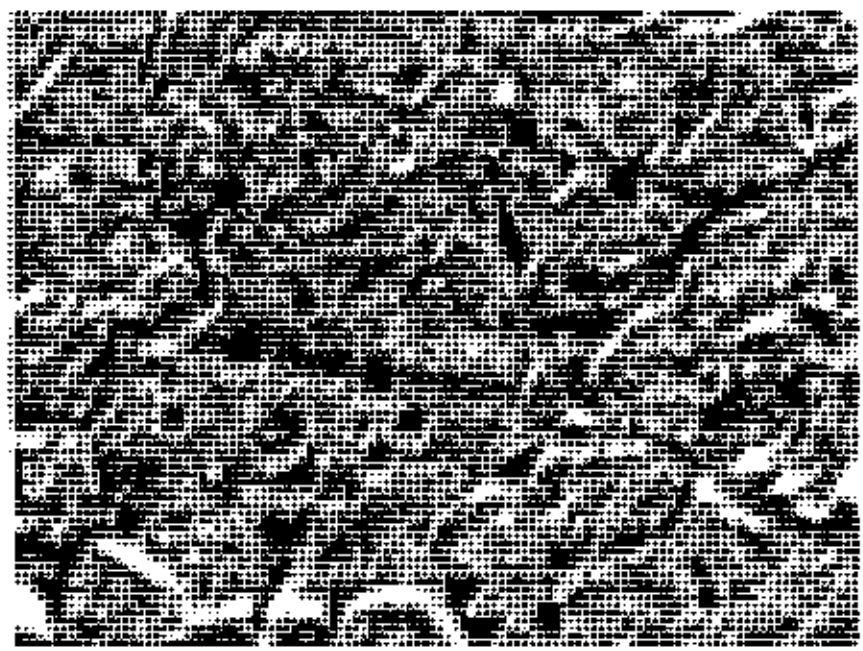

Figure 4.12: SEM micrograph shows twinning in polycrystalline $BaTiO_3$ in the polished and chemically etched section (×3500).

DeVries et al [37] found the same feature in polycrystalline $BaTiO_3$. Such a structure is very similar in appearance to the (111) plane frequently observed after annealing in face centered cubic metal.

### 4.2.3 Microstructure of Barium Strontium Titanate

Strontium is doped in $BaTiO_3$ by the solid solution of 0.9 mole fraction of $BaTiO_3$ with 0.1 mole fraction of $SrTiO_3$. Figure 4.13 shows the microstructure of $Ba_{.9}Sr_{.1}TiO_3$ sintered at 1250°C for 5 hours. Extensive grain growth is observed.

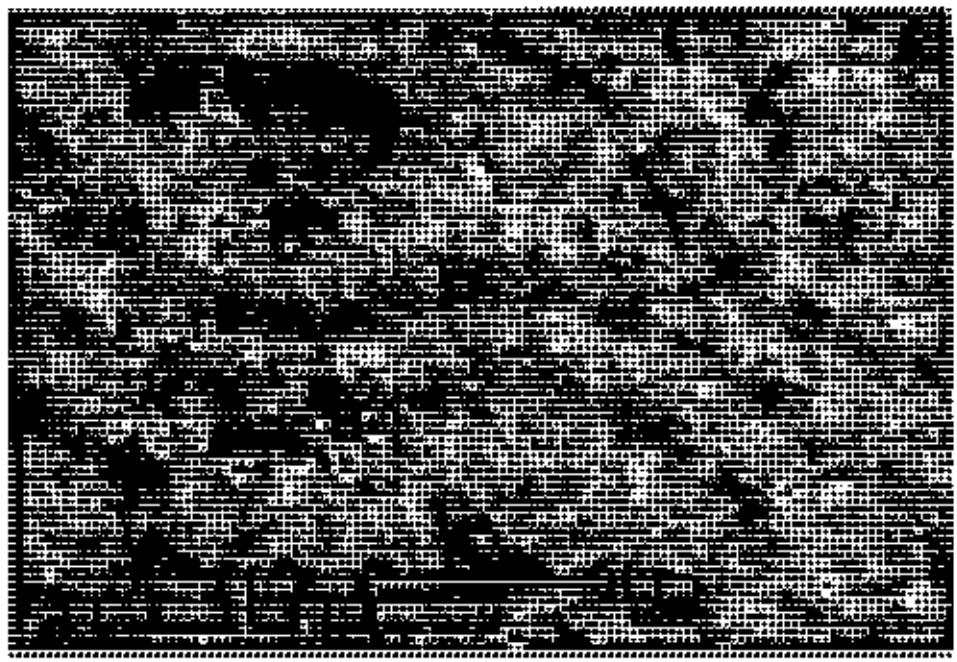

Figure 4.13: SEM micrograph of $Ba_{.9}Sr_{.1}TiO_3$ sintered at 1250°C for 5 hours.

Figure 4.14 shows the microstructure of $Ba_{.85}Sr_{.15}TiO_3$ sintered at 1275°C for 3 hours. Extensive grain growth is also observed in this microstructure Therefore, for doped sample the sintering temperature and time should be optimized to get a small grained microstructure.

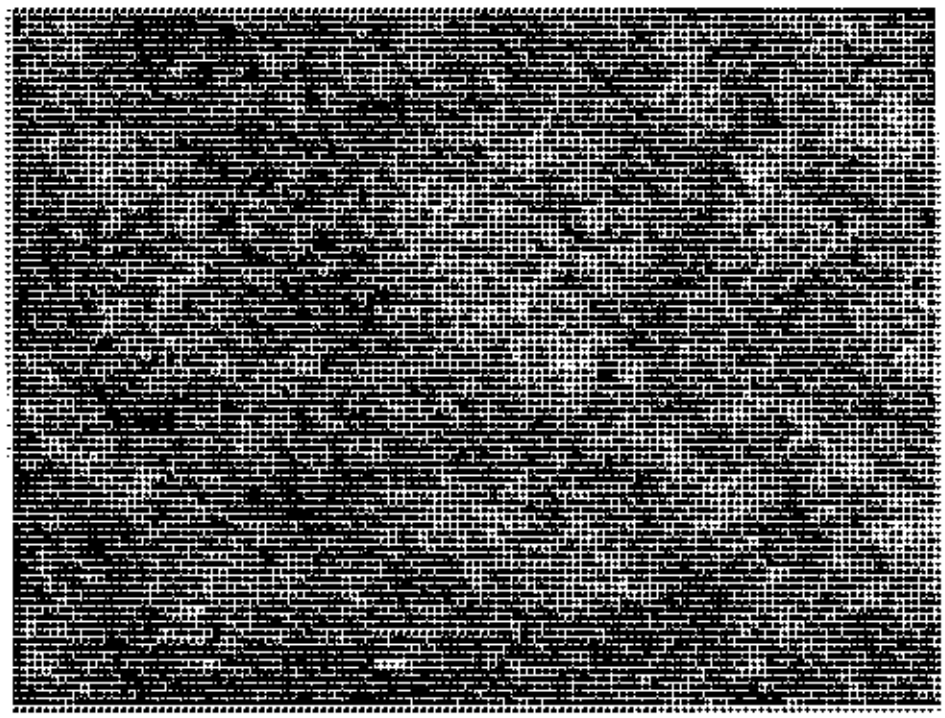

Figure 4.14: SEM micrograph of $Ba_{.85}Sr_{.15}TiO_3$ sintered at 1275°C for 3 hours.

### 4.2.4 Microstructure of Strontium Titanate

Pure $SrTiO_3$ sintered at 1200°C for 3 hours have very poor bulk density and this sample is very thick so a concentration gradient is set up during sample preparation and hence the density is reduced. The sample is thermally etched and microstructure could not be revealed. $SrTiO_3$ is sintered at 1250°C for 3 hours and at 1250°C for 5 hours. After sufficient polishing and chemical etching it seems that, the $SrTiO_3$ sample is not sintered properly. But some interesting microstructural features were revealed after the chemical etching as shown in Figure 4.15 and Figure 4.16. Some needle shape, X-shape, triangular shape morphologies have been revealed after chemical etching. This morphology was prominent in the sample sintered at 1250°C for 5 hours. For the sample sintered at 1250°C for 3 hours these special features are getting lighter but still prominent (Figure 4.17).

Figure 4.15: SEM micrograph of $SrTiO_3$ sintered at 1250°C for 5 hours.

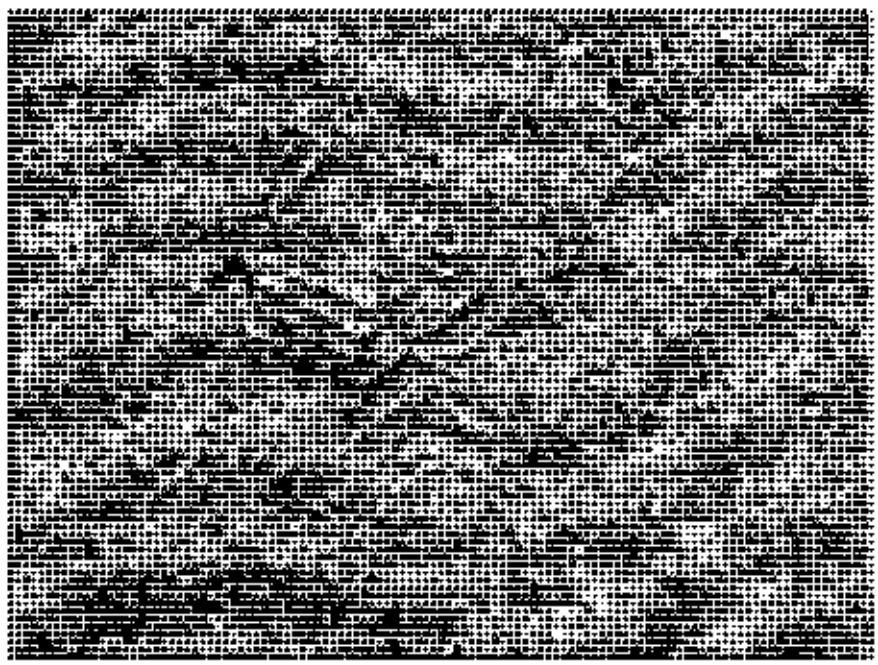

Figure 4.16: SEM micrograph of $SrTiO_3$ sintered at 1250°C for 5 hours.

Figure 4.17: SEM micrograph of $SrTiO_3$ sintered at 1250°C for 3 hour.

## 4.3 Microstructure-Property relation

Figure 4.18(a) shows frequency dependence of dielectric constant k′ of the pure $BaTiO_3$ in the frequency range 1 kHz to 5MHz. The dielectric constants were measured at room temperature. Higher dielectric constants were observed at room temperature for the Barium titanate sintered at 1225°C for 4hours than for 6 hours. This result was quite expected.

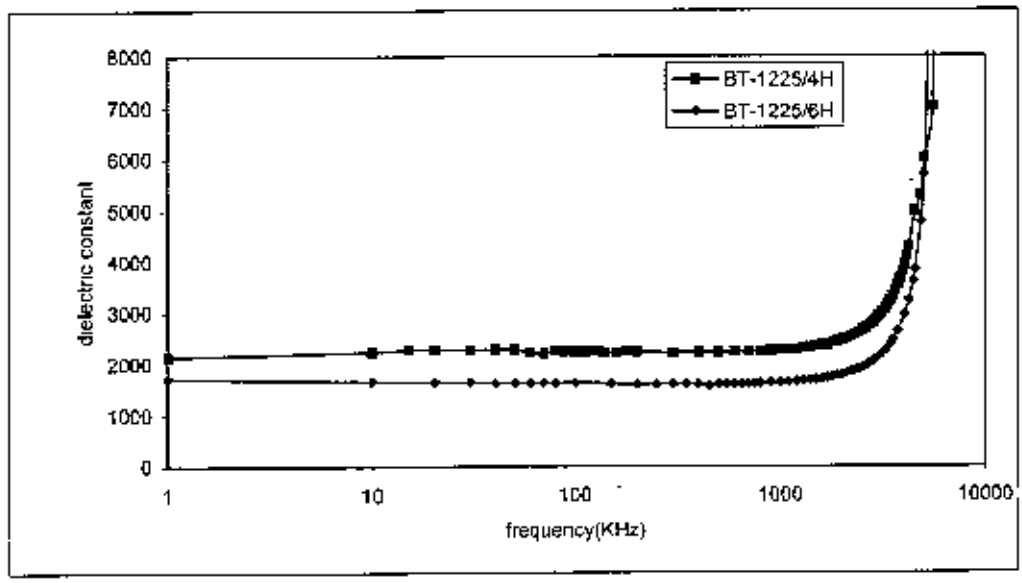


Figure 4.18(a): Dielectric constant as a function of frequency for $BaTiO_3$

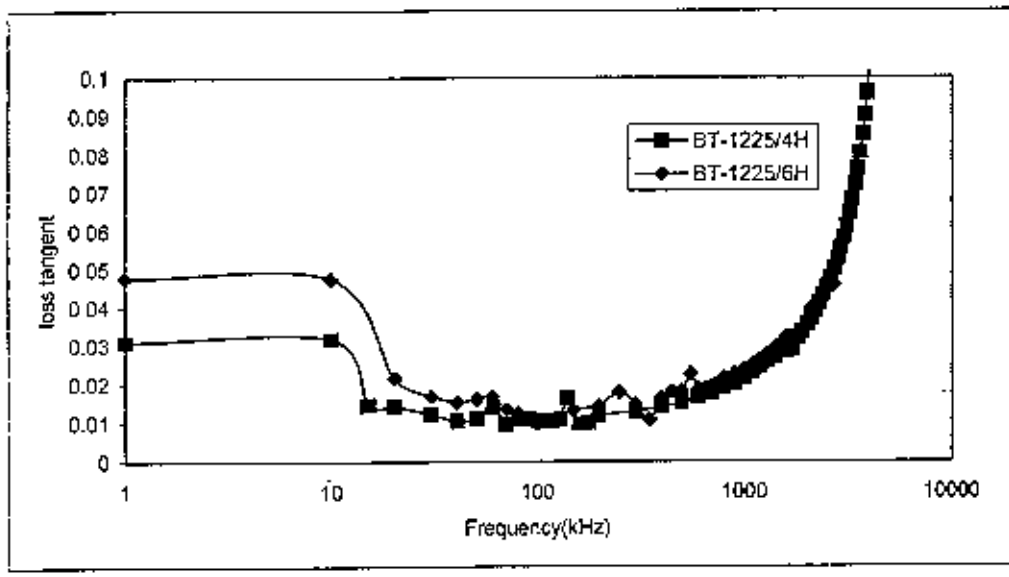


Figure 4.18(b): Loss tangent as a function of frequency for $BaTiO_3$

Lower holding time at the sintering temperature inhibited the grain growth and hence results in higher dielectric constant. The BT-1225/4H sample has smaller grain size as seen from the microstructure (Figure 4.6) where the BT-1225/6H sample has larger grain size (Figure 4.7).

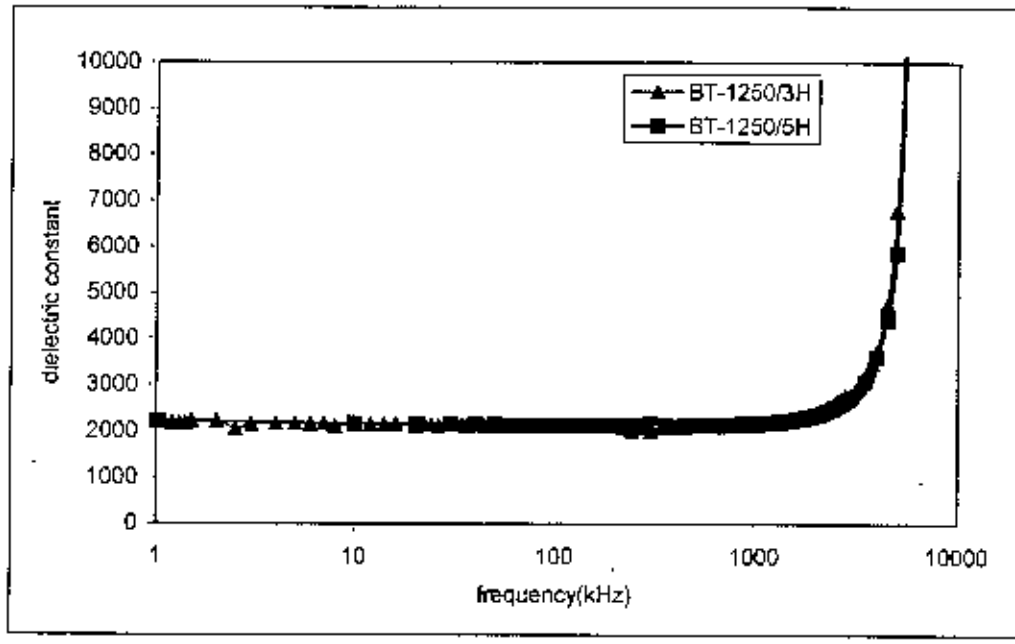


Figure 4.19(a): Dielectric constant as a function of frequency for $BaTiO_3$

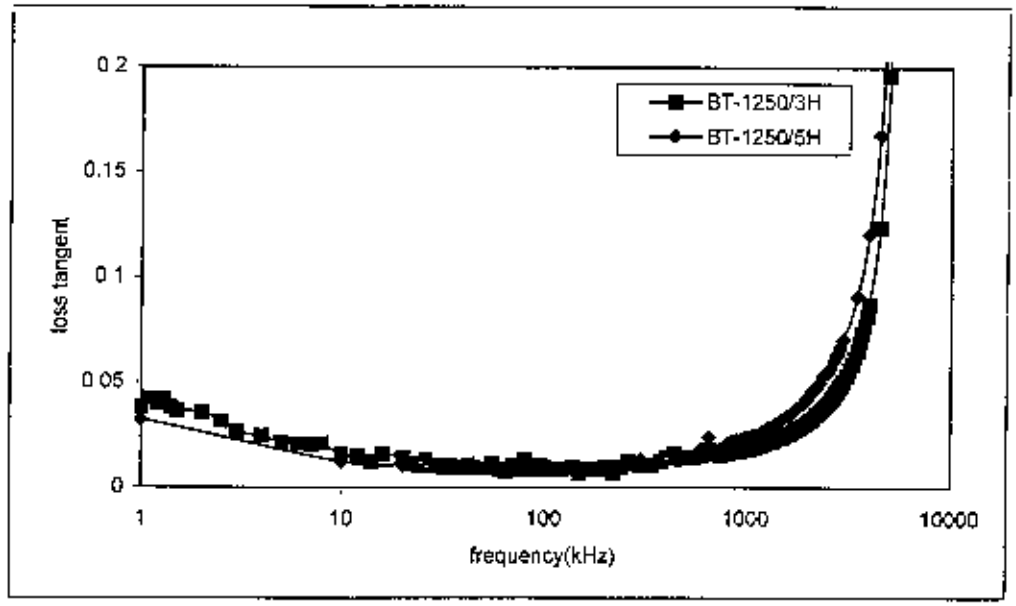


Figure 4.19(b): Loss tangent as a function of frequency for $BaTiO_3$

From both the figures, it can be seen that the average grain size is less than 10μm. According to G.Arlt et. al [22] higher dielectric constant can be explained in terms of domain wall contribution. In the range of 1<a<10μm, the decrease of domain width can be roughly expressed by the correlation d~√a, where d=domain width, a=grain size of a cubic grain. According to the decreasing width, the area of the 90° domain walls per unit volume strongly increases in fine grain $BaTiO_3$ The observed increase of dielectric constant in fine grain microstructure of $BaTiO_3$ can be therefore interpreted in terms of the increasing contribution of domain walls to the permittivity (or dielectric constant). The cause of the lower dielectric constant of the sample BT-1225/6H can also be attributed to the presence of porosity and the grain size. The presence of porosity in the grain inhibited the motion of the domain wall. The dielectric constant remains almost constant at room temperature in the frequency range 1 kHz to 5MHz. The loss tangents [Figure18 (b)] are also found to follow the same trend, higher loss tangent value were observed for the sample of larger grain size (Figure 4.7). On the other hand, low loss tangent was observed for the sample of relatively smaller grain size. The highest change in dielectric constant and loss tangent was observed at the resonance frequency. At the resonance frequency, the polarization reached at the maximum and maximum loss tangent was observed due to the dissipation of field energy as frictional heat. The frequency dependence of dielectric constant and the loss tangent of $BaTiO_3$ samples BT-1250/3H and BT-1250/5H are shown in the Figure 4.19(a) and Figure 4.19(b). Dielectric constant seems to be same for both the two sample sintered at the 1250°C for 3hours and 5 hours. Relatively high dielectric constant was observed. The reason can be attributed to the presence of less amount of porosity. The loss tangents are more or less same in the lower frequency range, but as the frequency increased, the loss tangent tends to be higher value for the sample BT-1250/5H. The reason is that some of the grains are too large so the total grain boundary area is small. As we know, that higher grain boundary area increases the resistivity of the polycrystalline material. Therefore, the smaller grain boundary area enhances the dc resistvity loss [58]. If we look at the microstructure, (Figure 4.3 and Figure 4.5) the average grain size obtained is higher than 10μm. Of course in both figures, some of the grains are small but in Figure 4.5 grain size as big as 20μm are observed. The ferroelectric

domain width remains essentially constant at the grain size larger than 10μm [22]. The simple correlation of the domain width and grain size seems to end at the grain size of about 10μm. It means that decreasing grain size in the range above 10μm will not decrease domain width that will not in return increase the total area of 90° domain wall per volume. That contribution of domain wall area to the real part of permittivity ends at 10μm. It is also clear from the micro structural observation that higher temperature actually initiated the grain growth. Grain size is larger in case of the sample BT-1250/3H than the sample BT-1225/4H.

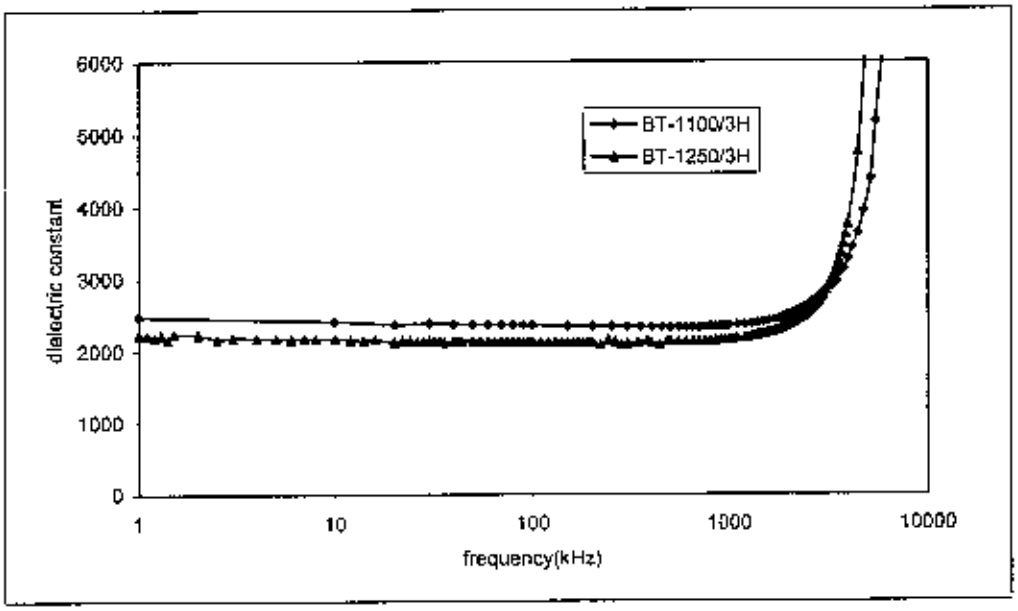


Figure 4.20(a): Dielectric constant as a function of frequency for $BaTiO_3$

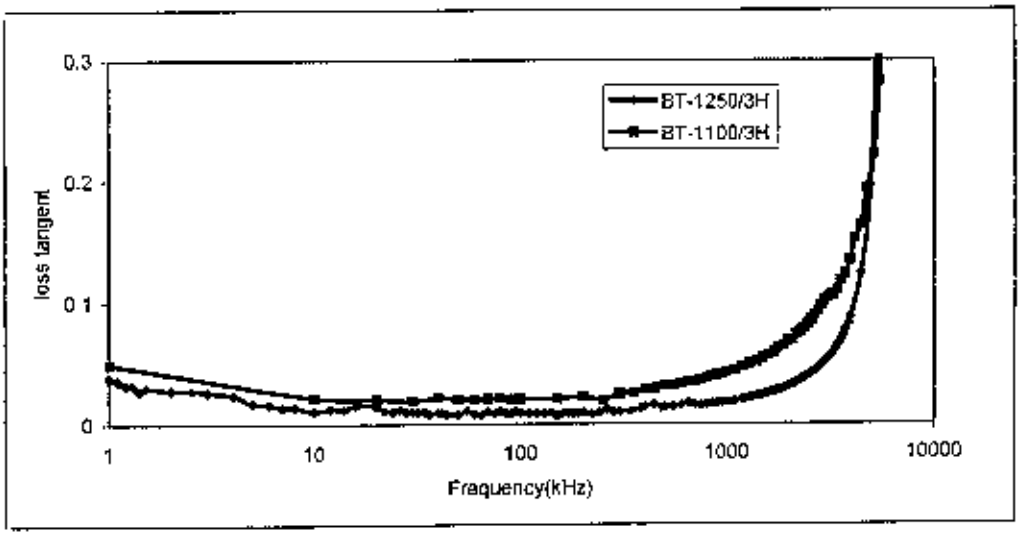


Figure 4.20(b): Loss tangent as a function of frequency for $BaTiO_3$

Figure 4.20(a) and 4.20(b) show the two extreme cases of the frequency dependence of dielectric constant for the samples BT-1100/3H and BT-1250/3H as far as the microstructure is concerned

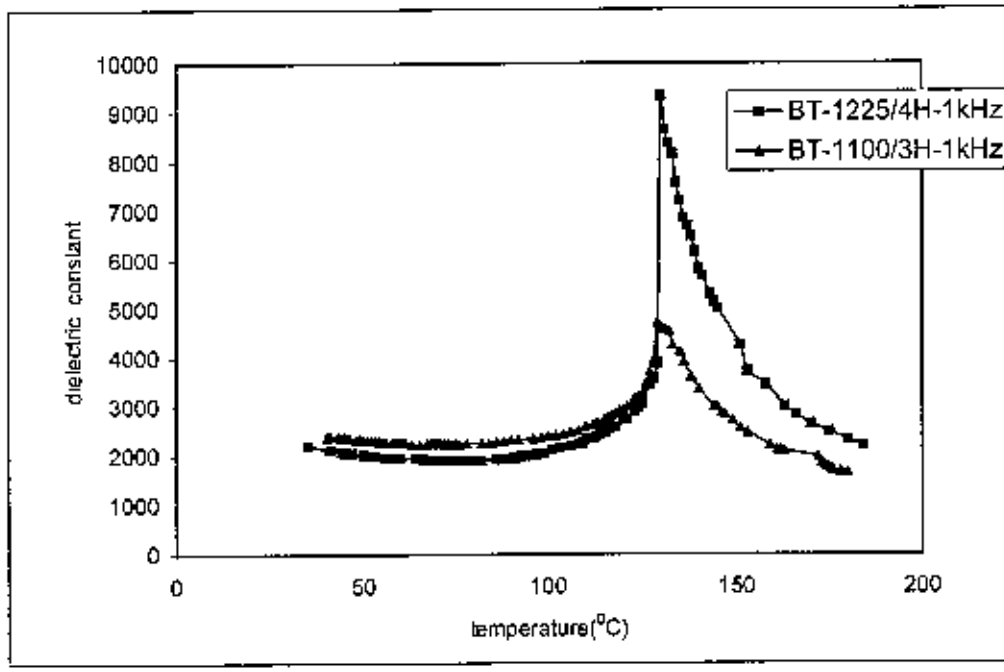


Figure 4.21(a): Dielectric constant as a function of temperature for $BaTiO_3$

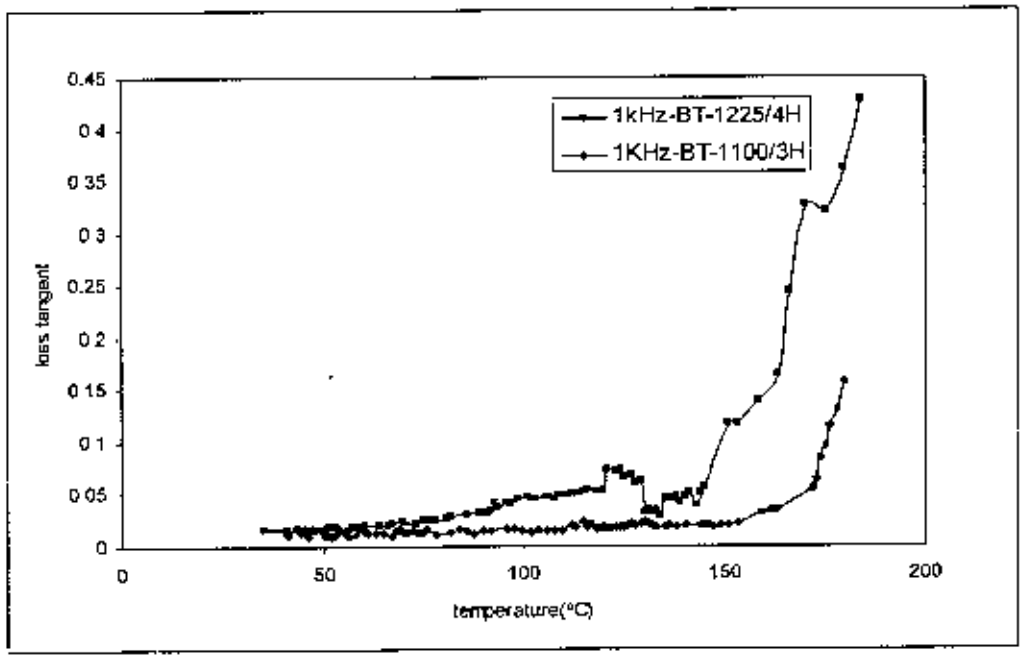


Figure 4.21(b): Loss tangent as a function of temperature for $BaTiO_3$

The sample BT-1100/3H is a $BaTiO_3$ sample sintered at 1100°C for 3 hours exhibits higher dielectric constant than the sample BT-1250/3H in the frequency range (1kHz-5MHz). But this is to note that the sample BT-1100/3H displayed higher loss tangent than that of the sample BT-1250/3H which increases above 1 MHz.

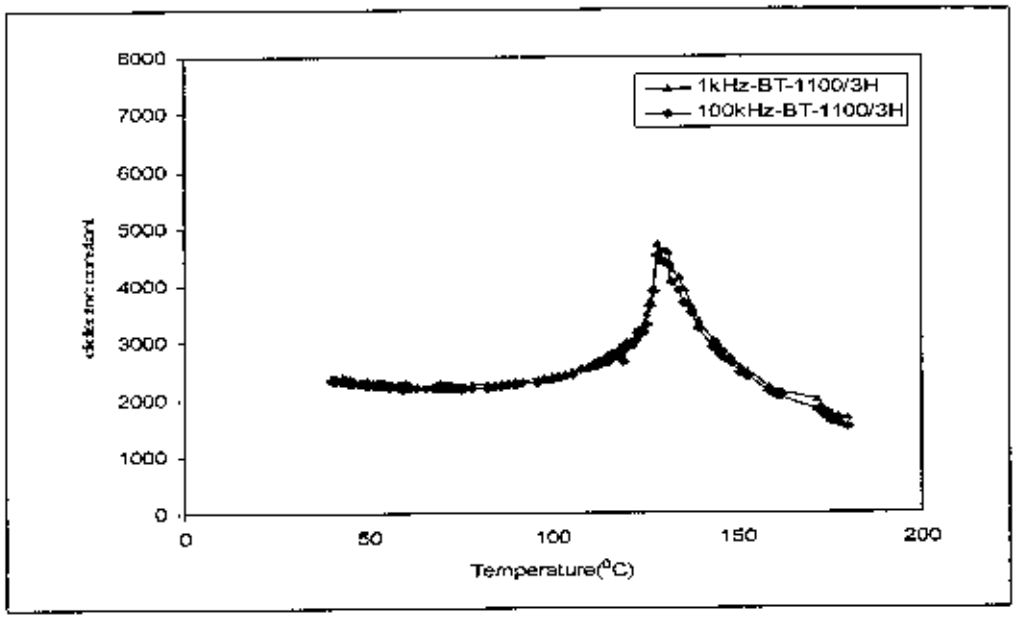


Figure 4.22(a): Dielectric constant as a function of temperature for $BaTiO_3$ at 1 kHz and 100 kHz.

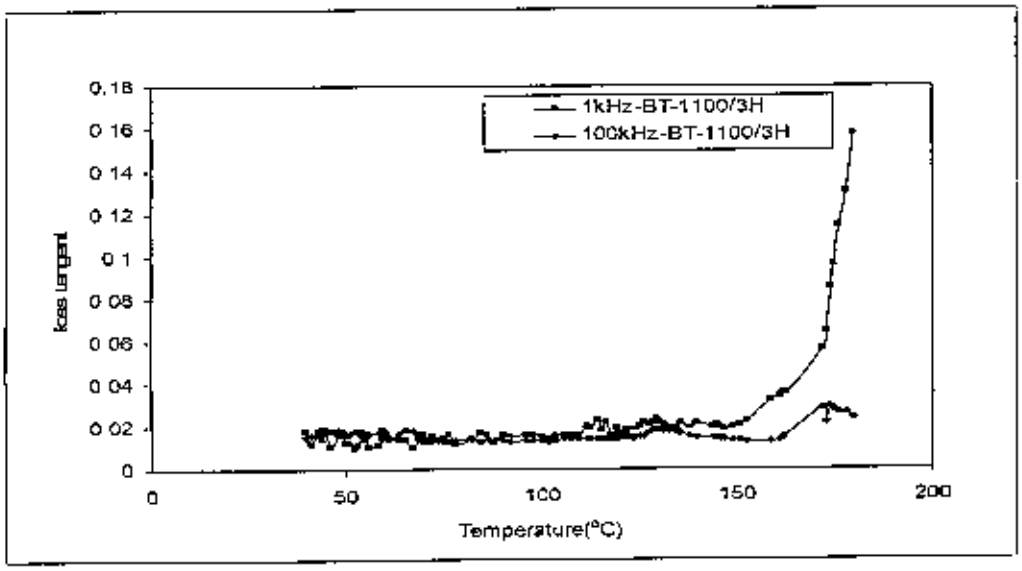


Figure 4.22(b): Loss tangent as a function of temperature for $BaTiO_3$ at 1 kHz and 100 kHz

The microstructure of the sample BT-1100/3H is shown in the Figure 4.1. This sample is very poorly sintered and the sintered bulk density is 77% of the theoretical density. The higher dielectric constant may be attributed to the smaller grain size and the higher loss may be due to the higher porosity. The difference between the two samples increased in the frequency range 1.2 MHz to 3.2 MHz.

Figure 4.21(a) and 4.21(b) give a classical example of grain size effect on microstructure and phase transformation in barium titanate. The BT-1100/3H sample shows lower permittivity peak at 129°C and the BT-1225/4H sample shows higher permittivity peak at 130°C. Lower grain size shows higher room temperature permittivity and the larger grain size shows lower permittivity at room temperature as already observed in the frequency dependence of dielectric constant. Figure 4.1 shows that the average grain size of the BT-1100/3H is 1μm. On the other hand, the BT.1225/4H sample has average grain size of 5μm (Figure 4.8). Although the dielectric constant for the lower grain sample should be higher [22] than the observed value of 2400, the reason for comparatively lower dielectric constant for the small grain structure is due to the presence of large amount of porosity. It is generally recognized that as the grain size is reduced to the micron level, the dielectric constant at the room temperature increased, and the temperature dependence of the dielectric constant is modified significantly below the Curie temperature ($T_C$). For large grain materials (grain size >1μm), the cubic–tetragonal transformation that occurs on cooling (130°C) drives the formation of a polydomain subgrain structure to minimize electrostatic elastic energies in polar anisotropic state. The polysynthetic twinning that take place serves largely to relieve stresses which would other wise be present throughout the transformed body [33]. The individual grains in the transformed microstructure of a large grain polycrystal are comprised of structural invariants. bounded by the domain walls of 90° and 180° types in the tetragonal state. Thus, large grain centers are usefully transformed and essentially unstressed. The dielectric response of such materials is readily rationalized in terms of an orientational average of values for the anisotropic dielectric constant, which characterizes a single domain of tetragonal $BaTiO_3$. It was observed that polycrystalline $BaTiO_3$ exhibited an enhanced dielectric response for ceramic specimens prepared with a grain size as small as 1μm. The increase in dielectric

constant is understood in terms of the twinning behavior of polycrystalline material with decreasing grain size. Despite the ability of the twinning mechanism to reduce the bulk strain energy that would be present after a homogeneous structural transformation occurred, stress still resides near grain boundaries, even in large grain ceramics. Minimization of the residual strain energy ultimately contributes to the resulting twin structure. The microstructure of a large grain ceramic contains 90° twins formed to relieve the strains generated when the c axis elongates on passing from the cubic to tetragonal symmetry; in the strained state highest permittivity is displayed. The domain boundary planes have surface energy proportional to the square of the grain diameter; the strain energy responsible for domain formation, a volume effect is relates to the cube of the grain diameter. With decreasing grain size a critical size is reached where it is energetically less costly to support an elastic strain than to relieve it by twin formation. This situation exists in the microstructure having grain size of the order of 1μm or less. These finer grain size materials are untwined, stressed; each grain has a single domain, has one orientation of spontaneous polarization, and tends to cubic symmetry. The decreasing tendency of the Curie temperature as the grain size is decreases that can be understood by the above-mentioned cause. That is at a higher grain size, tetragonal structure is stabilized by the formation of substantial amount of domain twining, and on the other hand transformational stress cannot be reduced by formation of domain twin in the small grain size structure because of the achievable lower volume free energy. This tends to shift the Curie point of small grain size to the lower temperature region as seen in Figure 4.21(a). The loss tangent as a function of temperature was shown in Figure 4.21(b). At the lower temperature range, the loss tangents are same but at higher temperature. BT-1225/4H sample exhibits higher loss because of large grain size and less amount of porosity. Porosity and grain boundary are believed to be the potential source of scattering. At higher temperature, ion-hopping effect is also pronounced which enhanced the dielectric loss. Temperature dependence dielectric properties of BT-1100/3H at two different frequencies 1 kHz and 100 kHz are shown in Figure 4.22(a) and 4.22(b). The dielectric constants are found to be same at both higher and lower frequency. A same trend is also observed in case of the loss tangent up to 150°C. Above 150°C loss tangent at low frequency range become

higher. The higher loss tangent can be attributed to the ion jump mechanism at high temperature.

Figure 4.23(a) and Figure 4.23(b) describe the frequency dependence of dielectric constant and loss tangent. The figure shows that BST20 that is $Ba_8Sr_2TiO_3$ has the higher dielectric constant and BST15 sample has lower dielectric constant.

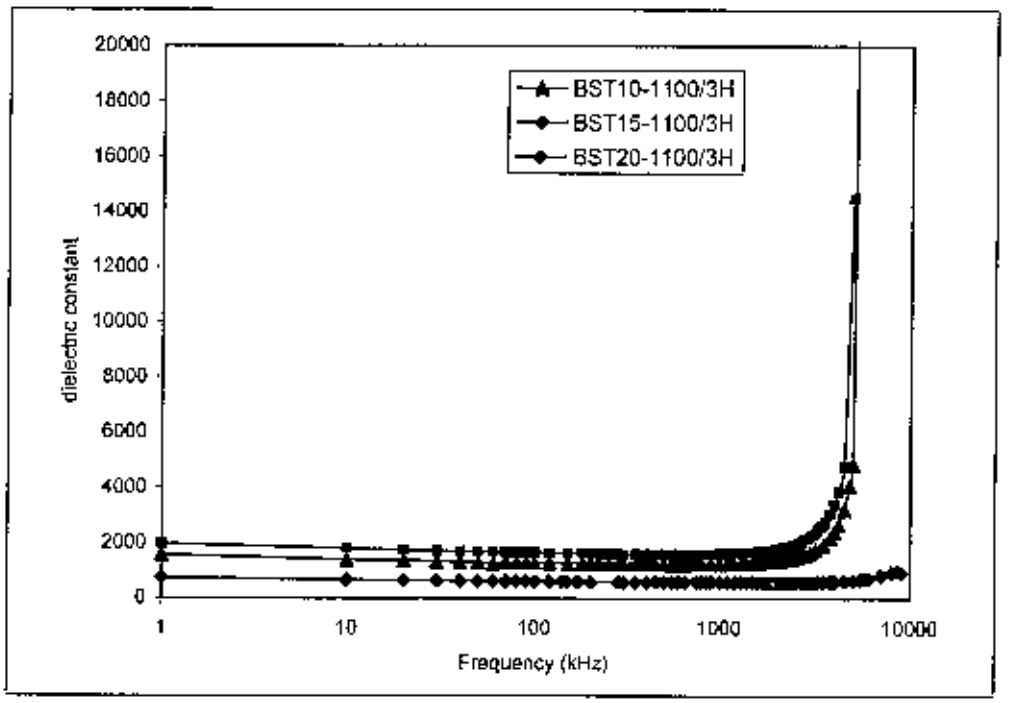


Figure 4.23(a): Dielectric constant as a function of frequency for $Ba_9Sr_1TiO_3$, $Ba_{85}Sr0_{15}TiO_3$ and $Ba_8Sr_2TiO_3$

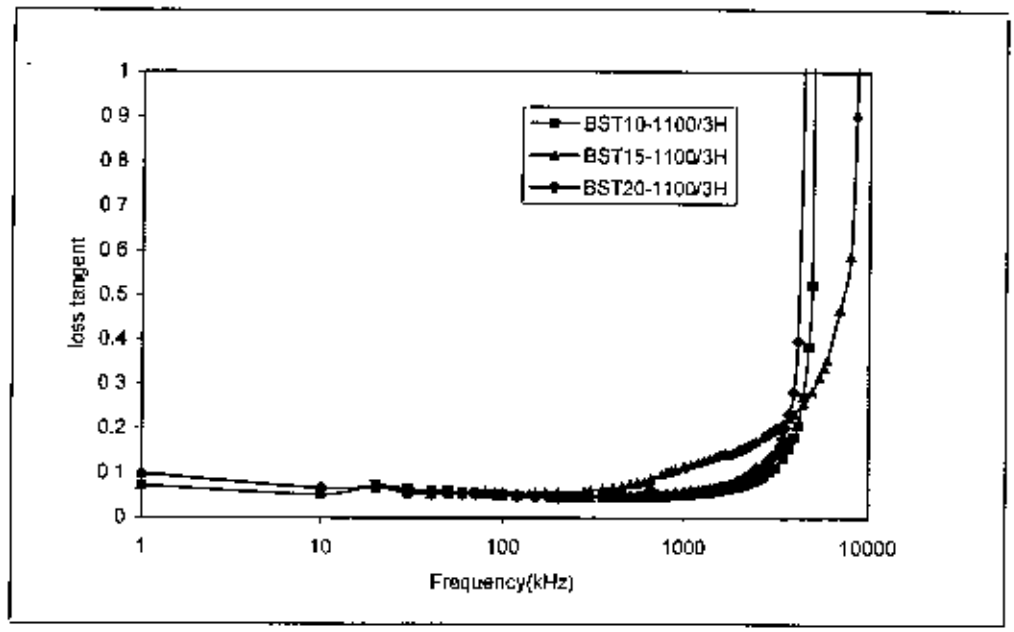


Figure 4.23(b): Loss tangents as a function of frequency for $Ba_{.9}Sr_{.1}TiO_3$, $Ba_{.85}Sr_{.15}TiO_3$ and $Ba_{.8}Sr_{.2}TiO_3$

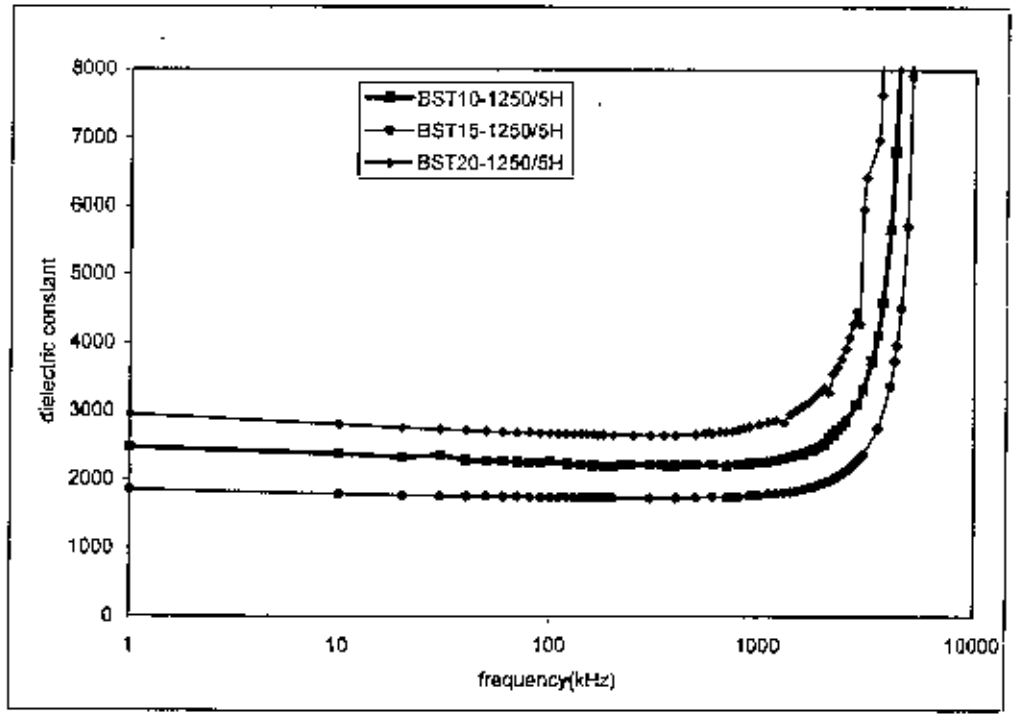


Figure 4.24(a): Dielectric constant as a function of frequency for $Ba_{.9}Sr_{.1}TiO_3$ $Ba_{0.85}Sr_{0.15}TiO_3$ and $Ba_{.8}Sr_{0.2}TiO_3$

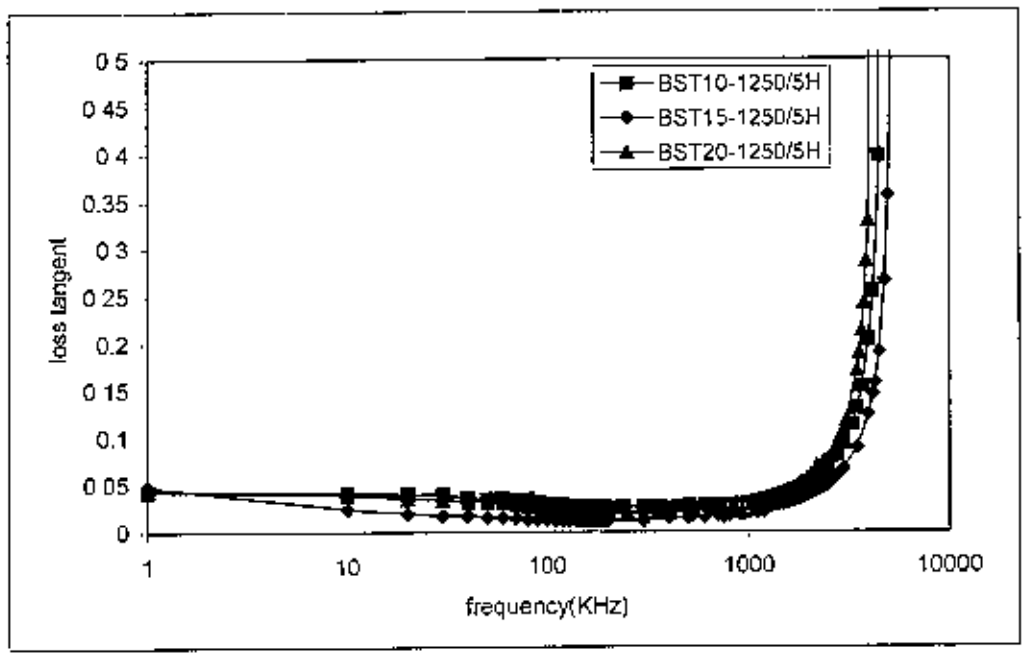


Figure 4.24(b): Loss tangent as a function of frequency for $Ba_{.9}Sr_{.1}TiO_3$, $Ba_{.85}Sr_{.15}TiO_3$ and $Ba_{.8}Sr_{.2}TiO_3$

The almost flat frequency response up to 10 MHz is observed in the case of BST15 sintered at 1100°C for 3 hours. If we see the loss tangent graph (Figure 4.23b), the BST10 and BST20 sample has almost same loss tangent property but for BST15 sample loss tangent is increased from 400 kHz. Lower dielectric constant values were observed in case of the BST samples sintered at 1100°C for 3 hours. From the DSC data it was confirmed that solid-state reaction was not completed as any sharp transition was observed (Figure 4.31). Therefore, both the high ($BaTiO_3$) and the low dielectric constant ($SrTiO_3$) phase were present in the BST sample sintered at 1100°C and as a result, the dielectric constant values decreased. Figure 4.24(a) and 4.24(b) shows the frequency dependence of dielectric properties of the BST samples sintered at 1250°C for 5 hours. It was observed that as the sintering temperature increased, all the three BST samples showed marked increase in their dielectric constant values. The BST20 sample shows dielectric constant as high as 3000 (Figure 4.24(a)). It was also observed that dielectric constant was strongly dependent on Sr doping concentration. Dielectric constant is decreased as the Sr

concentration increased up to 15%. For 20% Sr doping, the dielectric constant increased as seen in Figure 4.23 and Figure 4.24.

Temperature dependence of dielectric properties for the BST sample sintered at 1250°C for 5 hours is displayed in the Figure 4.25a-b, 4.26a-b and 4.27a-b. For pure $BaTiO_3$ Curie temperature is around 130°C, which was already shown in Figure 4.21(a). In generally, it is observed (Figure 4.25a-b, 4.26a-b and 4.27a-b) that the loss tangent displayed higher value at lower frequency and lower value at high frequency. This is because ion jump mechanism is prominent at lower frequency and absent at higher frequency. As the temperature increases, the loss tangent at lower frequency also increases for the sample BST10-1250/5H and BST15-1250/5H. It is well known that the number of successful ion jump increases constantly with temperature [7]. This mechanism prevailed up to 15% Sr doped $BaTiO_3$. Completely different tendency is observed for $Ba_{.80}Sr_{.20}TiO_3$. Figure 4.27(b) shows that loss tangent remains constant even at higher temperature for low frequency and for high frequency measurement, the loss tangent decreased as the temperature increased. For pure $SrTiO_3$ the tetragonal-cubic transformation temperature is 105K [59]. Therefore, the substitution of Sr instead of Ba in $BaTiO_3$ can reduce the Curie temperature. Figure 2.20 shows that, the Curie temperature decreased linearly with the increases of Sr content.

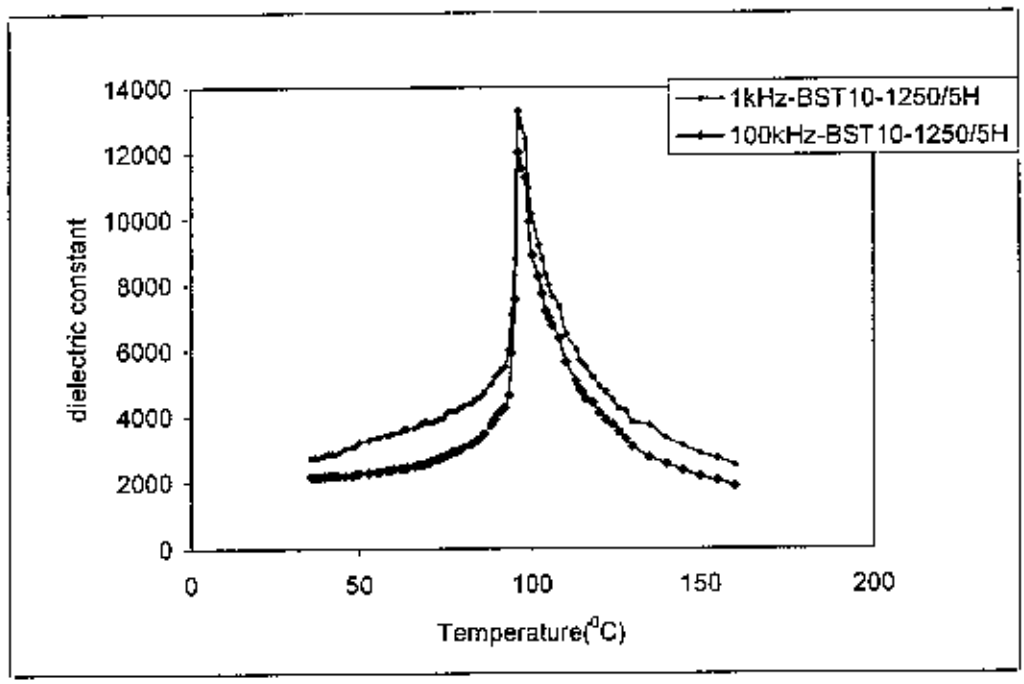


Figure 4.25(a): Dielectric constant as a function of temperature for $Ba_{.9}Sr_{.1}TiO_3$ at 1kHz and 100kHz.

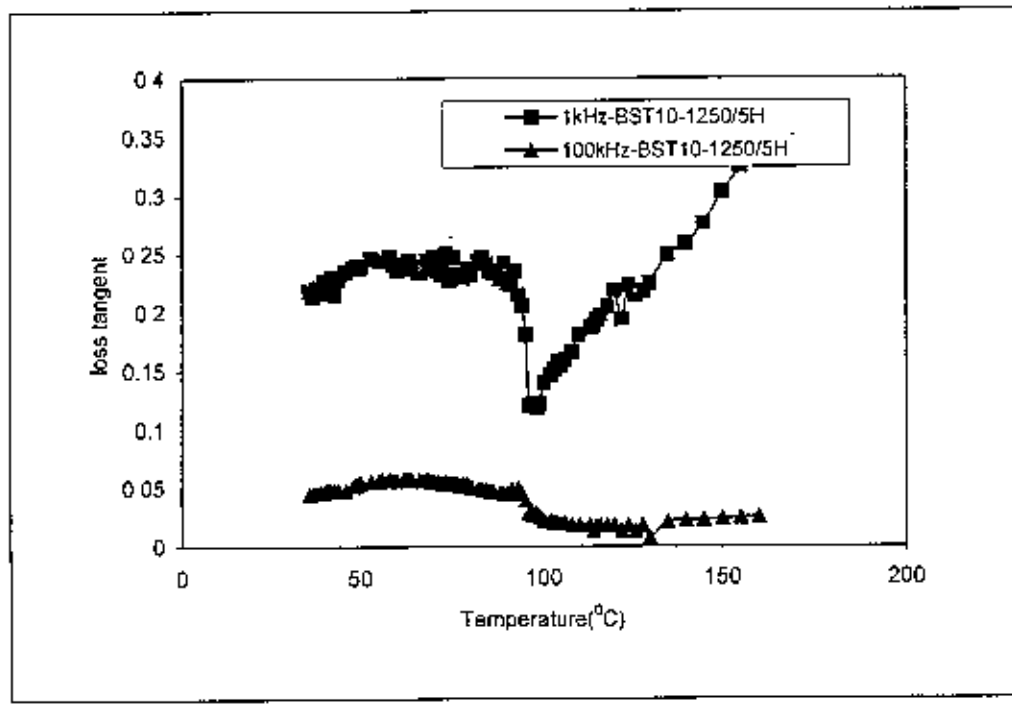


Figure 4.25(b): Loss tangent as a function of temperature for $Ba_{.9}Sr_{.1}TiO_3$ at 1 kHz and 100 kHz.

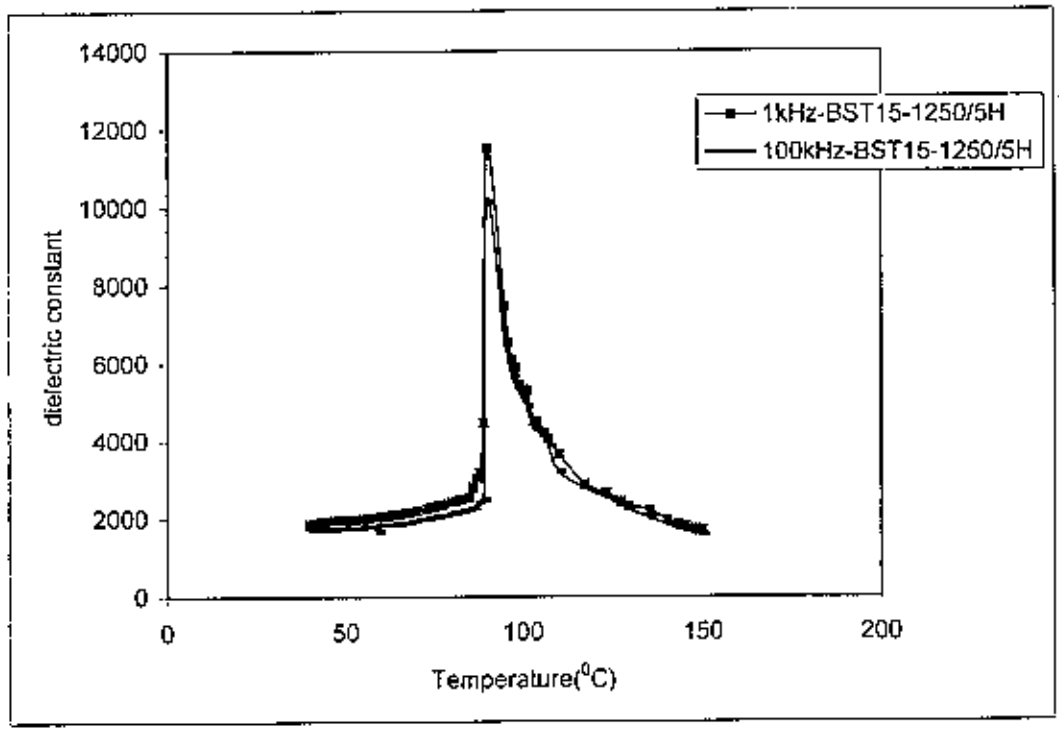


Figure 4.26 (a): Dielectric constant as a function of temperature for $Ba_{.85}Sr_{.15}TiO_3$ at 1 kHz and 100 kHz

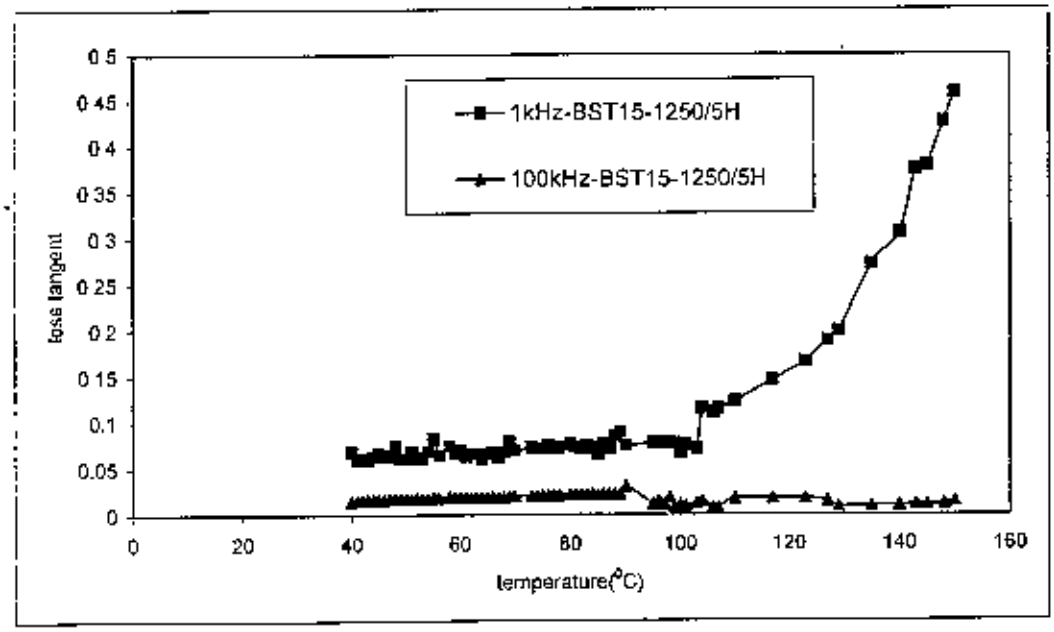


Figure 4.26(b): Loss tangent as a function of temperature for $Ba_{.85}Sr_{.15}TiO_3$ at 1kHzand 100kHz

Figure 4.25, Figure 4.26 and Figure 4.27 show the Curie point shifting towards the lower temperature as substitution of Sr2+ is increased. The reason of shifting the Curie temperature towards the lower temperature can be explained considering the ionic radius of Sr2+ and Ba2+. In perovskite crystal structure of $BaTiO_3$ (Figure 2.5(a)). Ti (titanium) atoms reside in octahedral interstitial position surrounded by six oxygen ions. The large size of the Ba ion makes the octahedral interstitial position quite large compare to the size Ti ion. The Ti ions are on the margin of being too small to be stable in the octahedral position. It is believed that there is minimum energy positions off-center in the direction of each of the six oxygen ions surrounding the Ti ion. The Ti ion positions randomly in one of these six possible minimum-energy sites. Above Curie temperature (120°C), the $BaTiO_3$ is cubic and every six possible minimum energy sites are equally probable.

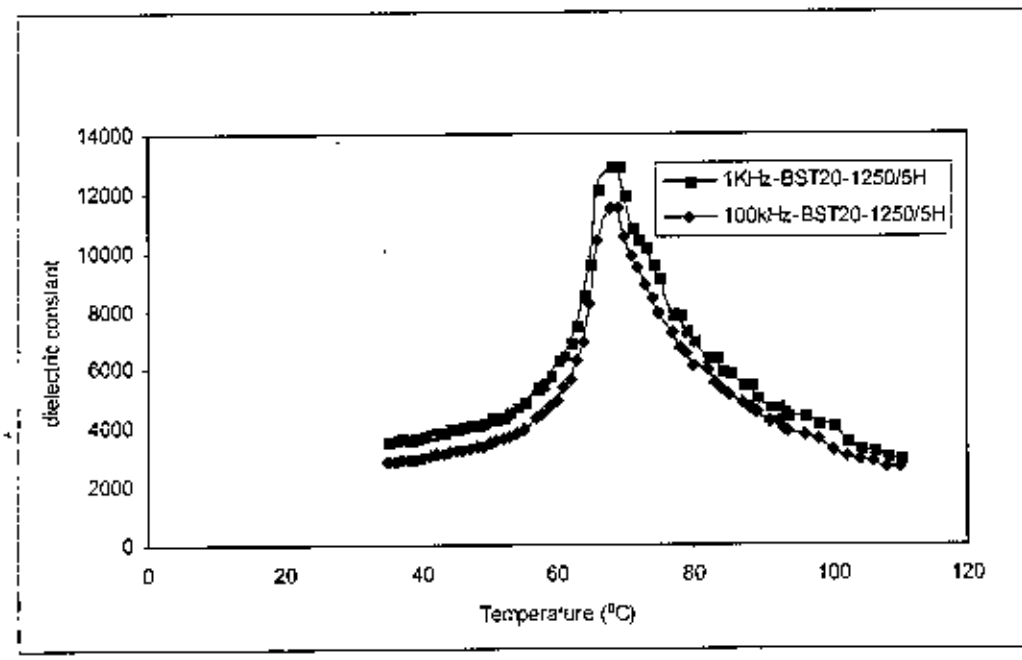


Figure 4.27(a): Dielectric constant as a function of temperature for $Ba_{.80}Sr_{.20}TiO_3$ at 1kHz and 100kHz

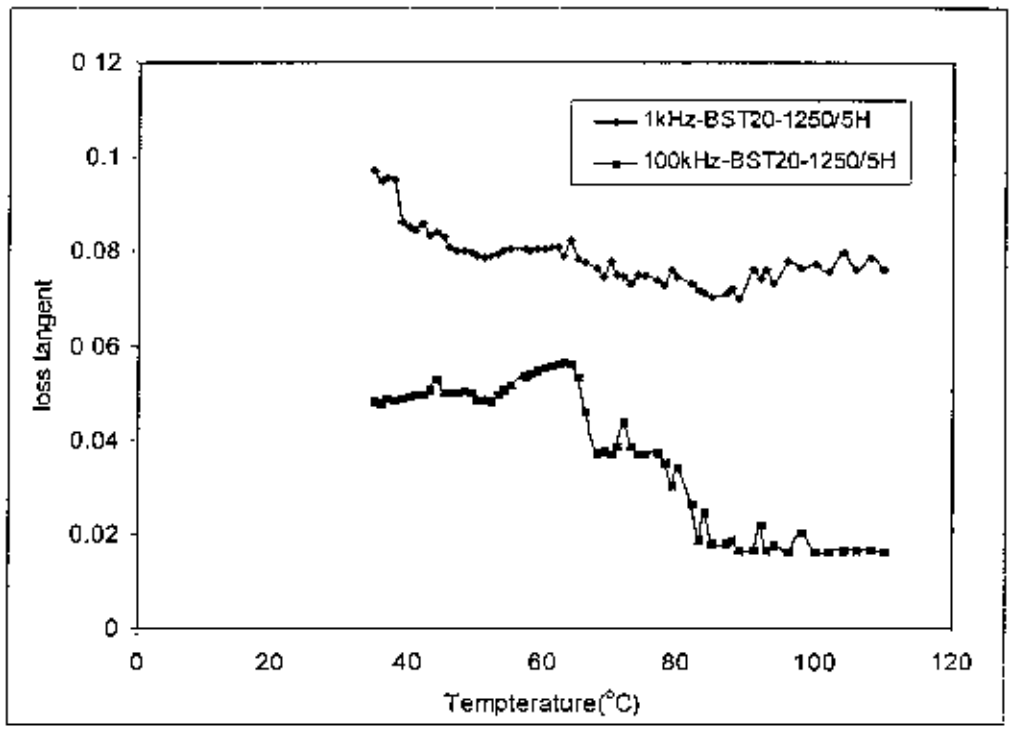


Figure 4.27(b): Loss tangent as a function of temperature for Ba $_{80}$Sr.$_{20}$TiO$_3$ at 1 kHz and 100 kHz.

Below the Curie temperature, the structure changes to tetragonal. The octahedral site is now distorted with the Ti ion in an off center position. If Ba ion is replaced by the Sr ion, because of the lower ionic radius of the Sr ion, Ti ion resides in a smaller octahedral interstitial position. This will result relatively stable position for Ti ion. This stable Ti ion stabilizes the cubic structure in the lower temperature range.

Figure 4.28(a-b) shows the frequency dependence of dielectric constant of pure strontium titanate sample sintered at 1250°C for 3 hour and 5 hours. The room temperature dielectric constant up to the frequency of 10 MHz is 210. The stable frequency range is quite long, up to 10 MHz, which is quite large as compared to the other sample investigated tested in this study. Lower dielectric constant can be understood by the paraelectric state of $SrTiO_3$ at room temperature causing no spontaneous polarization to take place.

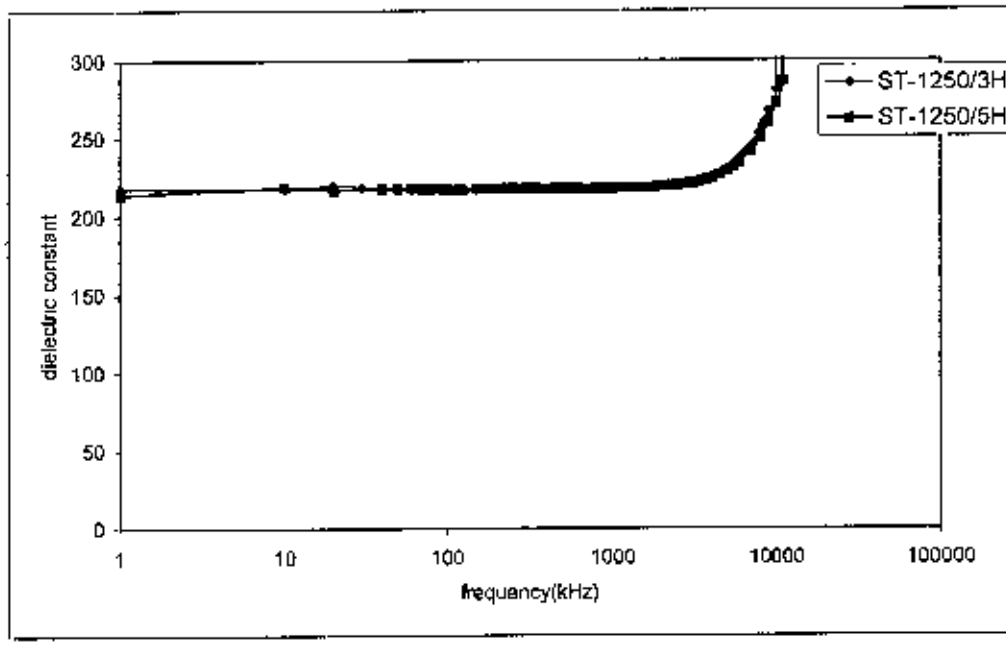


Figure 4.28(a): Dielectric constant as a function of frequency for $SrTiO_3$

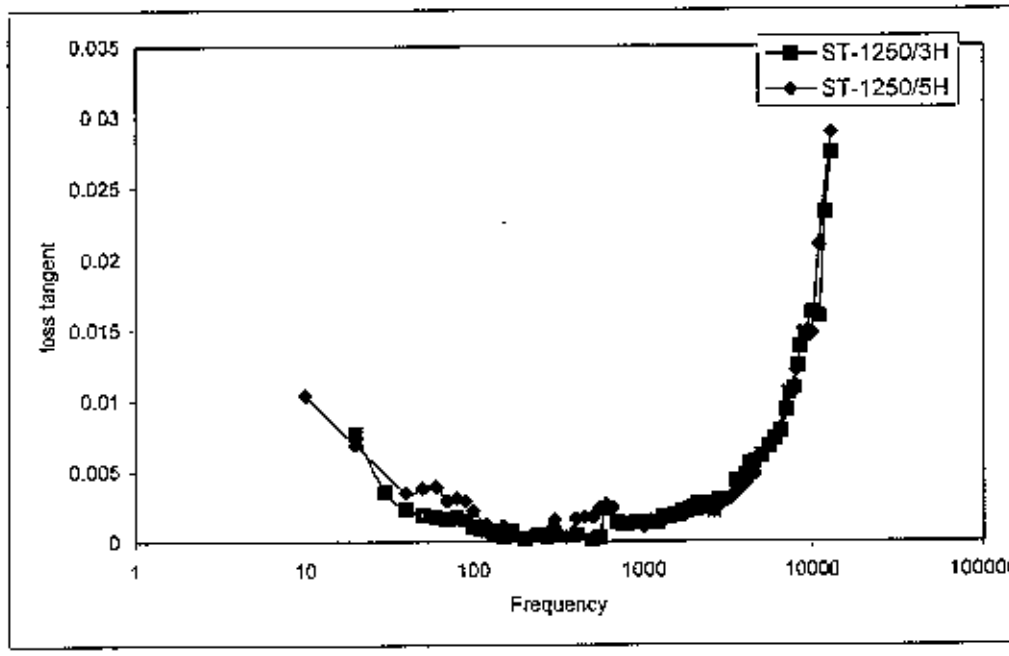


Figure 4.28(b): Loss tangent as a function of frequency for $SrTiO_3$

## 4.4 Differential Scanning Calorimetry (DSC)

Differential Scanning Calorimetry was used to find the tetragonal-cubic transition temperature for both $BaTiO_3$ and $Ba_{1-x}Sr_xTiO_3$. Crystallographic phase transition during heating was detected by a negative peak, thereby indicating that the process is endothermic. For $BaTiO_3$, the heating rate used was 5°C/min and that for $Ba_{1-x}Sr_xTiO_3$ heating rate was 2°C/min. The reason for taking higher heating rate was the thermal energy needed for the phase transformation can easily be acquired at the high temperature. Figure 4.29 shows the differential scanning calorimetry data recorded for $BaTiO_3$ polycrystals sintered at different temperature and holding time. From the microstructural study of $BaTiO_3$, it was observed that considerable grain growth occur at higher sintering temperature. Endothermic peak around 125°C may be attributed to the tetragonal-cubic phase transformation. There were clearly marked changes, which took place in the transformation behavior for materials with decreasing grain size. In particular, the tetragonal-cubic transformation shift to lower temperature with decreasing grain size as has been concluded previously based on dielectric constant data. It is also interesting to note that the peak shifting is accompanied with peak broadening. The heat flow, during the crystallographic phase transformation decreased with decreasing grain size. This reduction of heat flow during transformation suggested that small grain size $BaTiO_3$ exhibits suppressed transformation characteristics (tetragonal distortion).

The effect of substitution of Sr in $BaTiO_3$ is also shown the Figure 4.30. Increasing concentration of Sr decreases the Curie temperature, which has already been confirmed from the temperature dependence of dielectric constant experiment (Figure 4.25 to 4.27). The observable peak suggested that single phase is formed in the solid solution of $BaTiO_3$-$SrTiO_3$. No peak is observed in case of $Ba_9Sr_1TiO_3$ and $Ba_8Sr_2TiO_3$ sintered at 1100°C for 3 hours in the DSC data (Figure 4.31 and Figure 4.32). These results confirmed that the diffusion of Sr in $BaTiO_3$ has not been completed.

The Table 4.2 shows the Curie temperatures found using temperature dependent dielectric constant (k′) measurement and DSC experiment.

Table 4.2: Curie temperature of various BT and BST samples

| Composition | Sintering temperature and time | Curie temperature (Using k' measurement by LCR meter). | Curie temperature (Differential Scanning Calorimetry DSC) |
|---|---|---|---|
| $BaTiO_3$ | 1100°C for 3 hours | 129°C | 125°C |
| $BaTiO_3$ | 1225°C for 4 hours | 130°C | 126°C |
| $BaTiO_3$ | 1250°C for 3 hours | - | 127°C |
| $BaTiO_3$ | 1250°C for 5 hours | - | 127°C |
| $Ba_{.9}Sr_{.1}TiO_3$ | 1250°C for 5hours | 96°C | 92°C |
| $Ba_{.85}Sr_{.15}TiO_3$ | 1250 °C for 5hours | 90°C | 79°C |
| $Ba_{.8}Sr_{.2}TiO_3$ | 1250°C for 5hours | 69°C | 65°C |

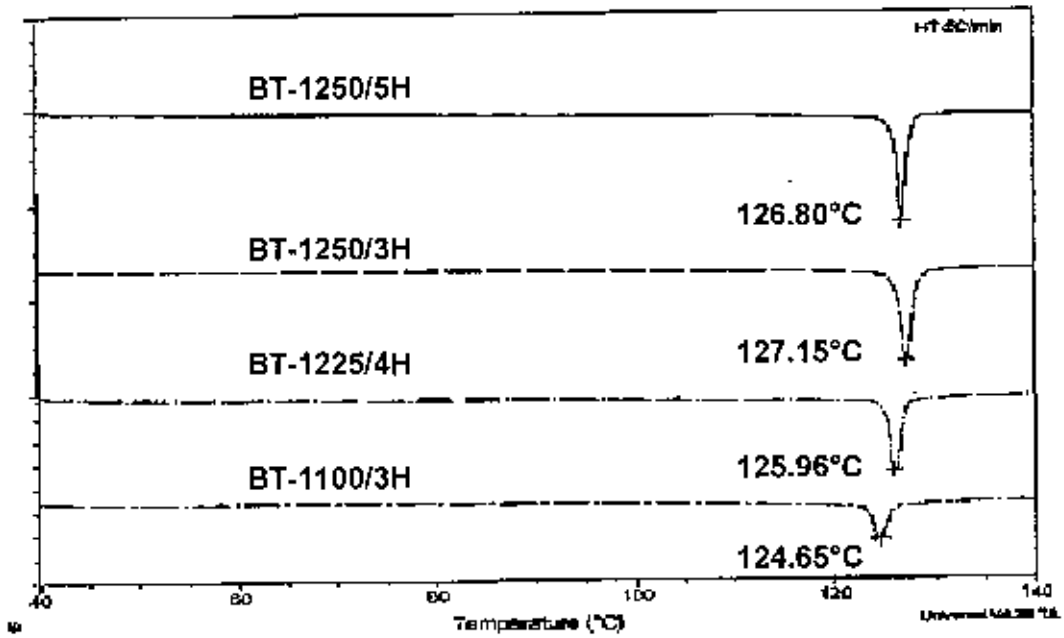


Figure 4.29: DSC data for polycrystalline $BaTiO_3$ sintered at different temperatures.

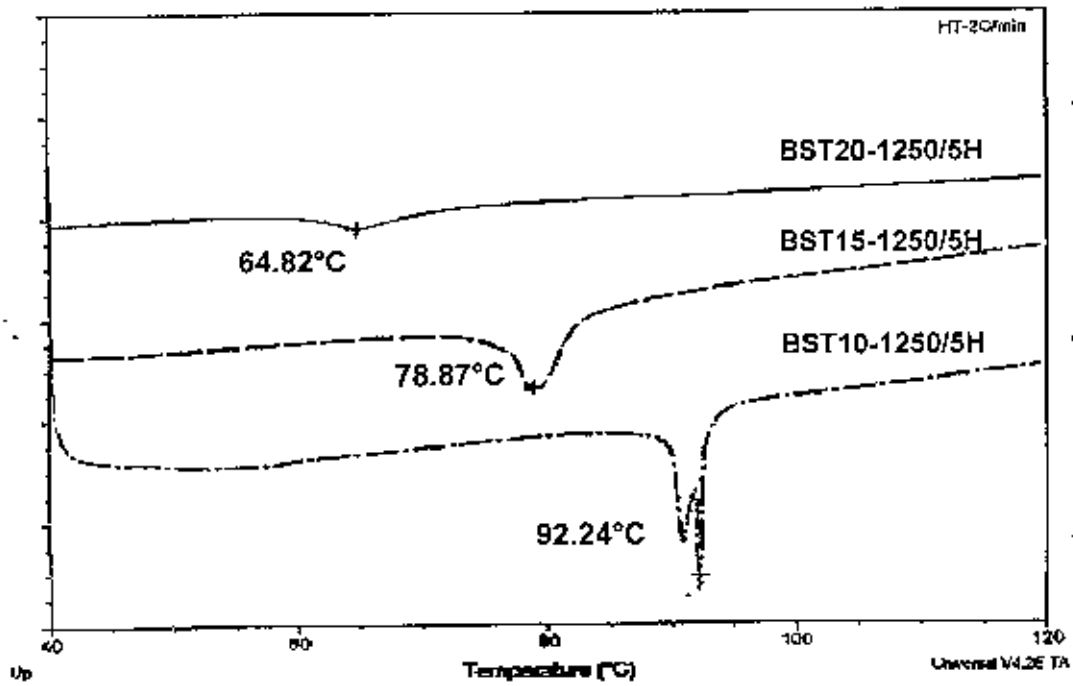


Figure 4.30: DSC data for $Ba_{1-x}Sr_xTiO_3$ (x=0.10, 0.15, 0.20) sintered at 1250°C for 5 hours.

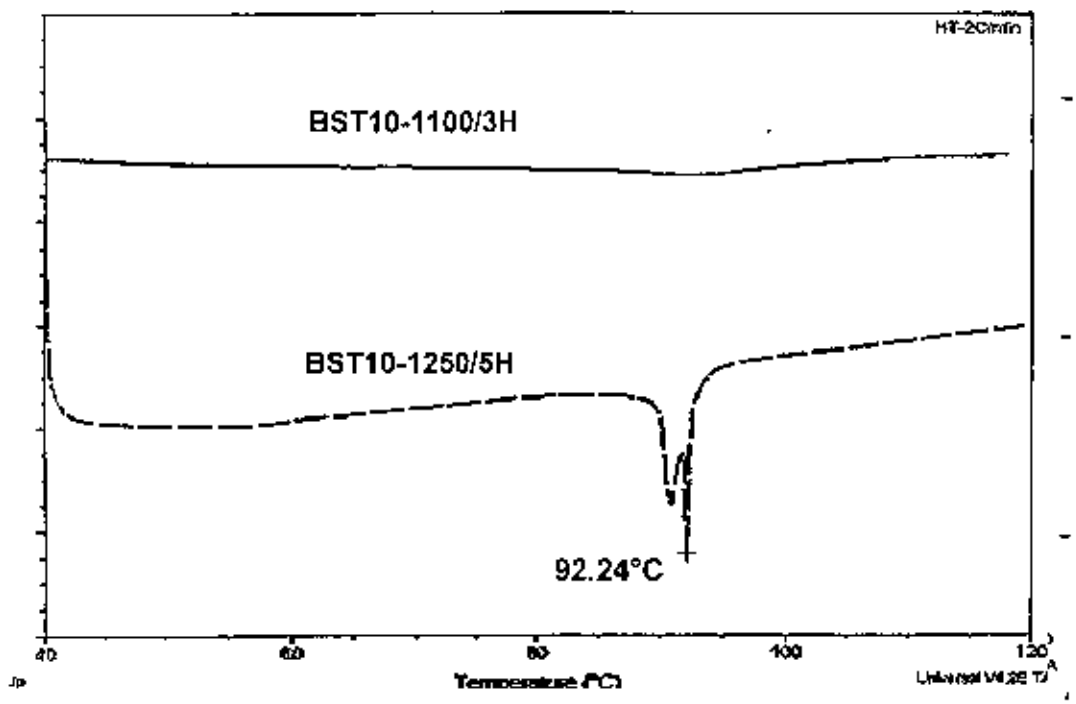


Figure 4.31: DSC data for $Ba_{1-x}Sr_xTiO_3$ (x=0.10) sintered at different temperatures.

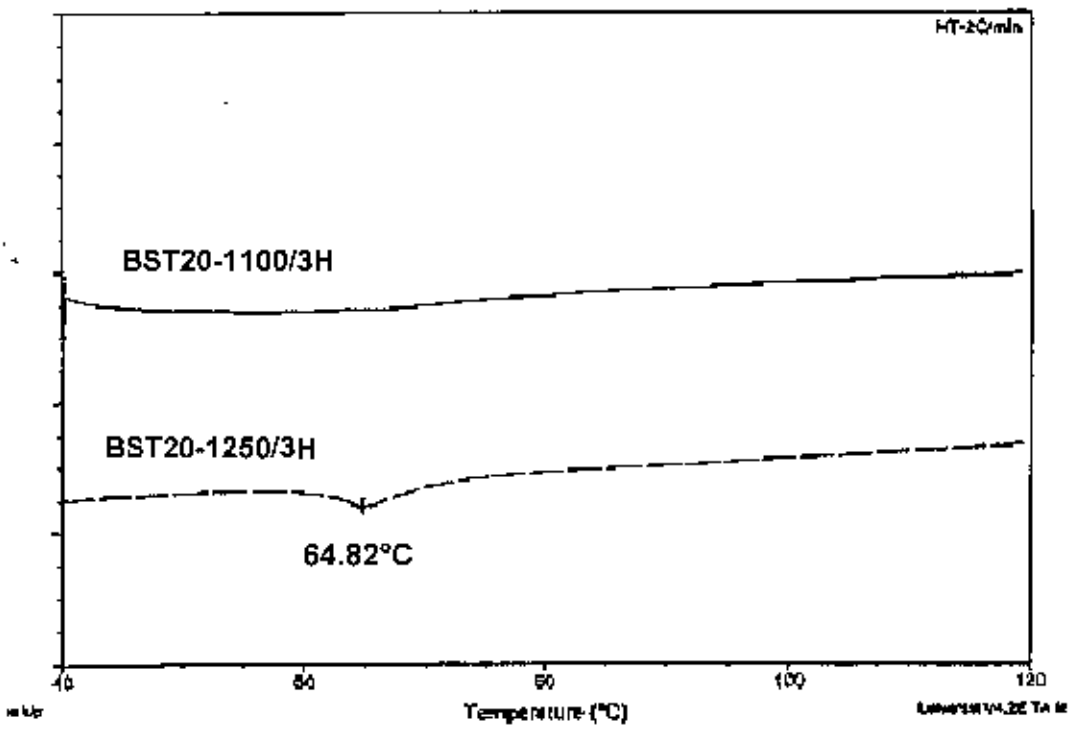


Figure 4.32: DSC data for $Ba_{1-x}Sr_xTiO_3$ (x=0.20) sintered at different temperatures.

## 4.5 X-ray diffraction analysis

Figure 4.33 shows the powder diffraction pattern of $BaTiO_3$ at room temperature sintered at 1100°C for 3hours. It is observed that at lower angle, tetragonality is suppressed but prominent at higher angle, that is (001) reflection is absent in Figure 4.33. On the other hand, at higher sintering temperature $BaTiO_3$ show tetragonality at lower angle. Figure 4.34 shows the XRD pattern of $BaTiO_3$ sintered at 1225°C for 4 hours. XRD data confirms the presence of (001) reflection. Microstructural study confirms that grain growth occurs at higher sintering temperature [Figure 4.1 and Figure 4.6]. Therefore, it can be concluded that tetragonality increases with the increase of grain size. These interesting results can be understood by 'internal stress model' proposed by Buessem et al [32]. When barium titanate is cooled through the Curie temperature, the individual grain experiences a complex stress system in it and its neighbors are transformed to the tetragonal state. The stress is minimized if the overall dimensional change of each grain is minimized, i.e. if the grain twins repeatedly. This very close mimetic twinning is an obvious feature of coarser grained (10μ to 50μ) barium titanate. In fine-grained barium titanate the frequency of occurrence 90° twins is very much reduced. Thus the fine grain barium titanate must be under much greater stress at room temperature than the coarse grained material. In general, however it is expected that the stress system would be of a type tends to suppress the spontaneous deformation, which decreased the tetragonality. This suppression of tetragonality is also observed in the temperature dependent dielectric constant data [Figure 4.21(a)].

Figure 4.35, 4.36 and 4.37 show the X-ray diffraction data of $Ba_{1-x}Sr_xTiO_3$ (x=0.1, 0.15, 0.20). The data confirms that solid state reaction is completed in $(Ba,Sr)TiO_3$ sintered at 1250°C for 5 hours. XRD data also shows that as the Sr concentration is increased the tetragonality becomes weaker. The X-ray diffraction data of $SrTiO_3$ nano powder is shown in Figure 4.38.

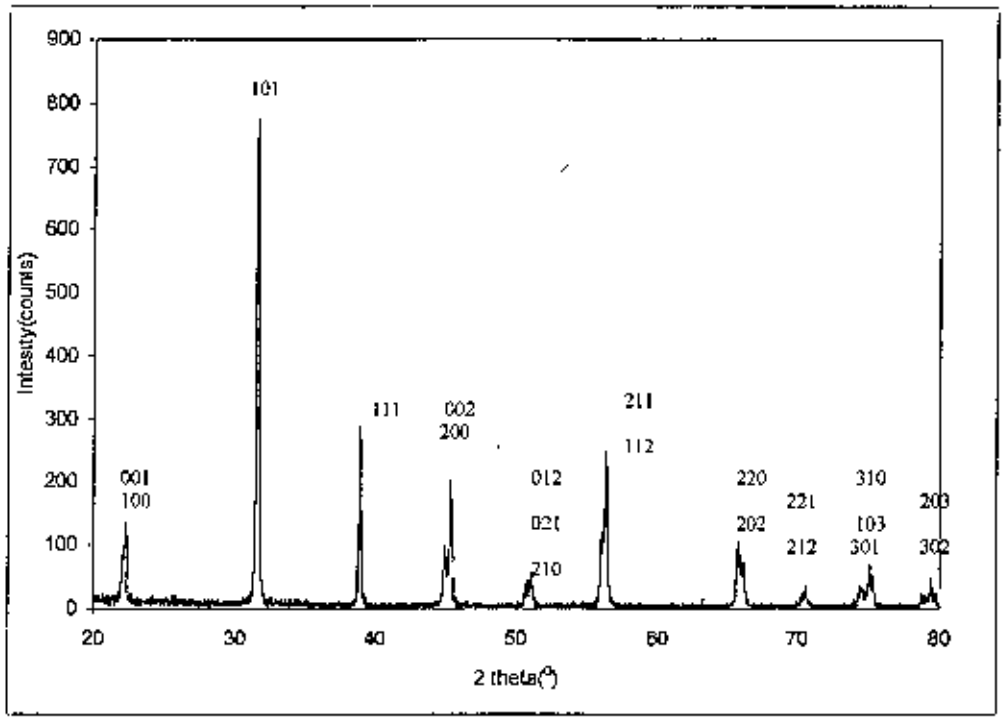


Figure 4.33: XRD pattern of $BaTiO_3$ sample sintered at 1100°C for 3 hours

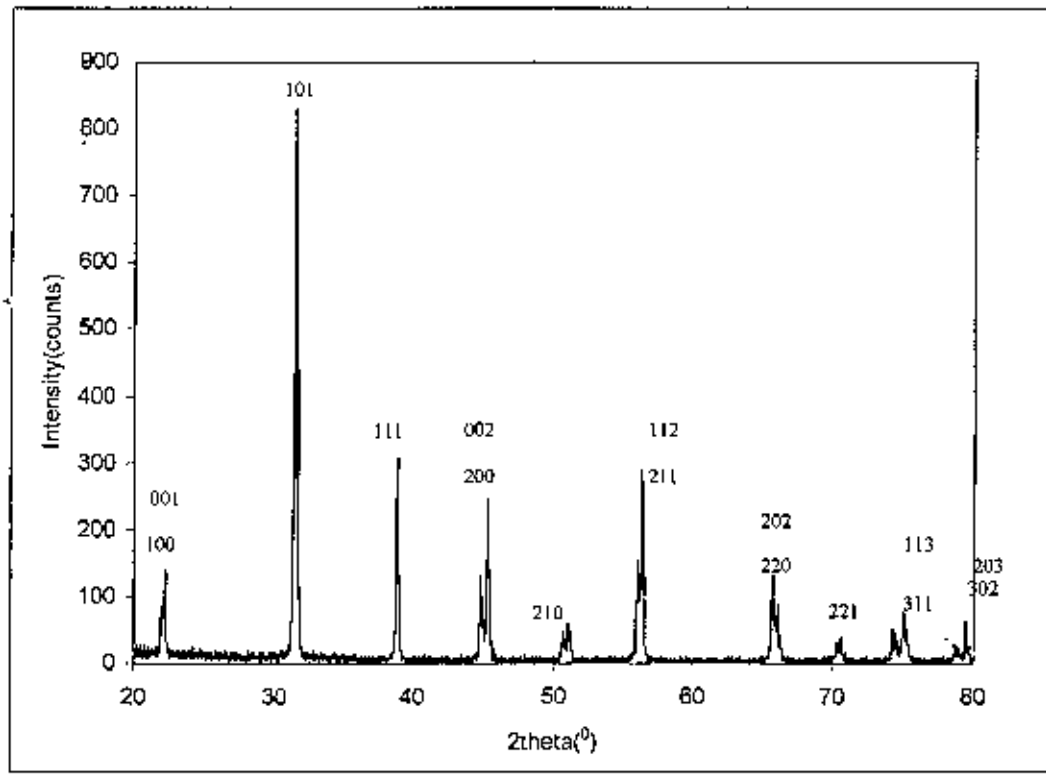


Figure 4.34: XRD pattern of $BaTiO_3$ sample sintered at 1225°C for 4 hours

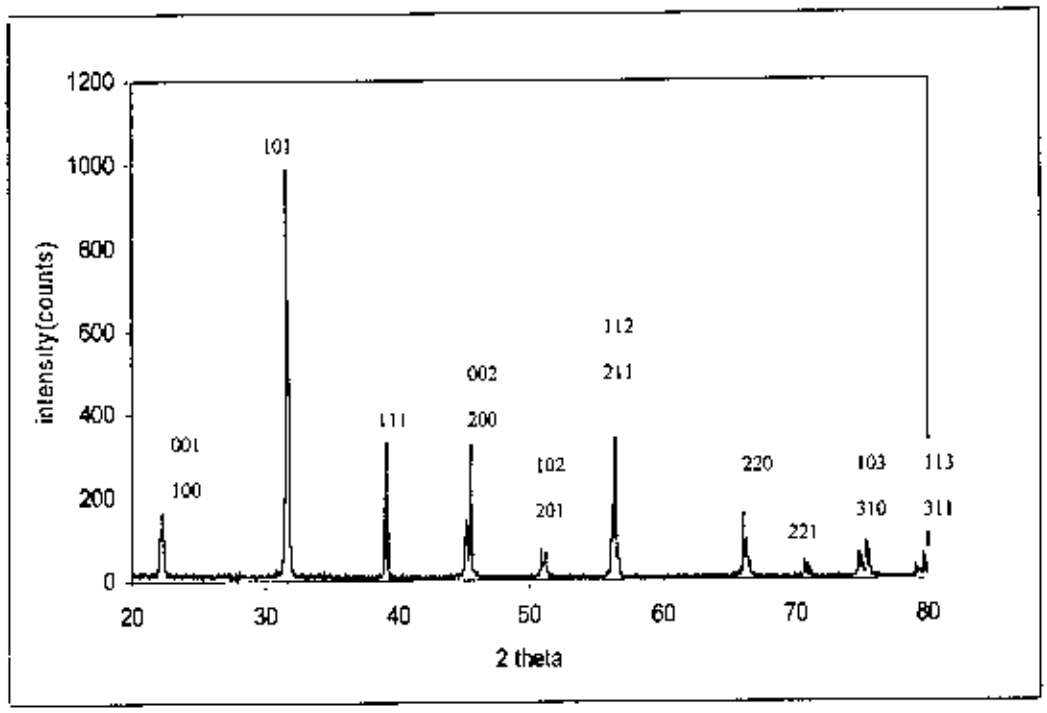


Figure 4.35: XRD pattern of $Ba_{.9}Sr_{.1}TiO_3$ sample sintered at 1250°C for 5 hours.

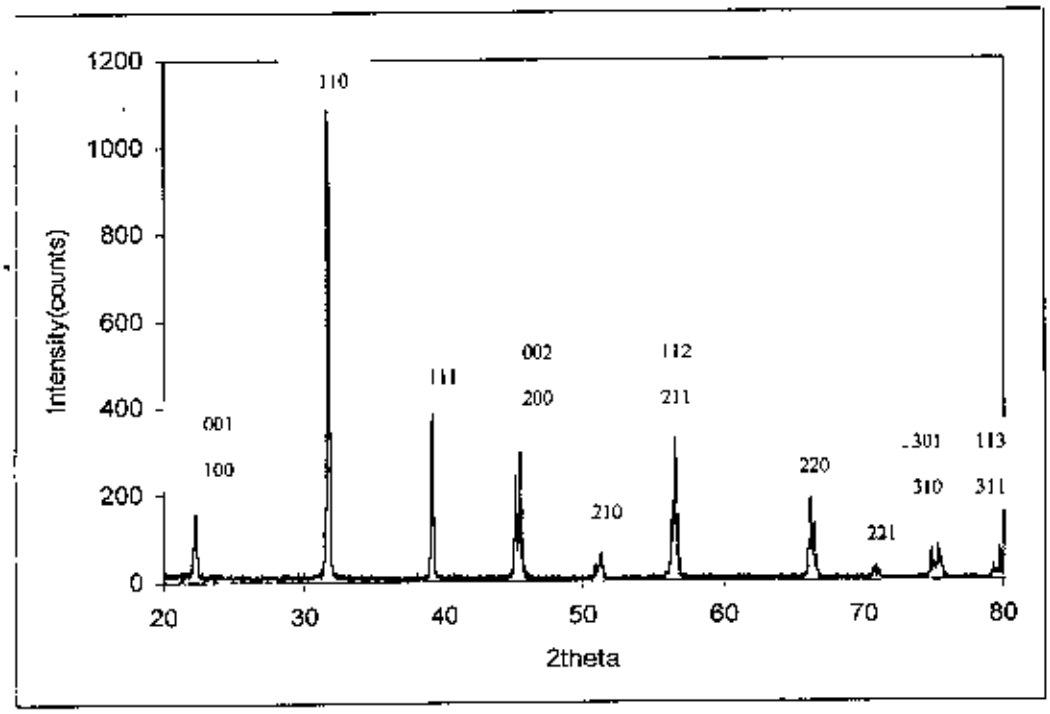


Figure 4.36: XRD pattern of $Ba_{.85}Sr_{.15}TiO_3$ sample sintered at 1250°C for 5 hours.

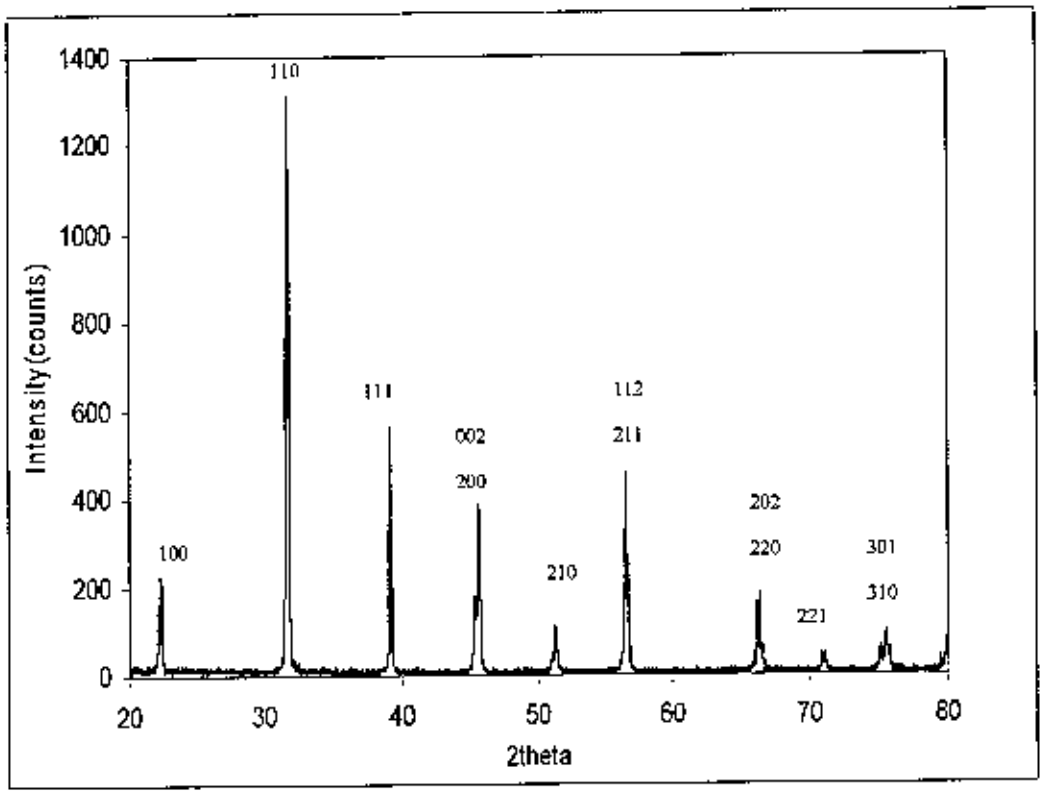


Figure 4.37: XRD pattern of $Ba_{.80}Sr_{.20}TiO_3$ sample sintered at 1250°C for 5 hour

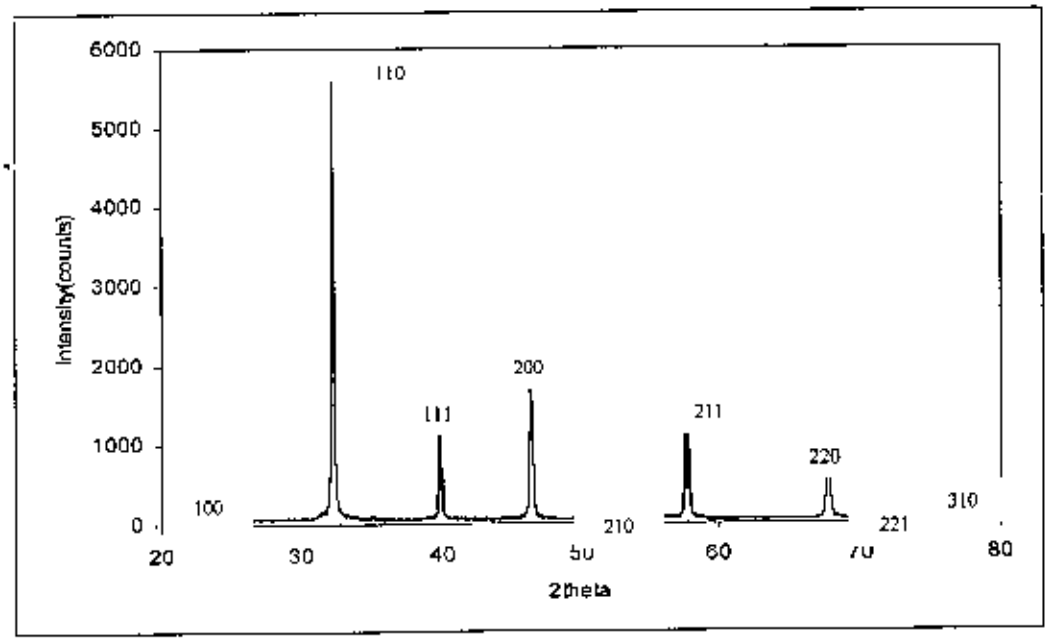


Figure 4.38: XRD pattern of $SrTiO_3$ nano powder

# 5. CONCLUSIONS

The study finally reached to the following conclusions:

1. 95% of theoretical density is obtained for $BaTiO_3$ in the temperature range 1225-1250℃. Few samples show lower theoretical density. This may be due to low sintering temperature and /or pressure gradient.

2. At higher temperature grain growth occurs as the holding time increased
3. Porosity was present in the microstructure indicates that grain growth rate is faster than the pore removal mechanism.
4. Ferroelectric domain twin was observed through chemical etching in large grained microstructure. Twin formation can be explained in terms of energy minimization and it is related to the grain size.
5. The presence of porosity may be the cause of not obtaining high dielectric constant.
6. At resonance frequency highest k' value and maximum loss due to the dissipation of field energy as frictional heat.
7. At low frequency (1kHz) loss tangent increases as the temperature increases- may be due to the ion migration. At High frequency (100kHz) loss tangent is low because ion migration is absent.
8. The dielectric constant at the Curie temperature found to be suppressed when the grain size is small. At room temperature, the fine grain $BaTiO_3$ shows high dielectric constant. On the other hand, room temperature dielectric constant was found to be low and at the Curie temperature the dielectric constant was found be higher than that of its fine grained counterpart.
9. At low sintering temperature, $Ba_{1-x}Sr_xTiO$ shows low k' and high loss tangent. This result can be attributed to the presence of more than one phase. This was confirmed by DSC, as no detectable endothermic peak was observed in DSC curve.
10. As the Sr concentration increased the Curie temperature ($T_C$) shifted to

the lower temperature. This result was confirmed from the temperature dependent dielectric constant graph and from DSC data.

11. X-RD confirmed single phase of $Ba_{1-x}Sr_xTiO_3$ (x=0.1, 0.15, 0.20) sample sintered at 1250°C for 5hours. The sharp endothermic peak also confirmed the presence of single phase.

12. The endothermic peak was observed to be decreased as the Sr concentration was increased. This indicates that cubic stability increased in lower temperature region.

# 6. SUGGESTIONS FOR FUTURE WORK

The topic just described here requires a great deal of research to find out more information about it. There are not much research work have been done in Bangladesh, regarding the structure property relationship of $BaTiO_3$-based dielectric materials. The future work should be directed to investigate the following important issues:

1. Effect of compaction pressure should be investigated more rigorously. Investigation should be carried on with the sample having pressure of 200MPa or more.
2. As the initial particle size is 100nm, the sintering temperature should not be more than 1225°C.
3. Investigation should be directed towards the heating rate during the sintering process, because it might have important effect on the microstructure (grain size, porosity) of the sample.
4. Ultimate goal of the research should be directed to find out the mechanisms of fabricating sample with pore free, fine-grained microstructure.

# 7. REFERENCES


**INTRODUCTION**

[1] H. Thurnauer, *Am.ceram. Society Bull.9*, 1977

[2] B.M Wul and N and F.L Vereschagen, Dokl. Akad. Nauk SSSR,48, 634

[3] K.Okazaki *Am Ceram Soc Bull*, 61, 932, 1932

[4] A.R Von Hipple, *Dielectrics and Waves*, Wily, New York 1954 p.203

[5] J. Merz, *Phys Rev.* 76,1221, 1949

[6] *Titanate materials Passive component industry* November/December 1999

[7] R. C. Buchanan, *Ceramic Material for Electronics*, Marcel Dekker, Inc., 1991

[8] L.L Hench ,J.K.West "*Principles of electronic ceramics*",John Wiley and Sons (SEA) Pte Ltd

[9] W. D. Kingery, *Introduction to Ceramics*, Jhon Wily & Sons.1975

[10] B. Jaffe, W. R. Cook and J. Jaffe, "*Piezoelectric Ceramics*", Academic Press Limited 1971

**LTERATURE REVIEW**

[11] Gene H Haertling * Motorola Inc., Albuqueque, New Maxico "Piezoelectric and electro optic ceramics" Ceramic *Material for Electronics*, Marcel Dekker, Inc., 1991

[12] W. Cady, *Piezoelectricity*, Mcgraw-Hill,New york,1946

[13] J. K. Lee, K. S. Hong, and J W Jang, *J. Am. Ceram. Soc.*, 84(9), 2001-2006. 2001

[14] R. E. Newnham, ' *Structure - Property Relations*', Springer-Verlag, New York, 1975

[15] R. E. Nettleton, *Ferroelectrics*. 1, 3, 87 207, 221, 1970

[16] R. E. Nettleton, *Ferroelectrics*, 2, 5, 77 93, 1971

[17] F. S. Galasso. *Structure, Properties and Preparation of Perovskite Type Compounds*, Pargamon Press, London, (1969)

[18] H. D. Megaw, *Acta Cryst.*, 7, 187-94, 1954

[19] J. P. Remeika, *J. Am. Chem. Soc.*, 76, 940-1, 1954

[20] M. Muller, E. Soergel, M. C. Wengler, K. Buse, *Appl. Phys. B.*, 78, 367-370, 2004

[21] Wang, J. E. Blendell, G. S. White. Q. Jiang, *Smart Mater. Struct.*, **12**, 217-222, 2003

[22] G. Arlt, D. Hennings and G. de With *J. Appl. Phys.* **58** (4) 1619-25, 1985

[23] Von. Hippel, *Rev. Modern Phys.*, **22**, 221, 1950

[24] A. Hooton and W. J. Merz, *Phys. Rev.* **98**, 409, 1955

[25] P. Cameron, *IBM Journal*, January 1957

[26] Bottger, *'Polar Oxides: Properites, Characteriazation and Imaging'*. Wiley-VCH, Weinheim, 2005

[27] I. K. Templeton, J. A. Pask, *J. Am. Cerm. Soc.*, **42**, 212, 1959

[28] A. Bauger, J. Mutin, J. C. Niepce, *J. Mater. Sci.*, **18**, 3548, 1983

[29] W. Kwestroo, H. A. M. Paing, *J. Am. Ceram. Soc.*, **42**, 292-9, 1959

[30] W. Maison, et al., *Science Asia*. **27**, 239-243, 2001

[31] S. L. Swartz. *IEEE Trans. Electrical Insulation*, **25**, 935, 1990

[32] W. R. Buessem, L.E. Cross, A. K. Goswami, *J. Am. Ceram. Soc.*,**75**, 2927 1966

[33] M.H. Frey and D.A. *Physical Review B* vol **54**, number 5p- 3158-3167 1996

[34] L.H Hench , J.K. West *Principle of Electronic ceramics* John Wily and Sons

[35] Yung H.Hu et.al . *J. Am. Ceram. Soc.*, **69**[8] 594 -602, 1986

[55] Suman Chatterjee and H. S. Maiti, *Materials Chemistry and Physics*, 67, 294-297. 2001.

[56] B. Huybrechts, K. Ishizaki and M. Takata, *Journal of Materials Science*, 30,2463-2474,1995.

**RESULTS AND DISCUSSION**

[57] Ulrike Taffner, Veronika Carle, UteSchafer, Michel J Hoffmann "*Preparation and Microstructural Analysis of High performance ceramics" ASM Hand book Vol-9*: Metallography and Microstructure(#06044G)

[58] Georg Koschek and Erich *J. Am. Ceram. Soc.*, vol-68, no-11November 1985

[59] Mathew trainer *Am.J.Phys* 69(9), September 2001

**APPENDIX**

[60] Wikipidea, a free encyclopidea

# 8. APPENDIX

## 8.1 Raw Powder Chemical Specification

Data provided here are taken from the label on the container.

Specification of the Nano powder

### Barium Titanate

| |
|---|
| Manufacturer: Inframet Advanced Materials |
| $BaTiO_3$ nano powder |
| Catalog#56220N-01 |
| Lot #IAM11066NBTO |
| Avg.Size ~100nm(SEM and BET) |

### Strontium Titanate

| |
|---|
| Manufacturer: Inframet Advanced Materials |
| $SrTiO_3$ nano powder |
| Catalog#38220N-01 |
| Lot #IAM6085NSTO |
| Purity -99.95% |
| Avg.Size ~100nm(SEM and BET) |

## 8.2 Basic Data of Elements involved

| Element | Molecular Weight | Atomic Number | Crystal Structure | Atomic Radius nm | Ionic Radius nm | Common Valance | Melting Point °C |
|---|---|---|---|---|---|---|---|
| Ba | 137.33 | 56 | BCC | 0.217 | 0.174(CN=12) | 2+ | 725 |
| Ti | 47.88 | 22 | HCP | 0.145 | .0745(CN=6) | 4+ | 1668 |
| Sr | 87.62 | 38 | | | 0.145(CN=12) | 2+ | |
| O | 15.99 | 8 | -- | - | 0.124(CN=4) | 2- | -218.4 |

## 8.3 Etching Reagent [57]

| Etchant composition | Condition | Uses |
|---|---|---|
| 95ml distilled $H_2O$+3ml HCl(32%)+2ml Hf(40%) | 5sec to 2min | $BaTiO_3$ |
| 100ml distilled $H_2O$+25ml Hf(40%) | 10sec to 5 min | $SrTiO_3$ |

## 8.4 Properties of Barium titanate [60]

| | |
|---|---|
| Molecular formula | $BaTiO_3$ |
| Appearance | White crystals |
| Density | 6.02gm/cm$^3$ |
| Melting point | 1625°C |
| Solubility of water | Insoluble |
| The data are given for materials in their standard state (at 25°C, 100kPa) | |

## 8.5 Properties of Strontium titanate [60]

| | |
|---|---|
| Molecular formula | $SrTiO_3$ |
| Appearance | Brown, redish, grey |
| Density | 5.13gm/cm$^3$ for synthetics |
| Melting point | Synthetics melt at 2080°C |
| Solubility of water | Synthetic resistant to most solvent |
| | |